



# Geomechanical and Petrophysical Studies to Reduce Risk in CO<sub>2</sub> Geological Storage

---

**Xiaojin (Andy) Zheng**

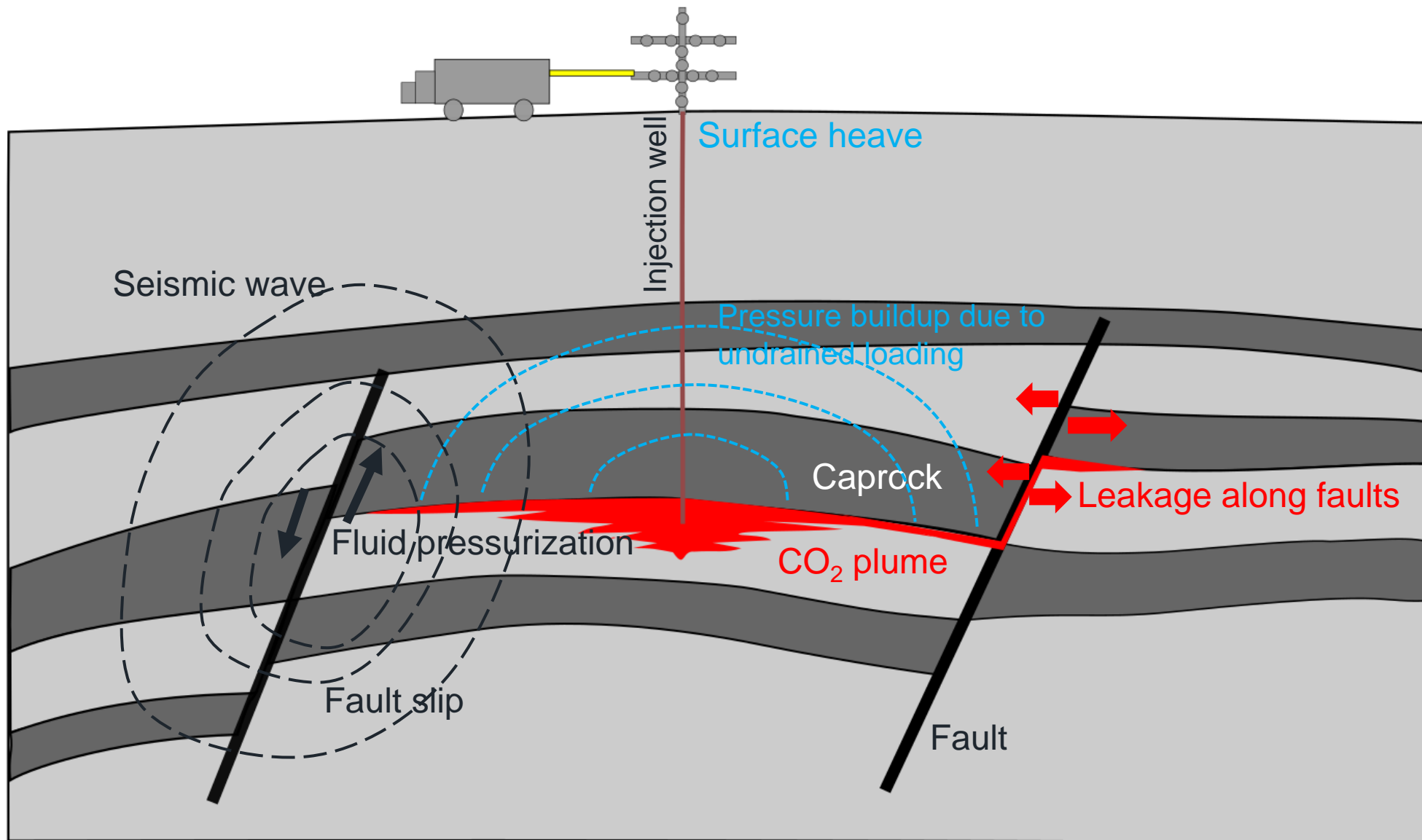
Ph.D. candidate

Hildebrand Department of Petroleum and Geosystems Engineering

The University of Texas at Austin

[xiaojin.zheng@utexas.edu](mailto:xiaojin.zheng@utexas.edu)

# Motivation

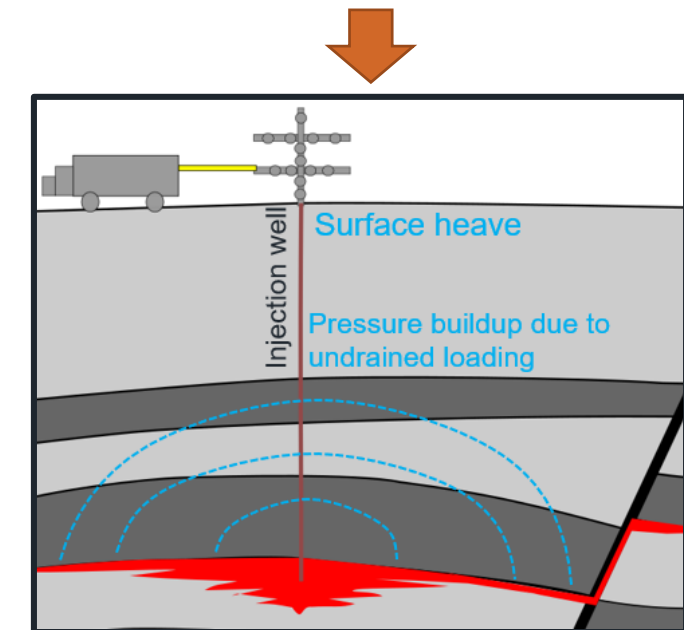
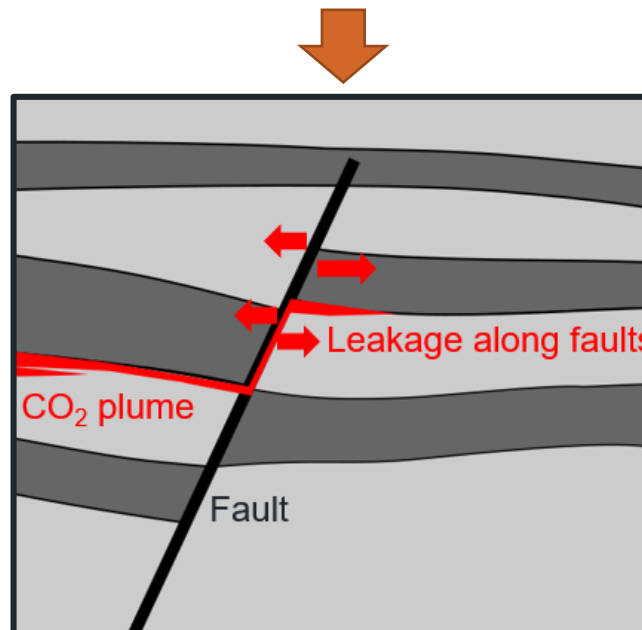
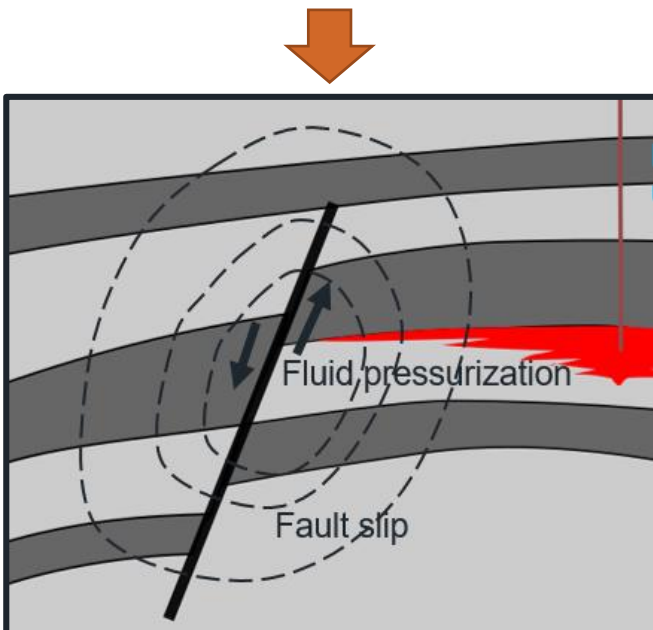


## Key problems in CO<sub>2</sub> geological storage

- Reservoir injectivity
- Reservoir sealing capacity
- Plume monitoring

# Research objectives

To reduce risk in CO<sub>2</sub> geological storage



## Reservoir injectivity:

- (1) How to manage CO<sub>2</sub> injection pressure in the reservoir?

*Experimental measurements on uniaxial strain unloading compressibility  
Fault transmissibility*

## Reservoir sealing capacity:

- (2) How much CO<sub>2</sub> can go through a fault?

*Measurements on transport properties of synthetic fault gouge*

- (3) What is the fault sealing capacity?

*Stochastic quantification on CO<sub>2</sub> column height*

## Subsurface monitoring:

- (4) How to monitor subsurface leakages?

*Reservoir modeling on poroelastic response induced by CO<sub>2</sub> injection*

# Contents

## Reservoir injectivity

- How to manage CO<sub>2</sub> injection pressure in the reservoir?

## Reservoir sealing capacity

- How much CO<sub>2</sub> can go through a fault?
- What is the height of CO<sub>2</sub> column?

## Subsurface monitoring

- How to monitor subsurface leakages?

### Chapter 1

**Measurement of Unloading Pore Volume  
Compressibility of Frio Sand under Uniaxial-strain  
Stress Path and Implications on Reservoir Pressure  
Management**

### Chapter 2

**Multiphase CO<sub>2</sub>-brine Transport Properties of Synthetic Fault Gouge**

### Chapter 3

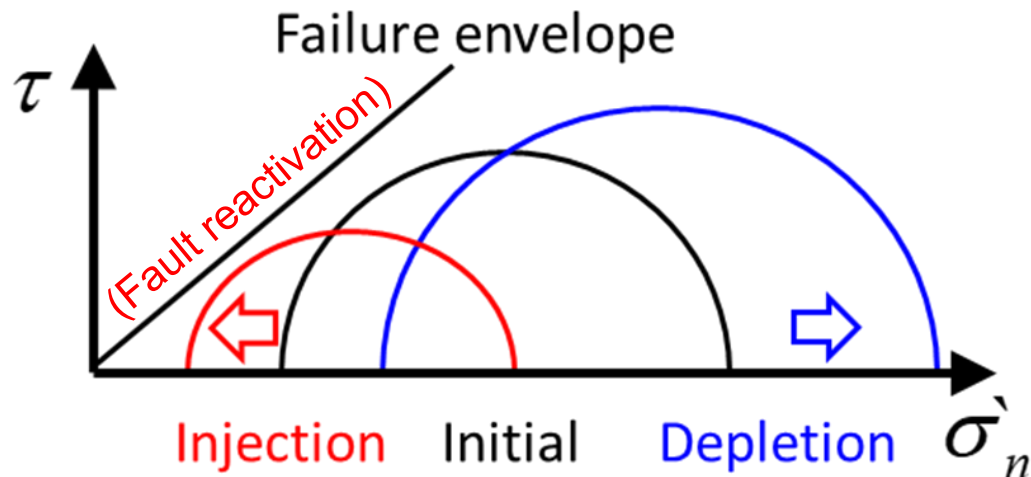
**Stochastic Quantification of CO<sub>2</sub> Fault Sealing Capacity in Sand-Shale Sequences**

### Chapter 4

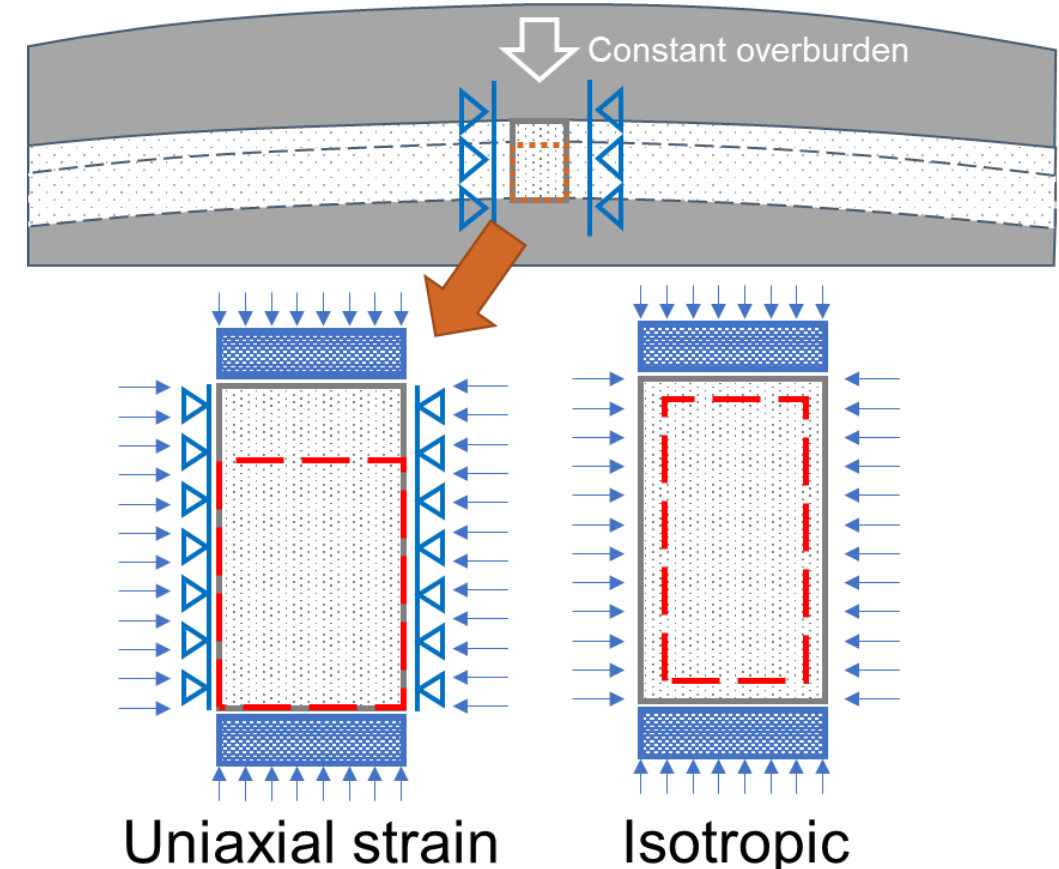
**Poroelastic Monitoring above the Injection Zone for CO<sub>2</sub> Geological Storage**

# Uniaxial strain unloading compressibility

- CO<sub>2</sub> injection unloads the stress on rocks.
- Reservoir rock is closer to uniaxial strain.

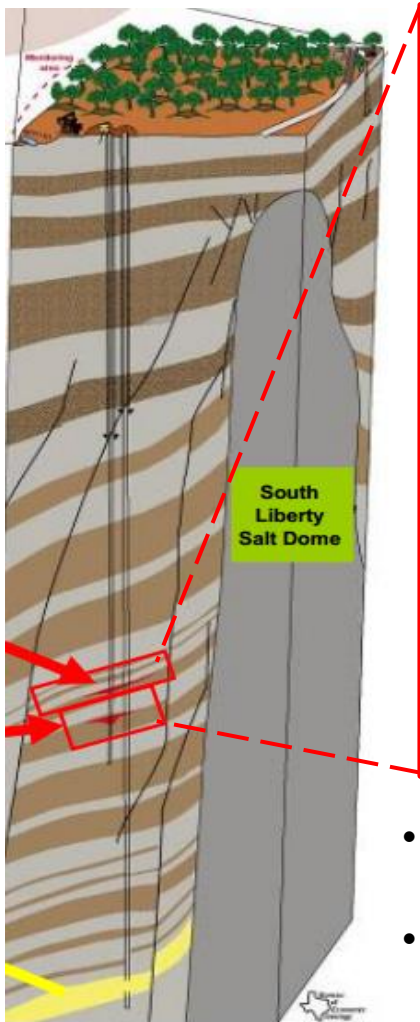


$$C_{pp}^{uni} = \frac{1}{V_p} \frac{dV_p}{dP_p} \Big|_{S_v, \varepsilon_h}$$

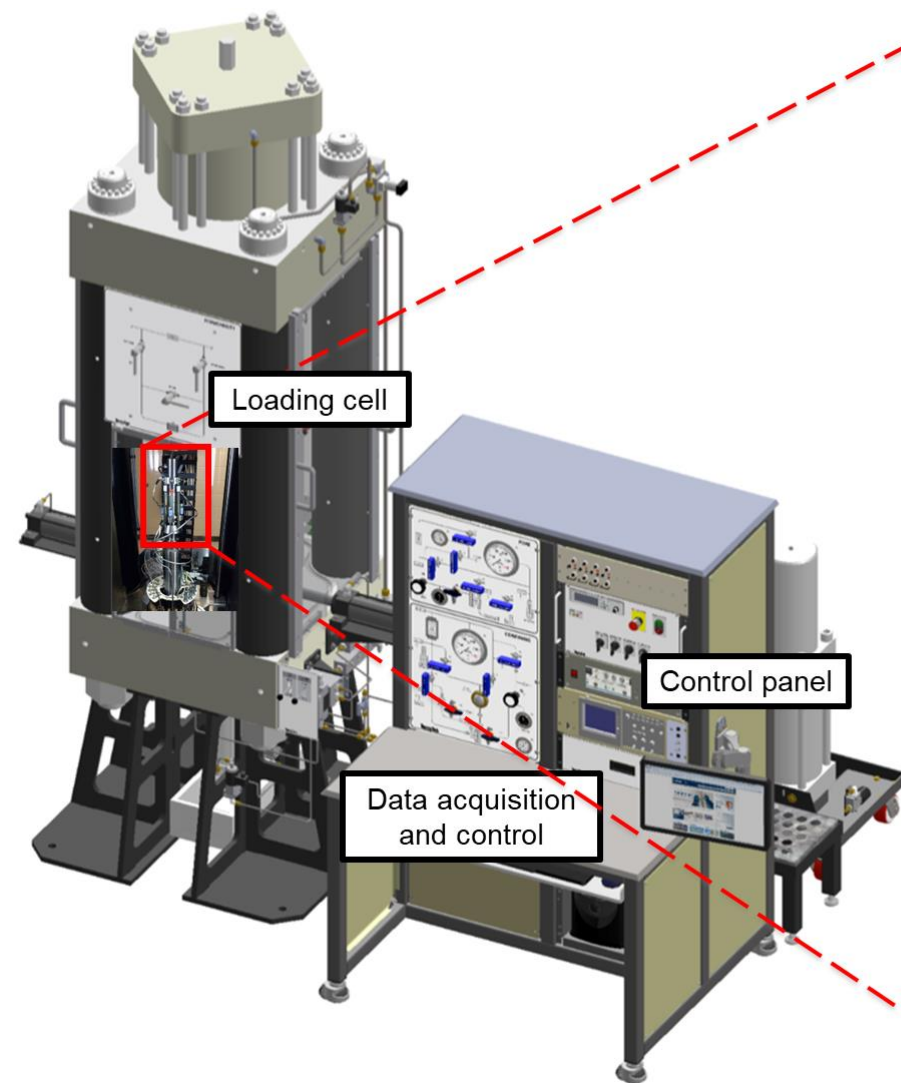


Uniaxial strain unloading compressibility can capture the real pressure change in CO<sub>2</sub> injection.

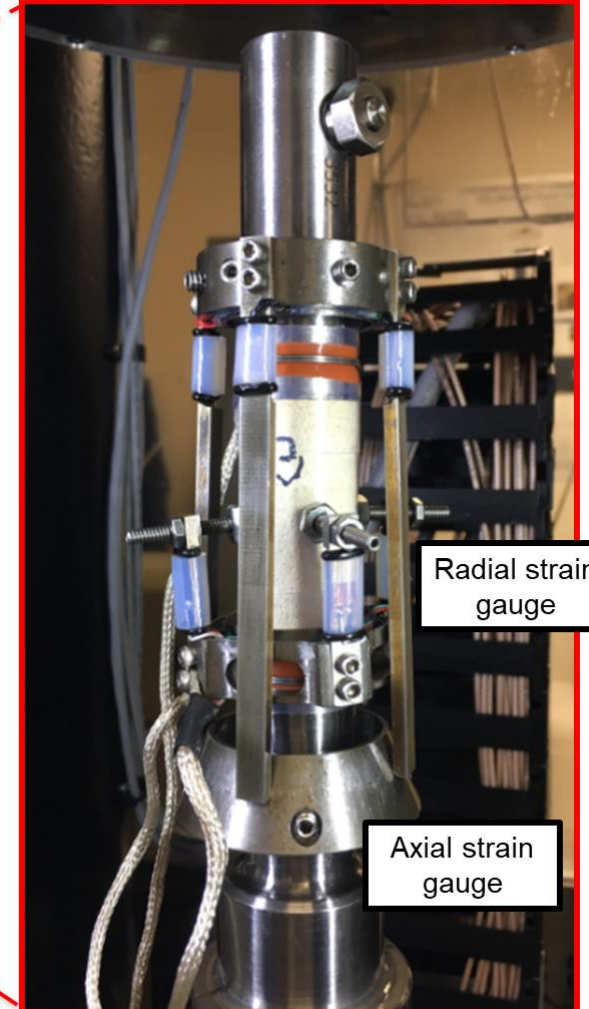
# Experimental cores and testing device



- South Liberty oil field, a region of the Gulf Coast
- Unconsolidated sand: courtesy of GCCC-BEG

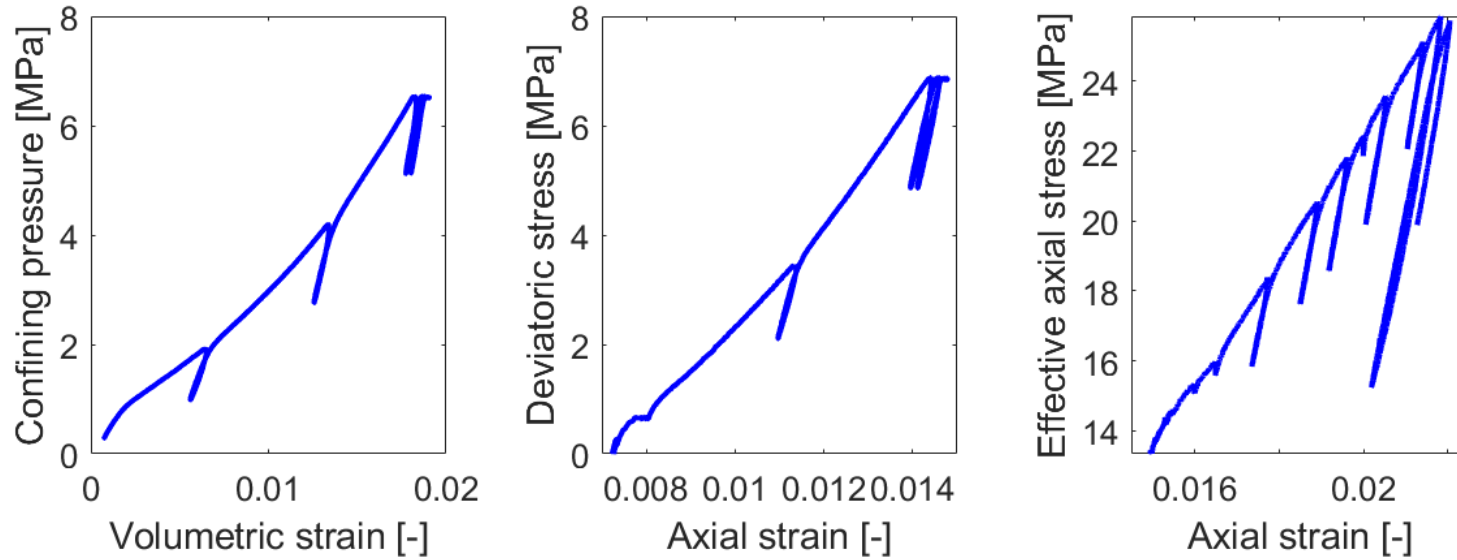


TerraTek triaxial frame

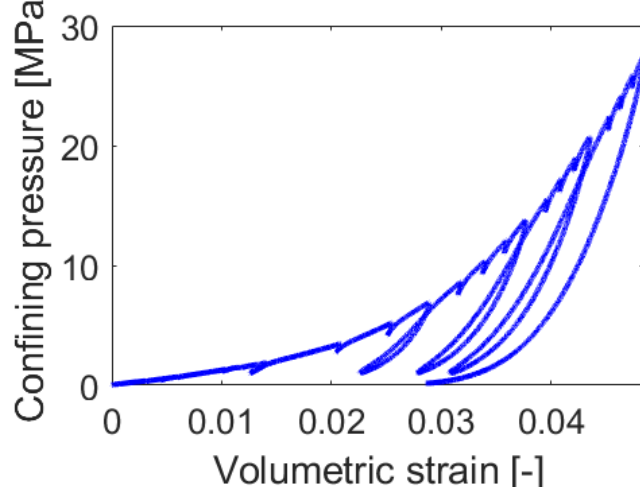


# Stress path

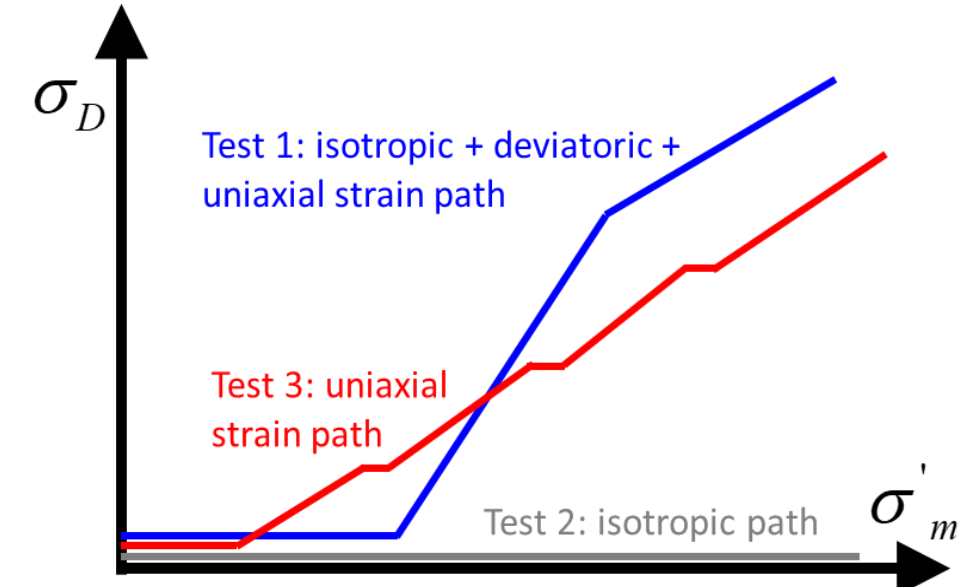
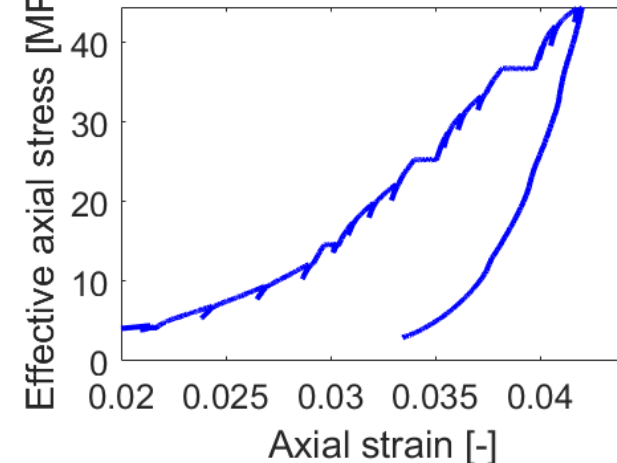
**(a) Test 1: Isotropic, deviatoric, and uniaxial strain path**



**(b) Test 2: Isotropic path**



**(c) Test 3: Uniaxial strain path**

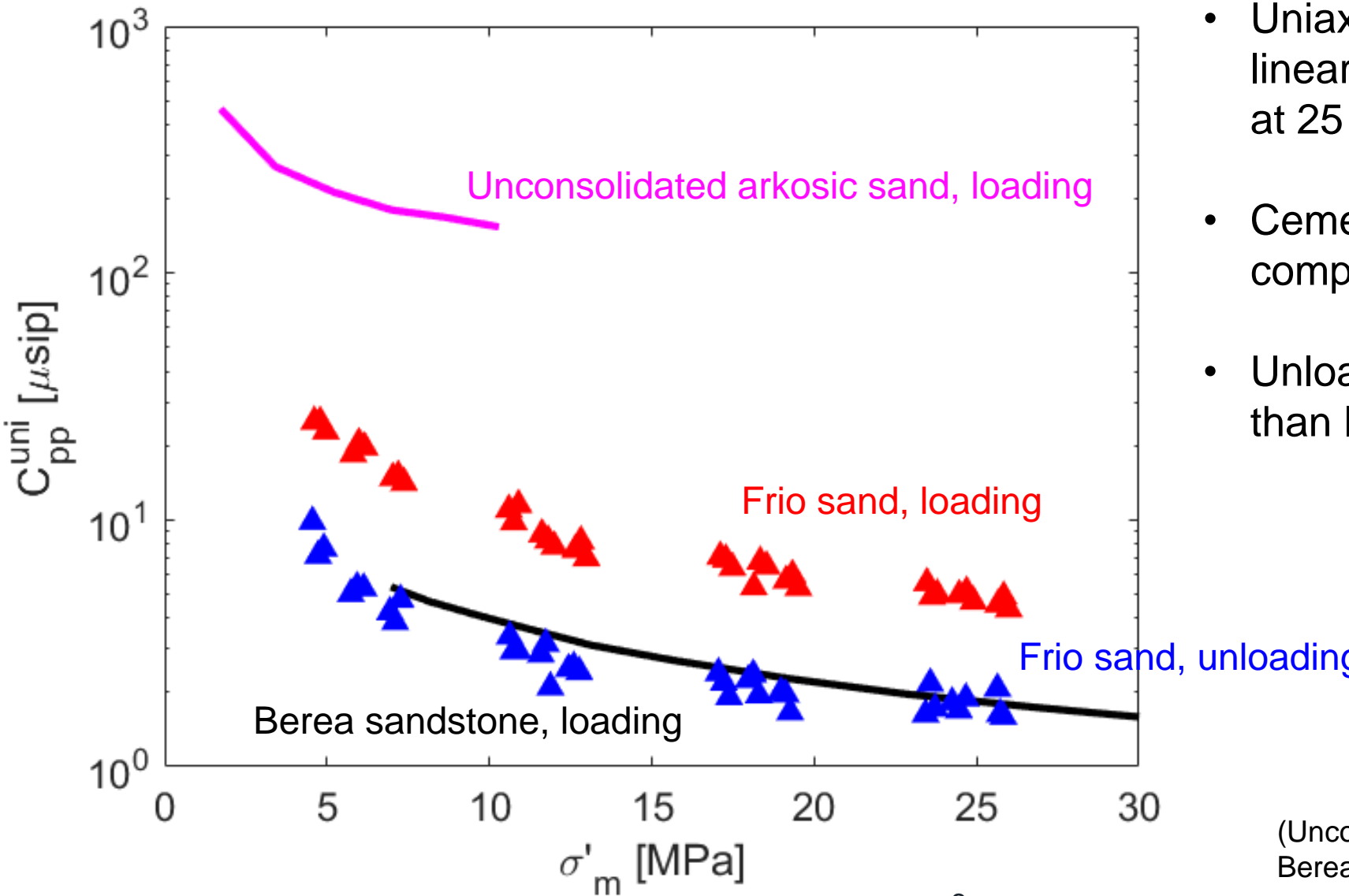


$$K = \frac{\Delta P_c}{\Delta \varepsilon_{vol}} \quad E = \frac{\Delta \sigma_D}{\Delta \varepsilon_{zz}} \quad M = \frac{\Delta \sigma_{zz}'}{\Delta \varepsilon_{zz}}$$



$$C_{pp}^{iso} = \frac{1}{\phi K} \quad C_{pp}^{uni} = \frac{1}{\phi M}$$

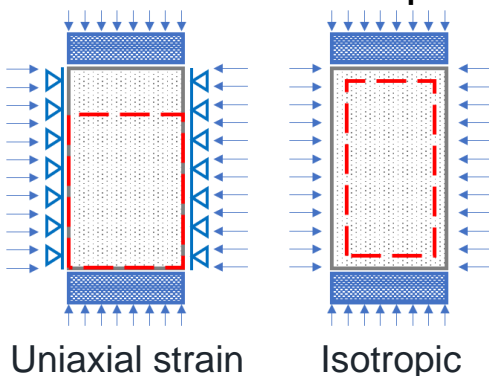
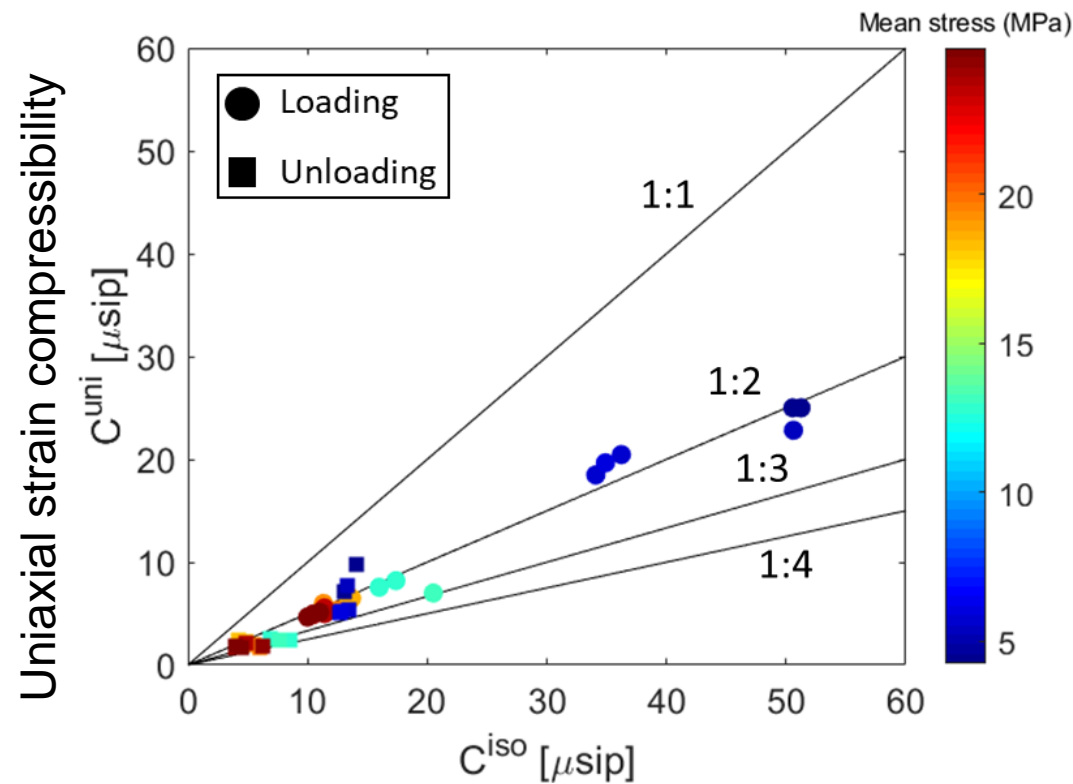
# Results of uniaxial strain unloading compressibility



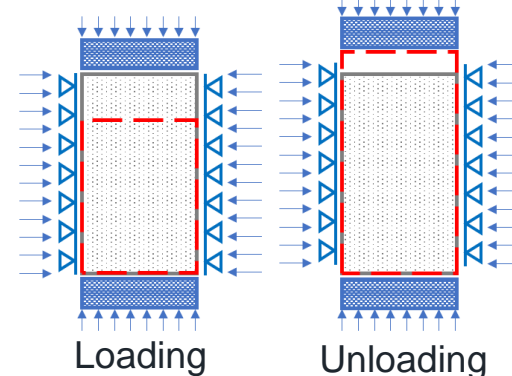
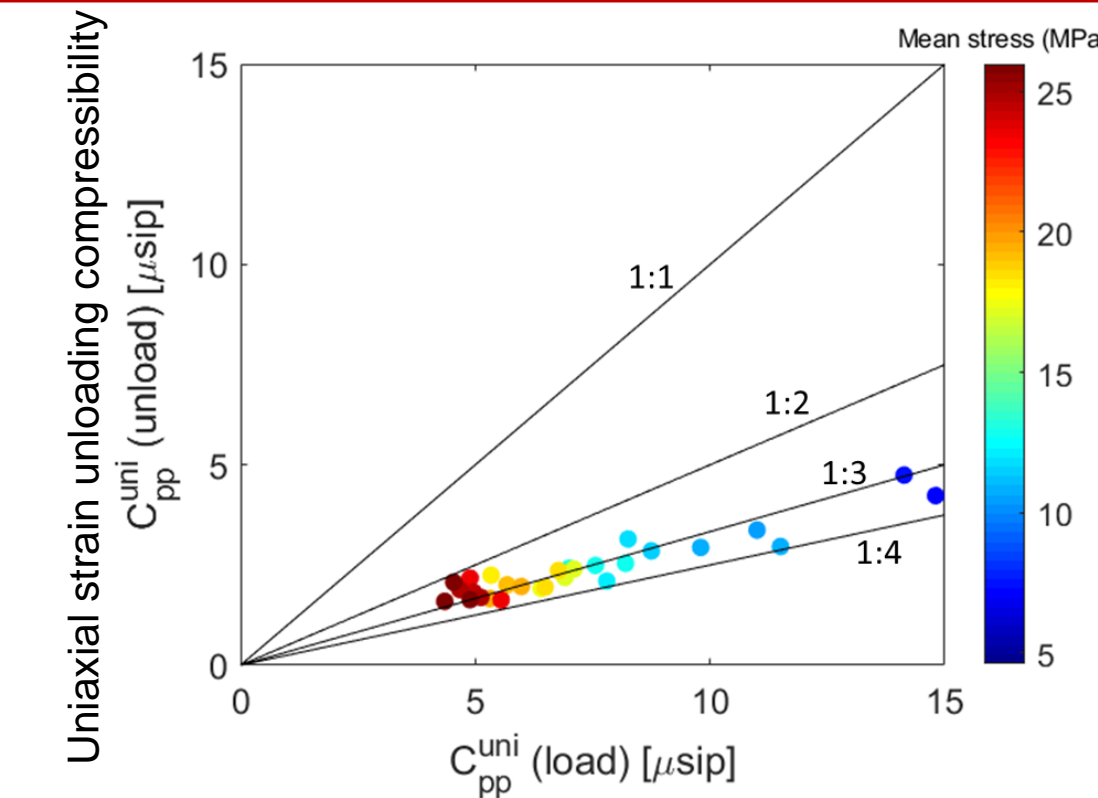
- Uniaxial strain compressibility is non-linearly stress-dependent ( $4 - 6 \text{ } \mu\text{sip}$  at 25 MPa).
- Cemented rock has lower compressibility.
- Unloading compressibility is smaller than loading compressibility.

(Unconsolidated arkosic sand, Sawabini, 1974;  
Berea sandstone, Andersen, 1985)

# Compressibility comparison

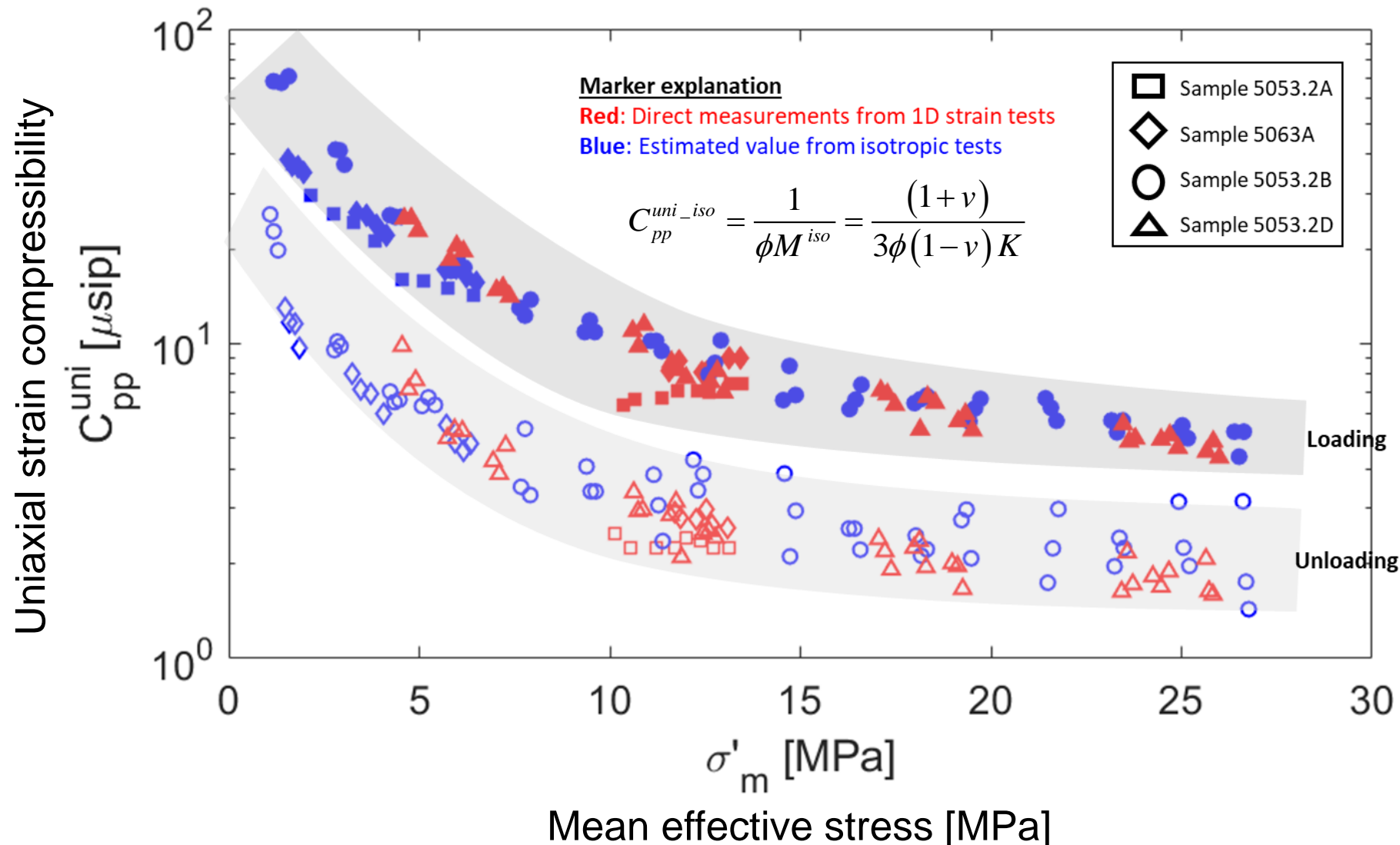


Uniaxial strain compressibility  
is about one half of isotropic  
compressibility.

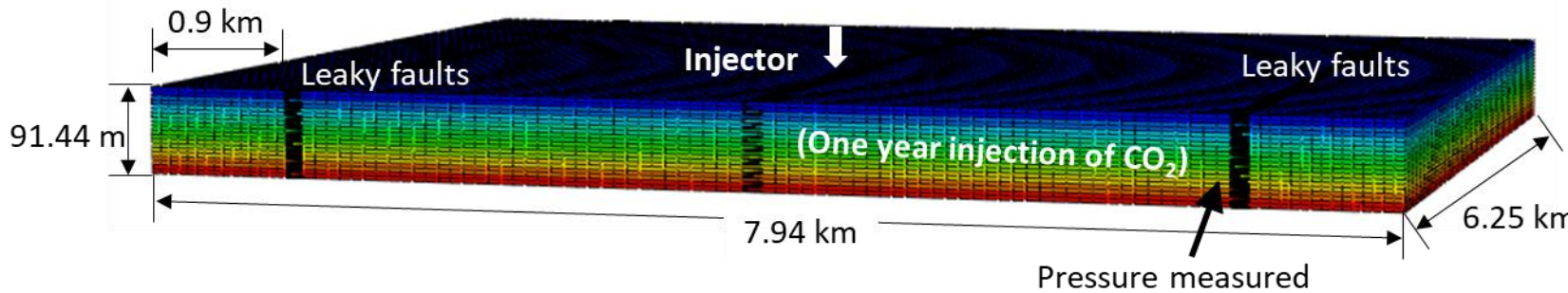


Unloading compressibility  
is about 1/3 of the loading  
compressibility.

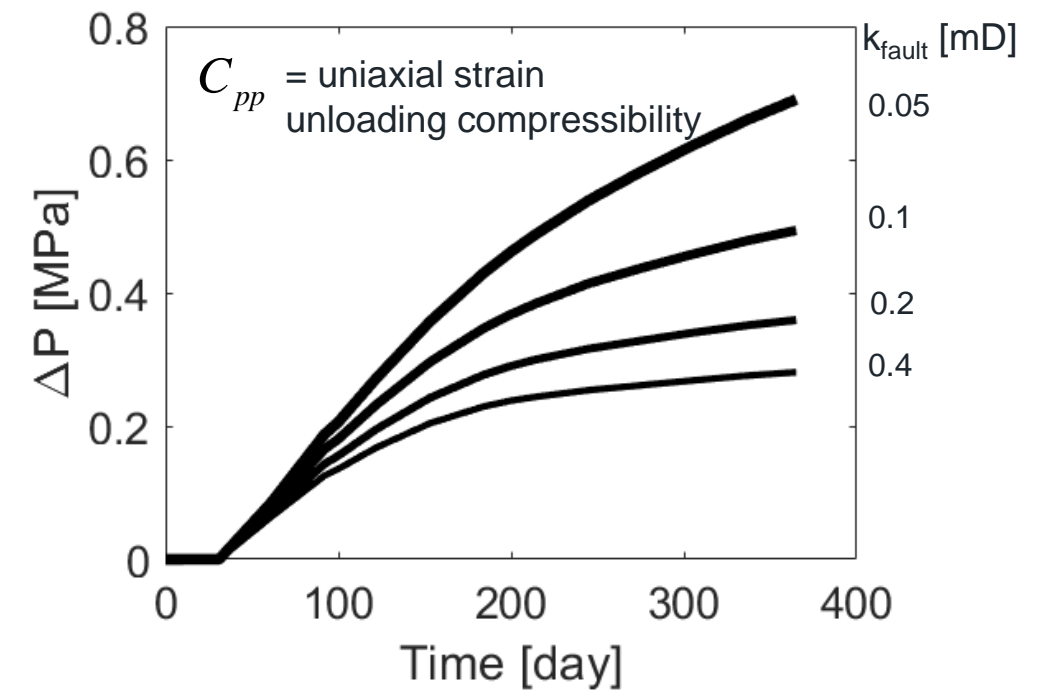
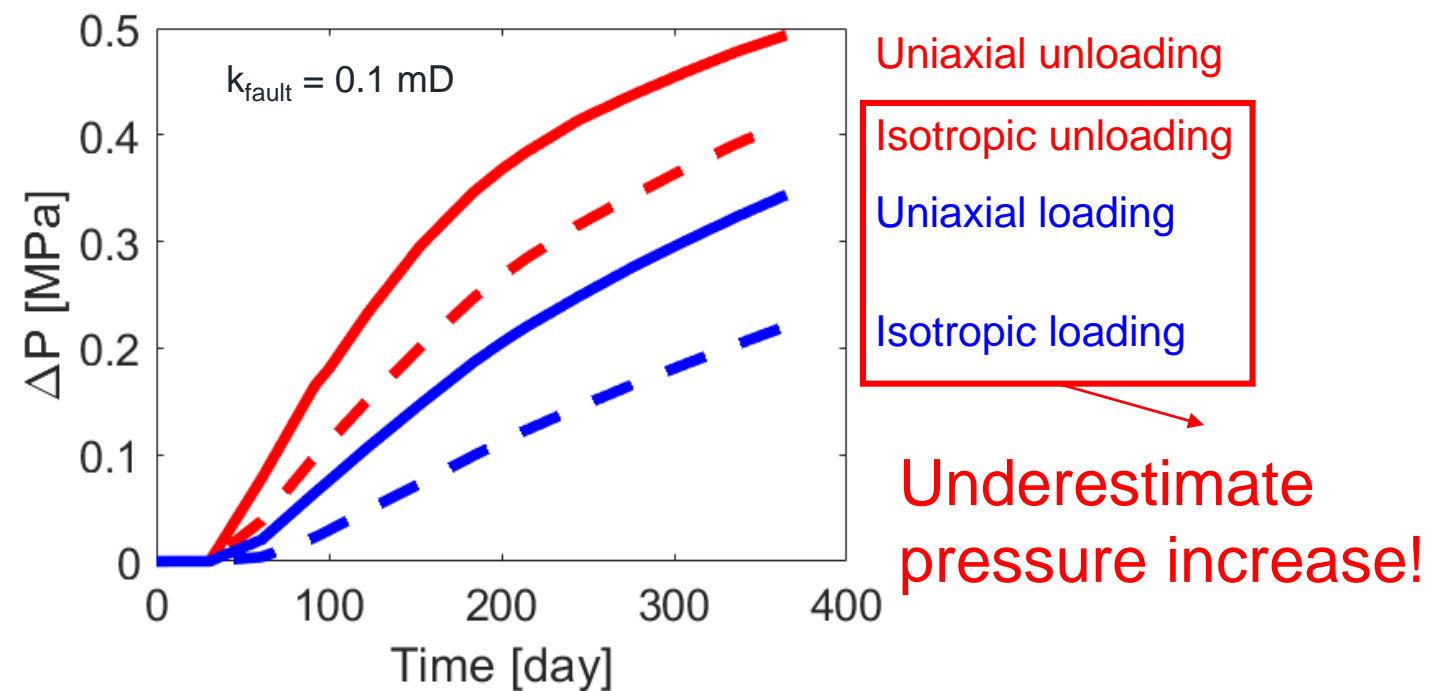
# Compressibility summary



# Reservoir simulation



- Sand porosity: 0.34
- Fault porosity: 0.1
- Sand perm: 100 mD
- Fault perm: 0.1 mD
- Injection rate: 0.9 Mt CO<sub>2</sub> / year
- Injection period: 1 year



# Summary

## Reservoir injectivity

- How to manage CO<sub>2</sub> injection pressure in the reservoir?

## Reservoir sealing capacity

- Can CO<sub>2</sub> migrate through a fault?
- What is the height of CO<sub>2</sub> column?

## Subsurface monitoring

- How to monitor subsurface leakages?

- Uniaxial strain unloading compressibility captures reservoir deformation better than traditional isotropic loading compressibility and should be used in reservoir simulation of CO<sub>2</sub> injection.
- Incorrect compressibility input for CO<sub>2</sub> storage projects may underestimate the risk of fault reactivation.

# Contents

## Reservoir injectivity

- How to manage CO<sub>2</sub> injection pressure in the reservoir?

## Reservoir sealing capacity

- How much CO<sub>2</sub> can go through a fault?
- What is the height of CO<sub>2</sub> column?

## Subsurface monitoring

- How to monitor subsurface leakages?

### Chapter 1

Measurement of Unloading Pore Volume Compressibility of Frio Sand under Uniaxial-strain Stress Path and Implications on Reservoir Pressure Management

### Chapter 2

Multiphase CO<sub>2</sub>-brine Transport Properties of Synthetic Fault Gouge

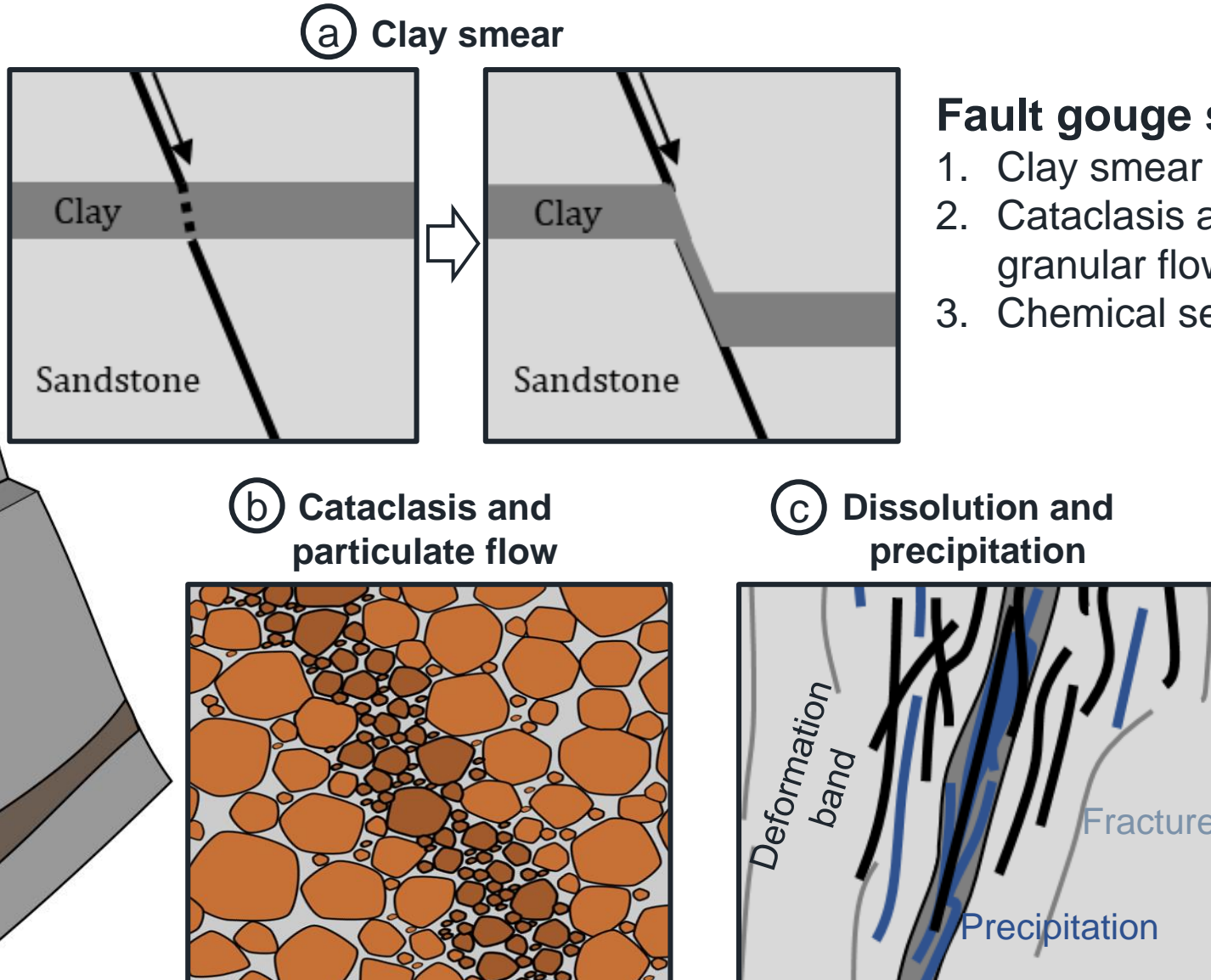
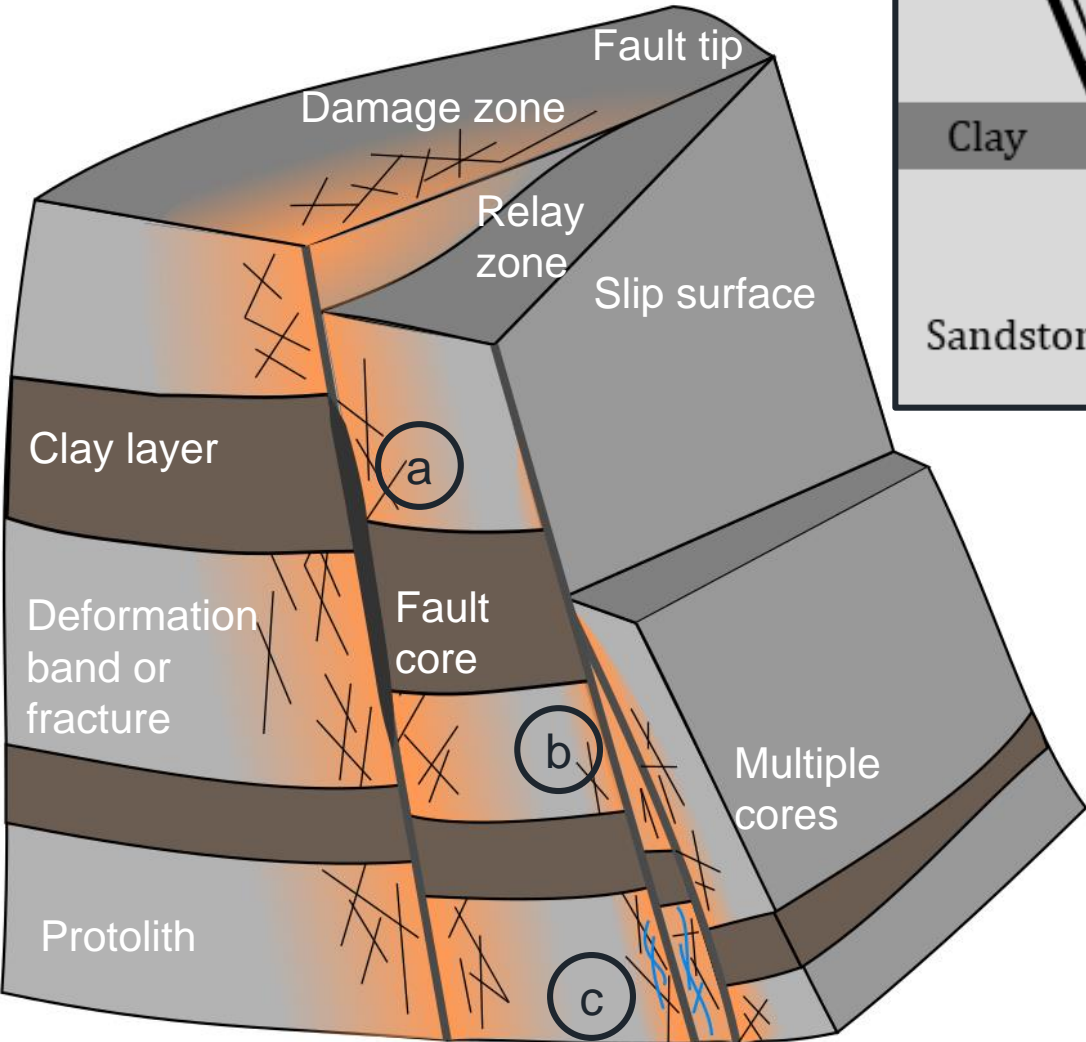
### Chapter 3

Stochastic Quantification of CO<sub>2</sub> Fault Sealing Capacity in Sand-Shale Sequences

### Chapter 4

Poroelastic Monitoring above the Injection Zone for CO<sub>2</sub> Geological Storage

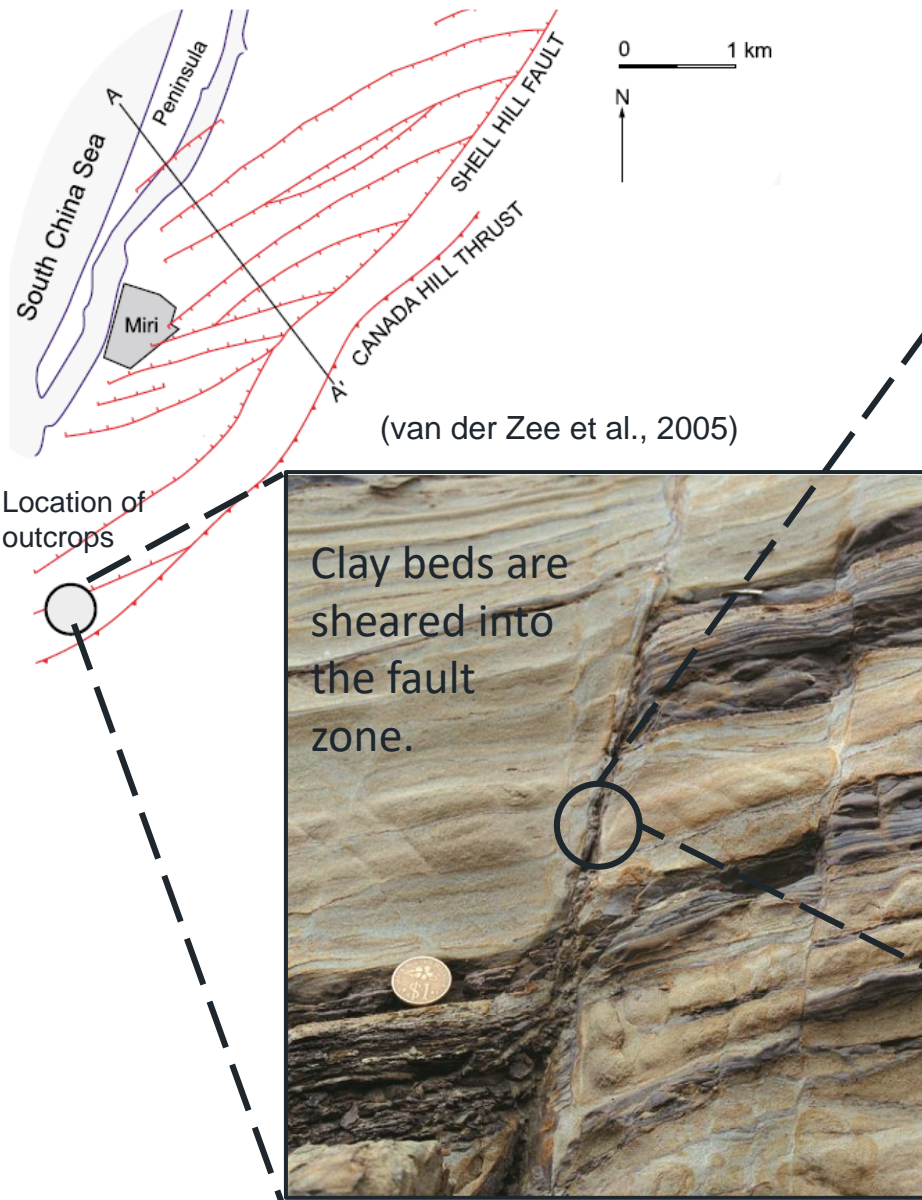
# Fault architecture and fault gouge sealing



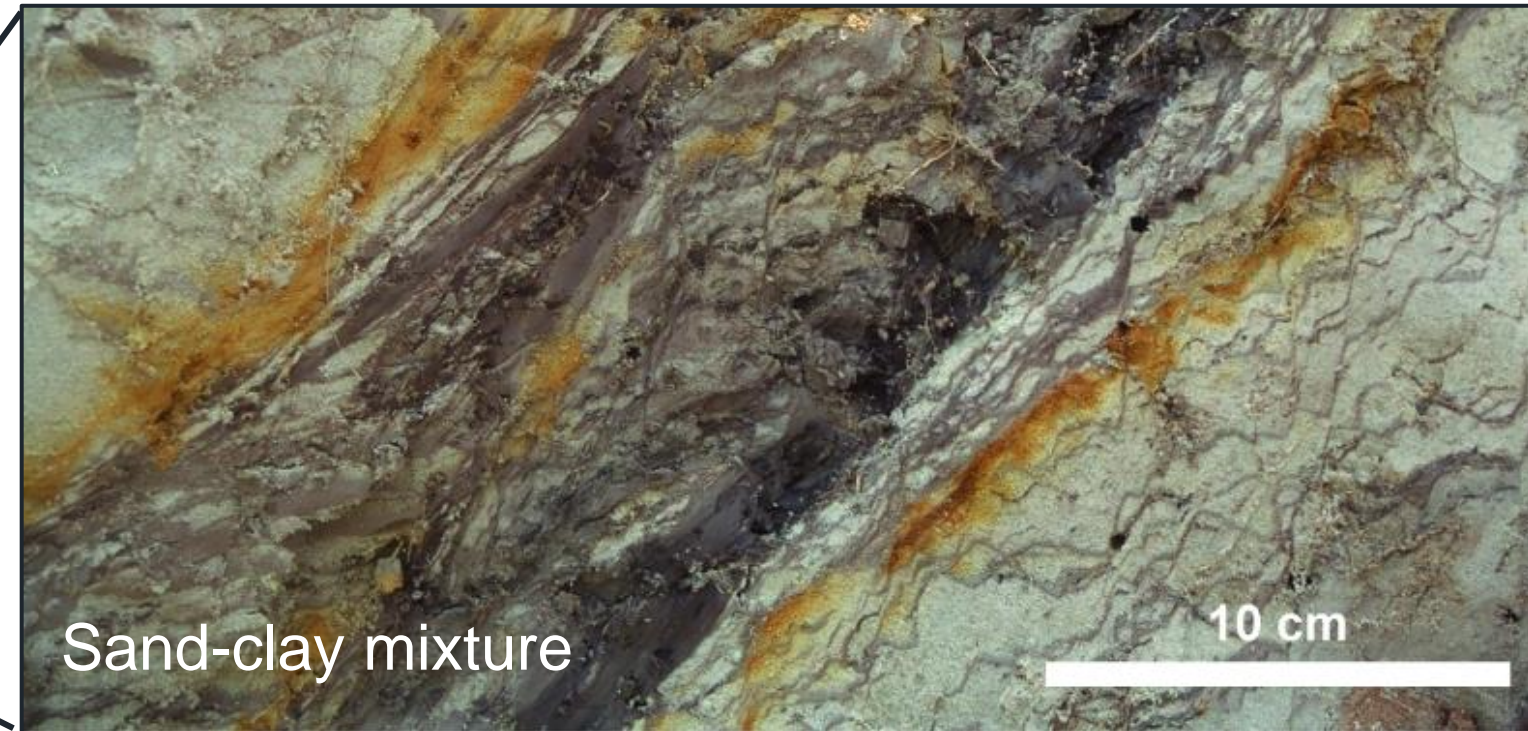
## Fault gouge sealing

1. Clay smear
2. Cataclasis and granular flow
3. Chemical sealing

# Natural fault gouge



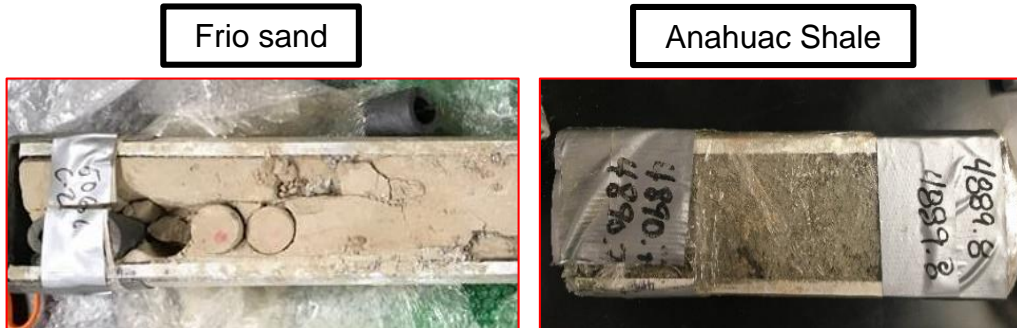
An example of clay-rich fault gouge in Miri, Malaysia



Outcrops of normal faults in layered deltaic sediments near Miri, Malaysia

# Preparation of synthetic fault gouge

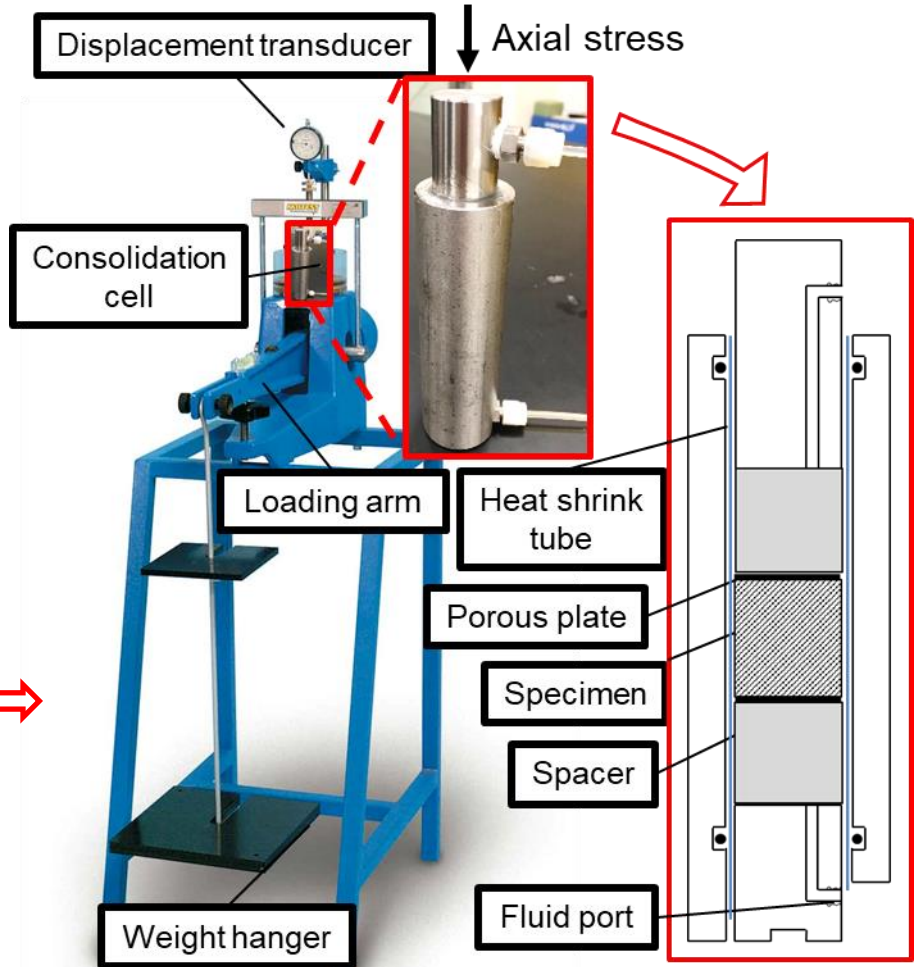
(1) Cores: GCCC-BEG



(2) Disaggregation



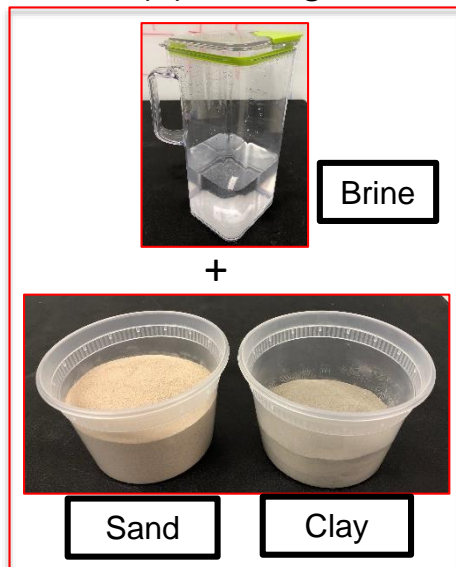
(6) Consolidation



(3) Sieving



(4) Mixing



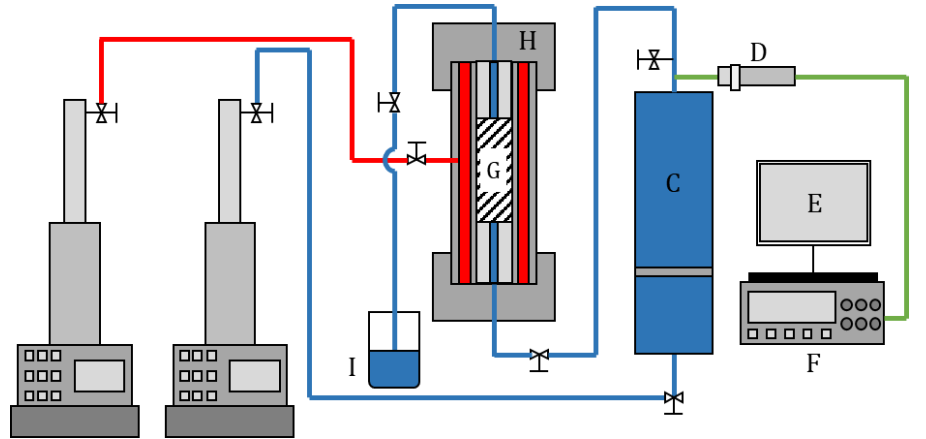
(5) Re-sedimentation



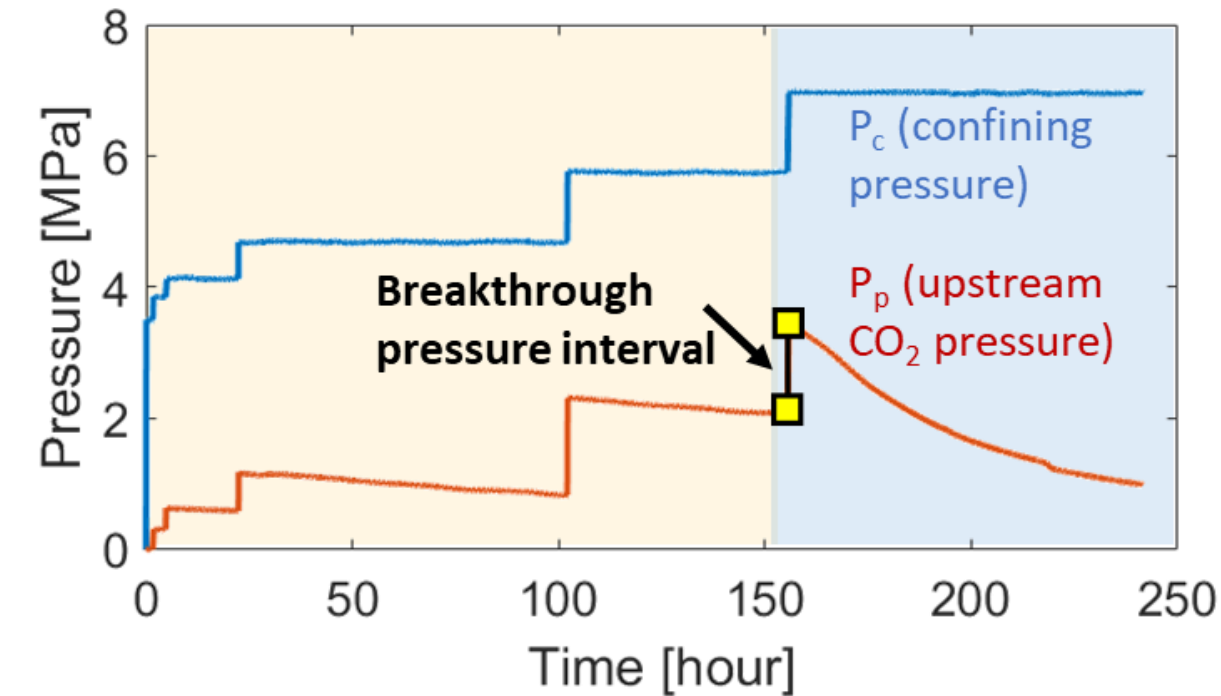
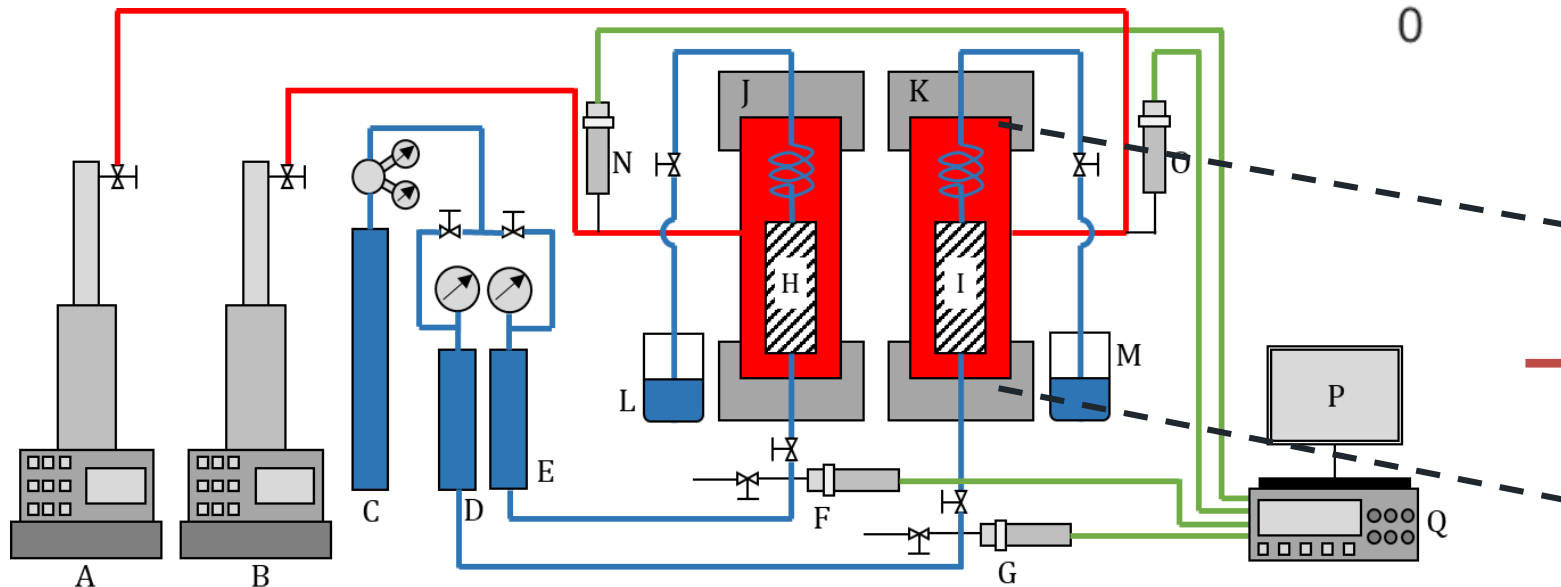
Adjusting proportion  
of sand and clay

# Experimental setup

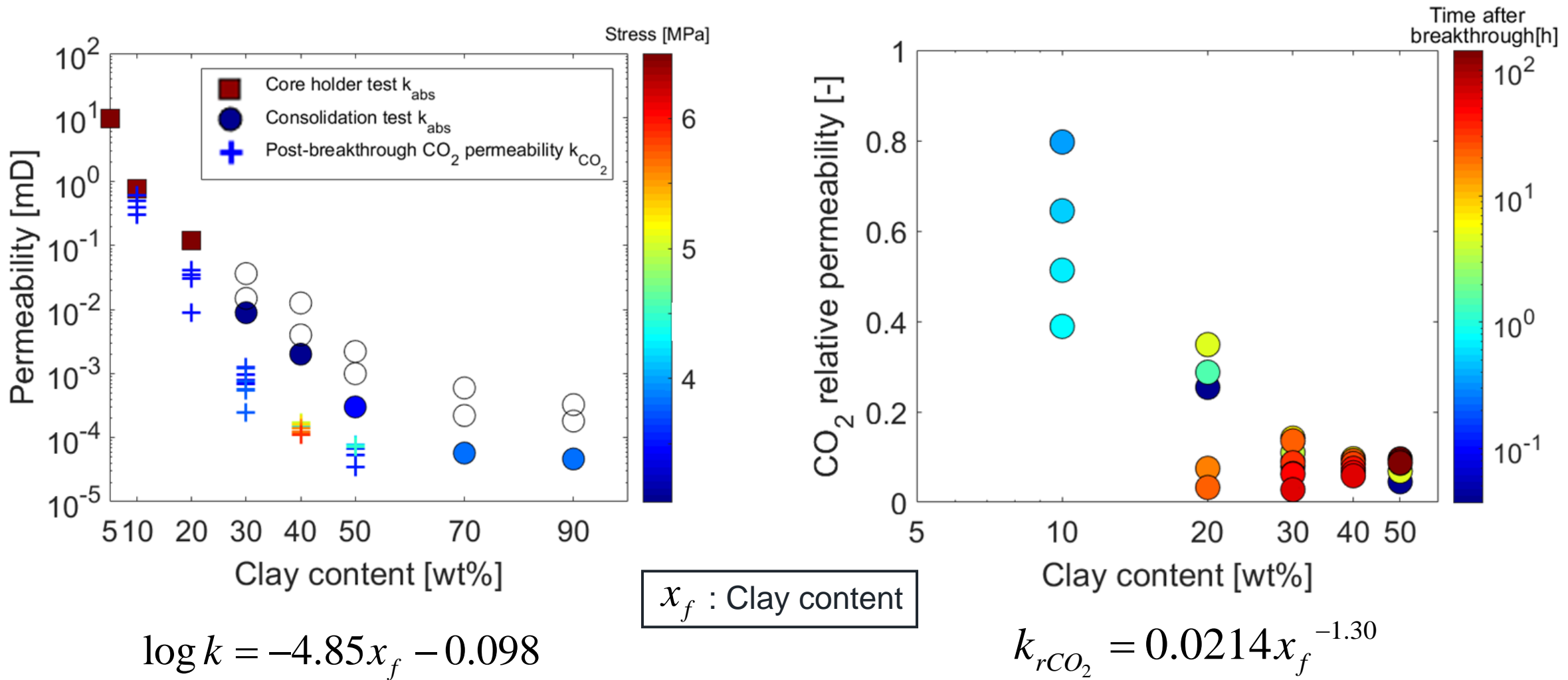
Core holder setup



$\text{CO}_2$  breakthrough pressure setup

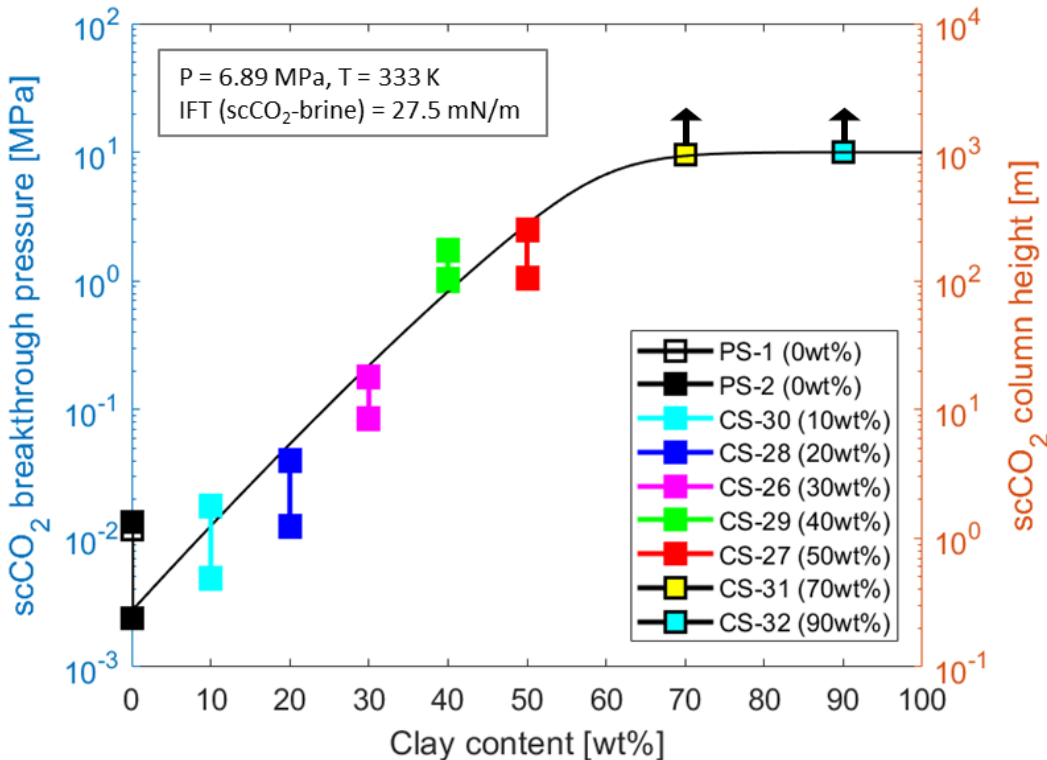


# Permeability tests

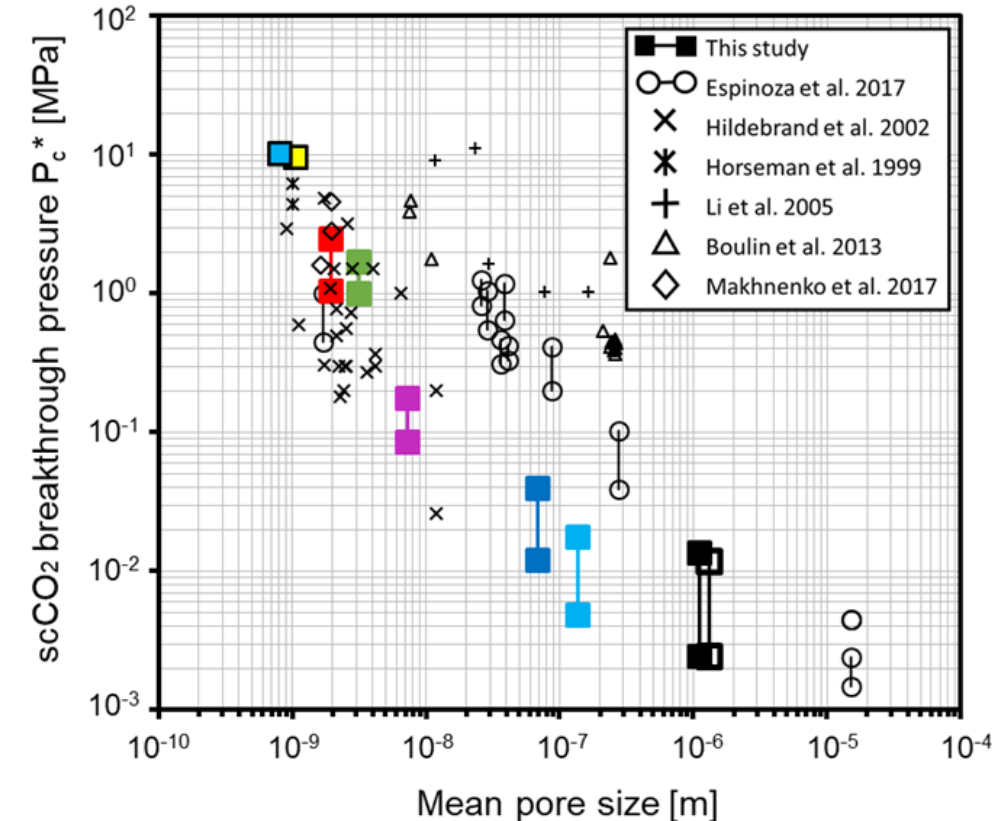


Fault gouge permeability decreases about one order of magnitude when adding 10 wt% clay.

# CO<sub>2</sub> breakthrough pressure tests

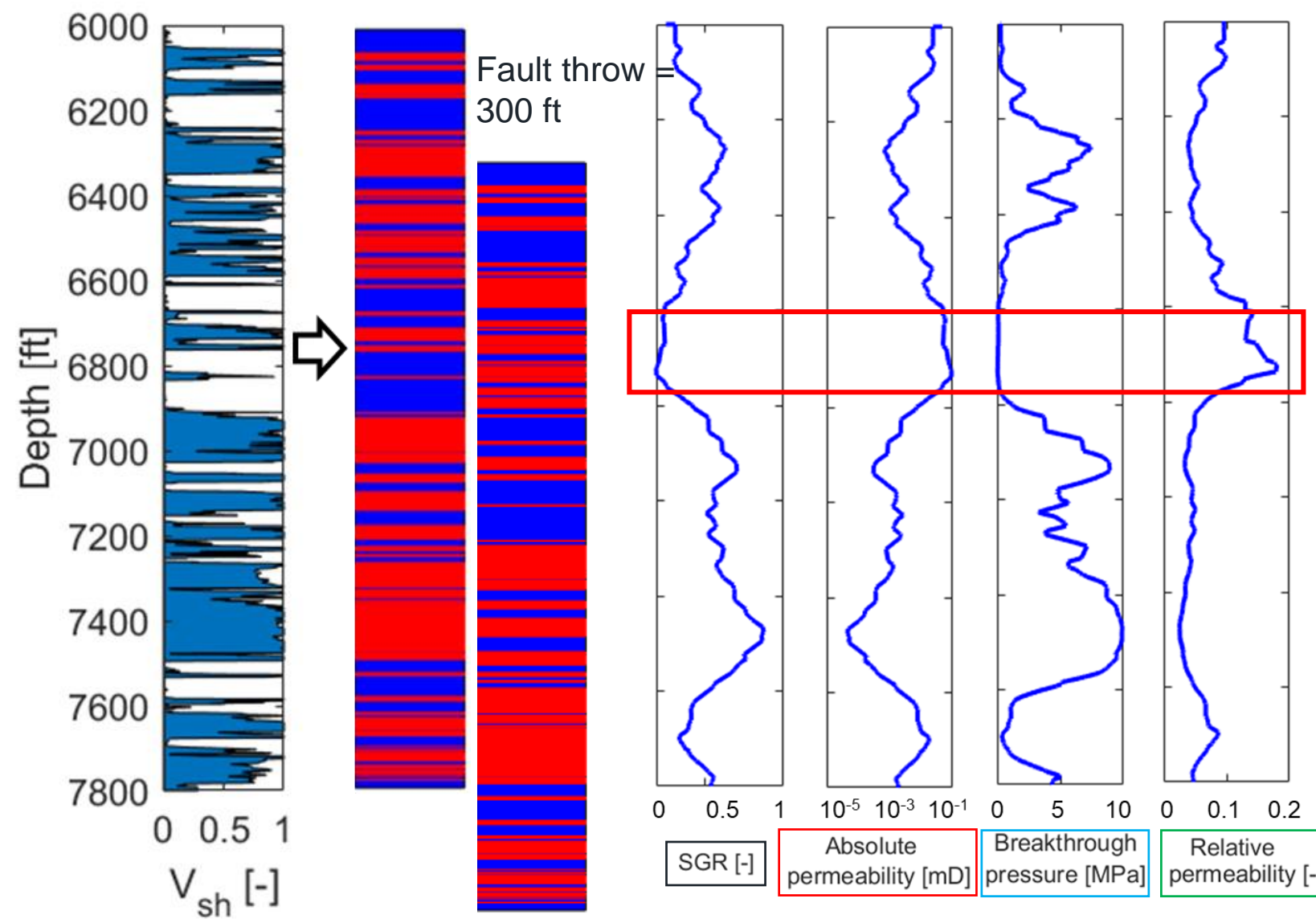


$$P_c^* = \frac{10}{1 + e^{-14.51x_f + 8.12}}$$



The breakthrough pressure increases by half order of magnitude with increments of 10 wt% clay into synthetic fault gouge.

# Applications in the High Island field



Example fault in the High Island field, representative of Gulf of Mexico Basin.

Shale gouge ratio (SGR)

$$SGR = \frac{\sum_{i=1}^n T_i \times (y_f)_i}{D} \approx x_f$$

Absolute permeability

$$\log k = -4.85x_f - 0.098$$

Breakthrough pressure

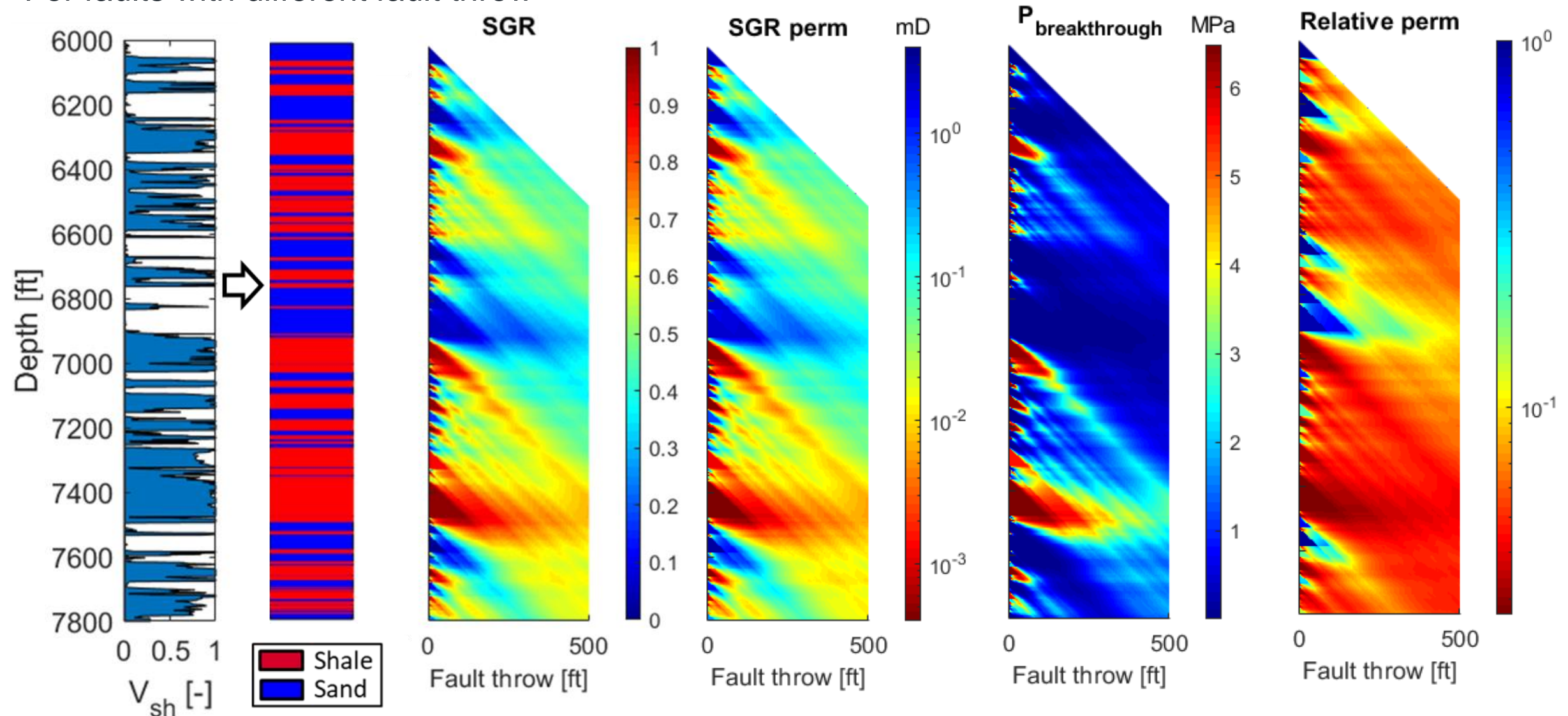
$$P_c^* = \frac{10}{1 + e^{-14.51x_f + 8.12}}$$

Relative permeability

$$k_{rCO_2} = 0.0214x_f^{-1.30}$$

# Applications in the High Island field

For faults with different fault throw



# Summary

## Reservoir injectivity

- How to manage CO<sub>2</sub> injection pressure in the reservoir?

## Reservoir sealing capacity

- Can CO<sub>2</sub> migrate through a fault?
- What is the height of CO<sub>2</sub> column?

## Subsurface monitoring

- How to monitor subsurface leakages?

- The absolute permeability of synthetic fault gouge decreases by about one order of magnitude and the CO<sub>2</sub> breakthrough pressure increases approximately by half order of magnitude with increments of 10 wt% of clay.
- The measurements on fault gouge properties help more reliable predictions on CO<sub>2</sub> migration through a fault.

# Contents

## Reservoir injectivity

- How to manage CO<sub>2</sub> injection pressure in the reservoir?

## Reservoir sealing capacity

- How much CO<sub>2</sub> can go through a fault?
- What is the height of CO<sub>2</sub> column?

## Subsurface monitoring

- How to monitor subsurface leakages?

### Chapter 1

**Measurement of Unloading Pore Volume Compressibility of Frio Sand under Uniaxial-strain Stress Path and Implications on Reservoir Pressure Management**

### Chapter 2

**Multiphase CO<sub>2</sub>-brine Transport Properties of Synthetic Fault Gouge**

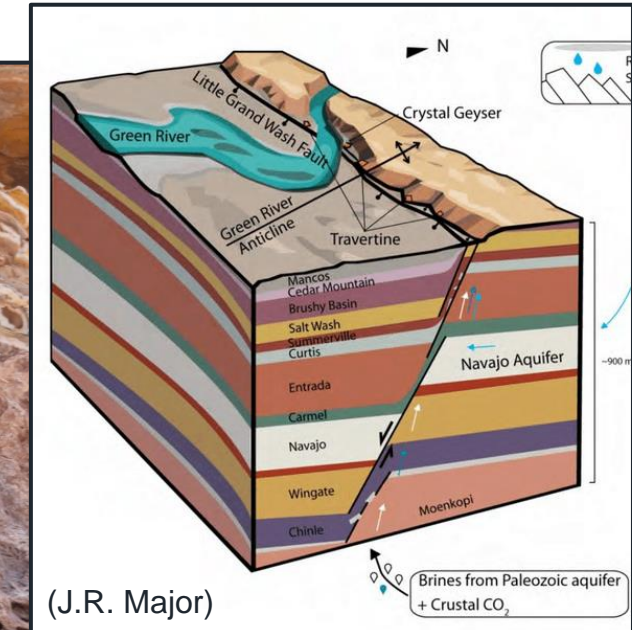
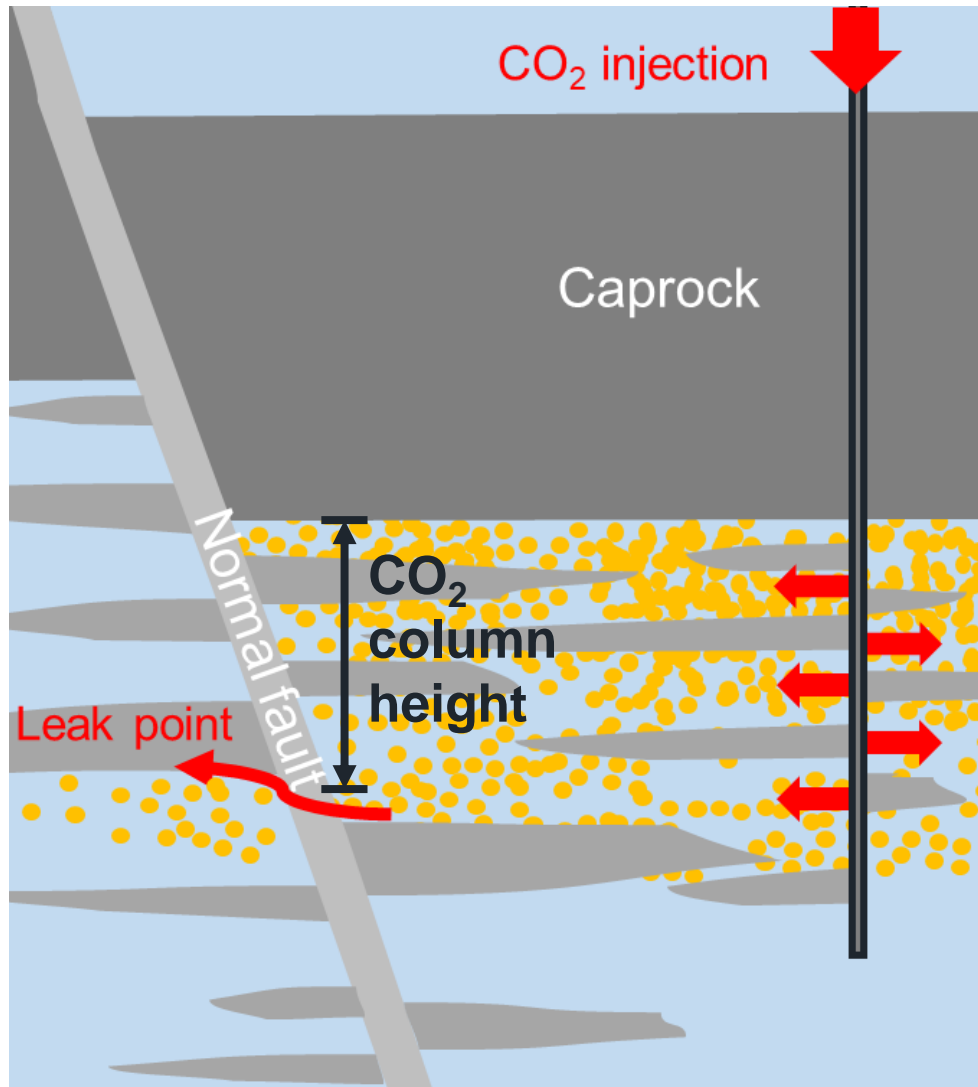
### Chapter 3

**Stochastic Quantification of CO<sub>2</sub> Fault Sealing Capacity in Sand-Shale Sequences**

### Chapter 4

**Poroelastic Monitoring above the Injection Zone for CO<sub>2</sub> Geological Storage**

# $\text{CO}_2$ column height and $\text{CO}_2$ leaks



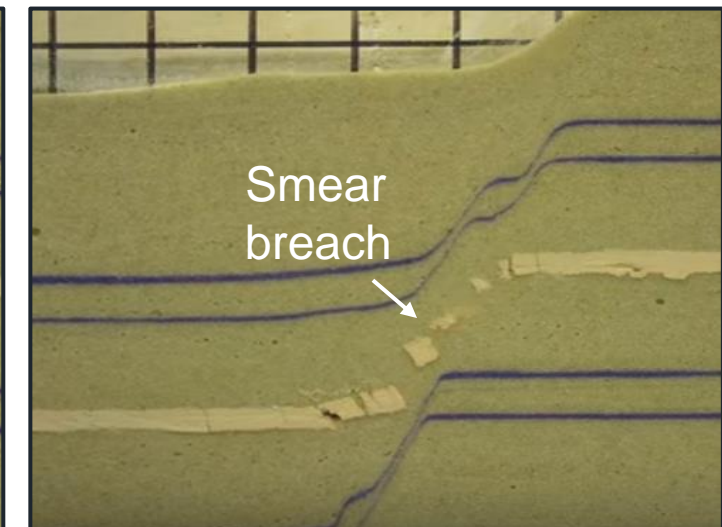
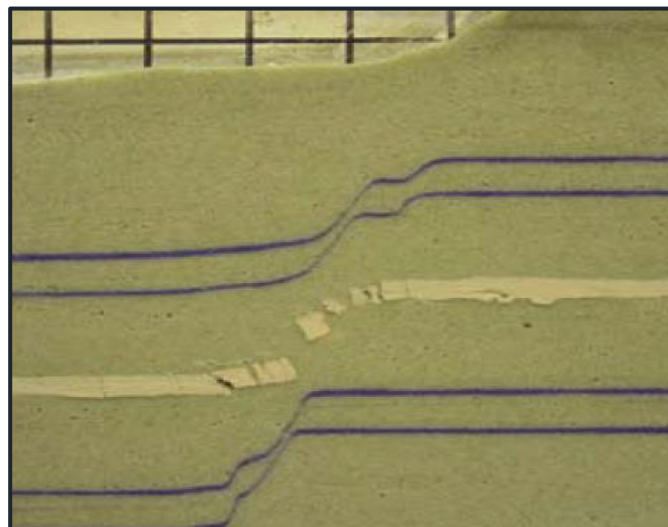
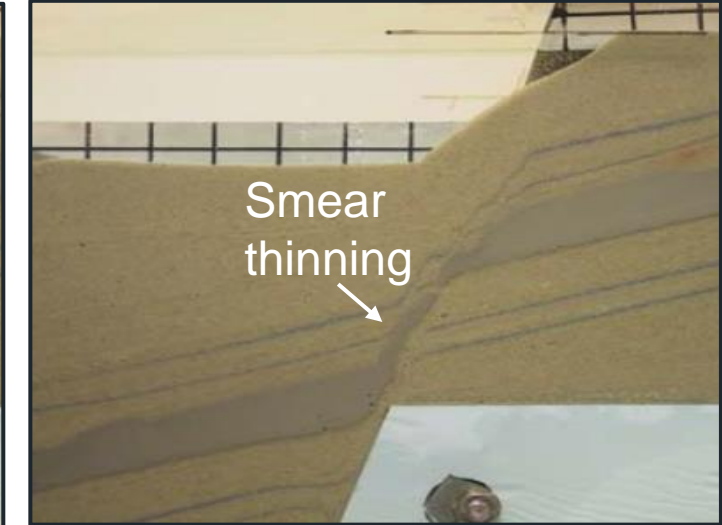
# Clay smear evolution

Homogeneous  
fault gouge

Discontinuous  
fault gouge



## Sandbox experiments



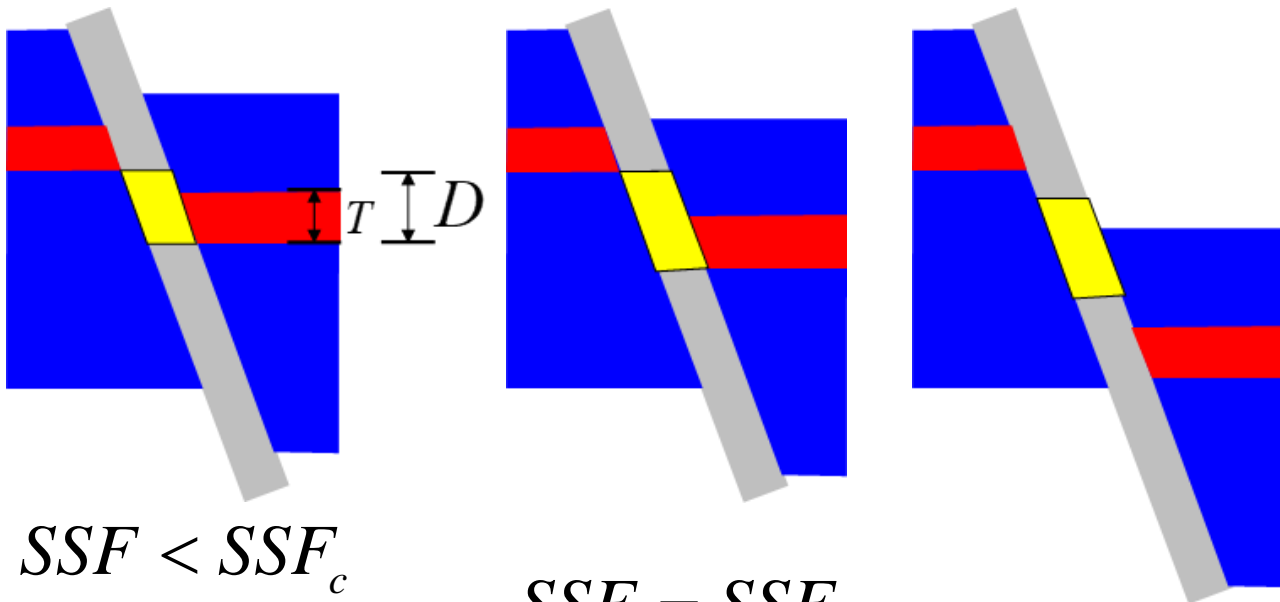
(Schmatz et al, 2010)

# Shale smear predictor

**Shale Smear Factor**  $SSF = \frac{\text{Throw}}{\text{Shale thickness}} = \frac{D}{T}$

**Probabilistic Shale Smear Factor**  $PSSF$

Increase fault throw



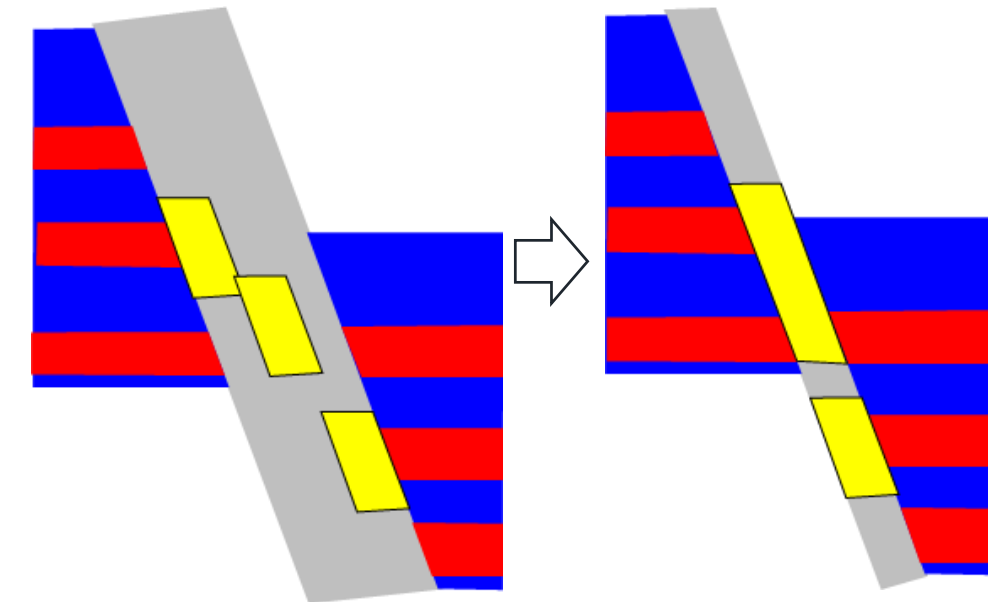
$$SSF < SSF_c$$

$$SSF = SSF_c$$

(Critical shale smear factor)

$$SSF > SSF_c$$

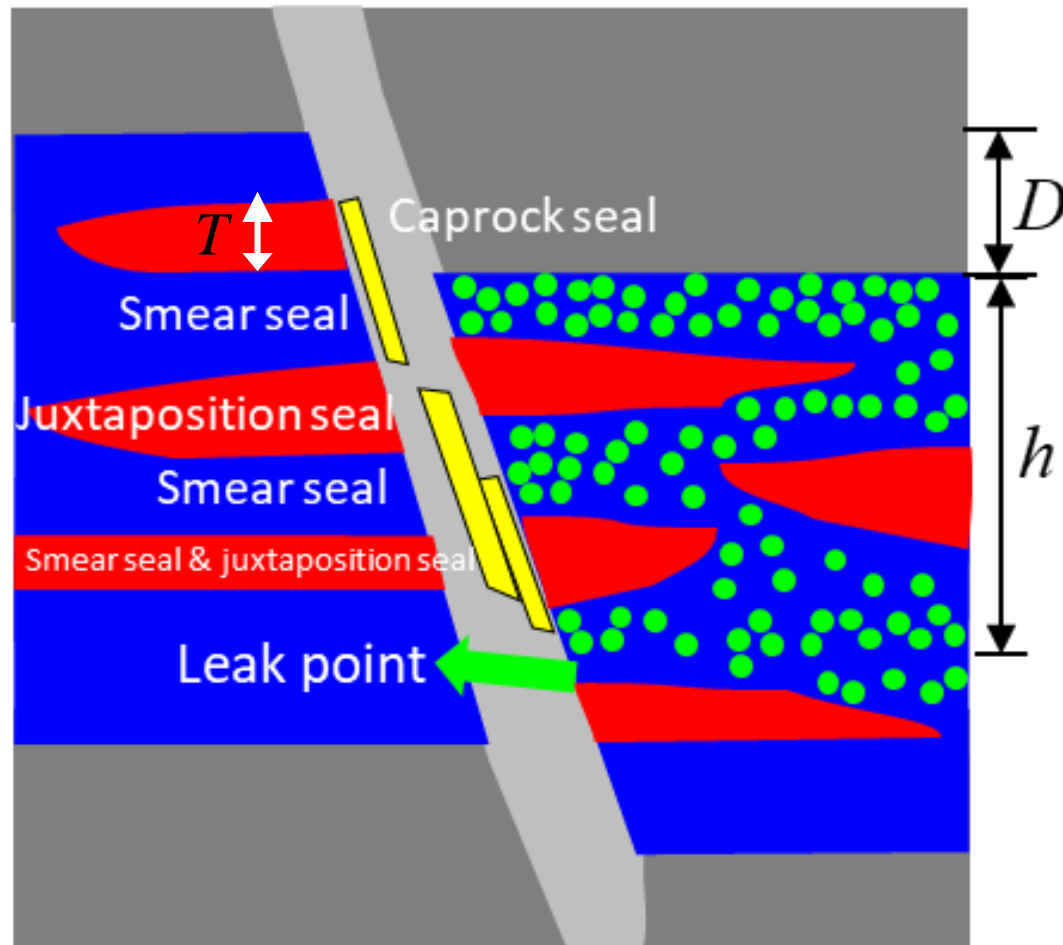
- Clay smear extension until breach
- Breached smear randomly placed in faults



(Lindsay, 1993; Childs, 2007; Yields, 2012;  
Noorsalehi-Garakani et al., 2013, 2015;  
Schmatz et al., 2010; )

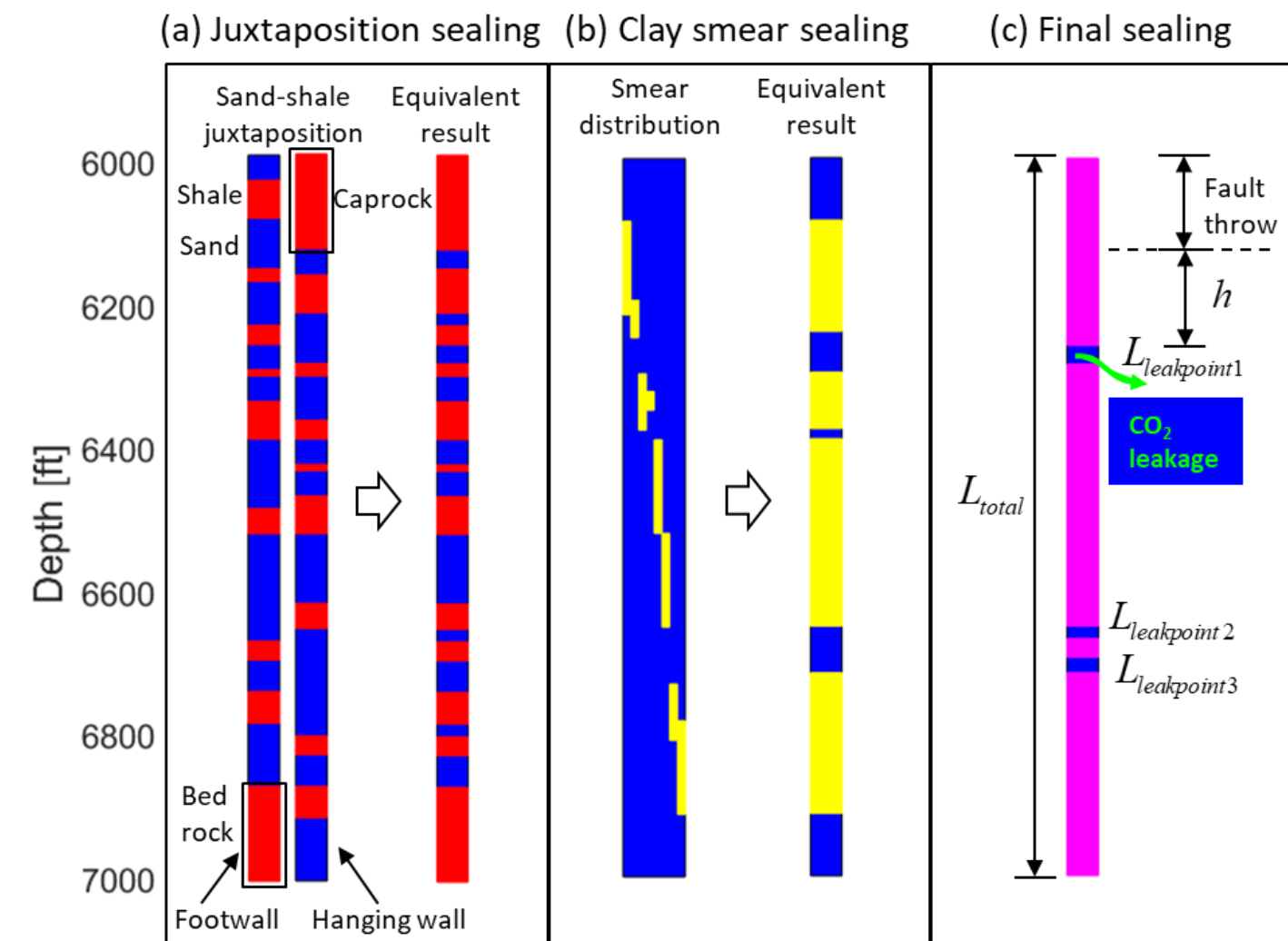
# Probabilistic Shale Smear Factor (PSSF) based predictor

## Sealing mechanisms



The sand-sand contact with no smear is the leak point.

## Workflow

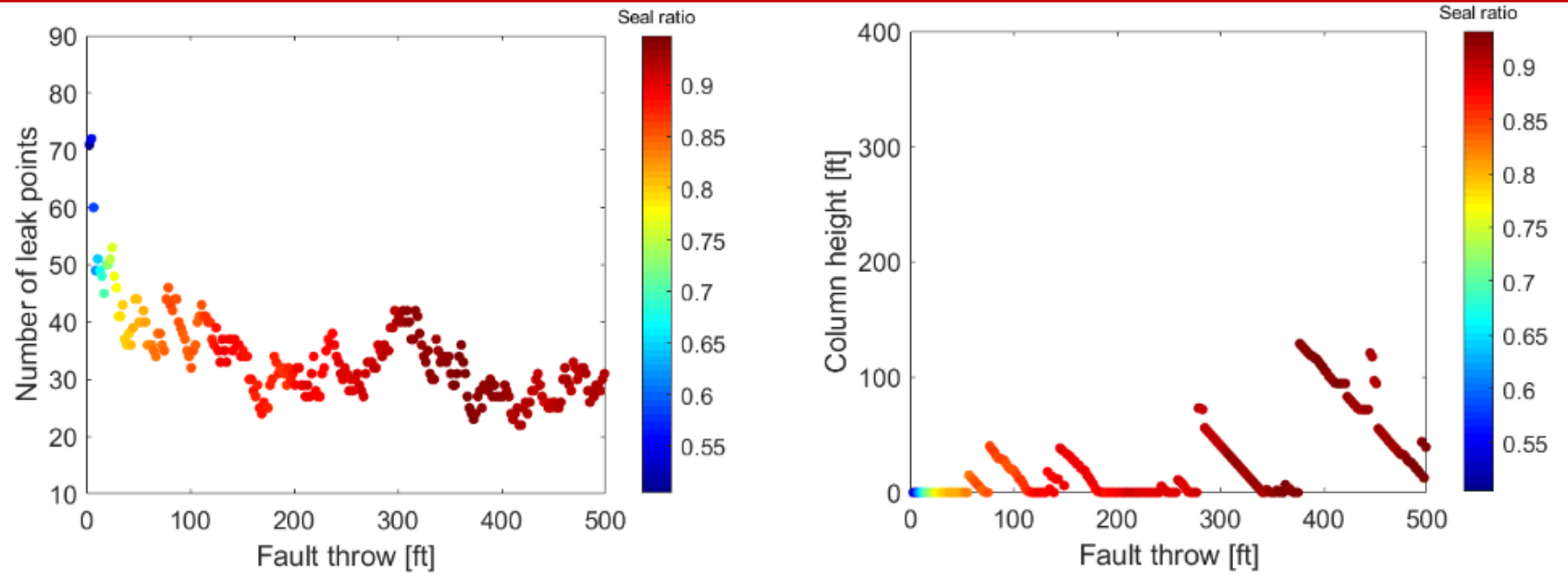


# Predicted CO<sub>2</sub> column height

- High Island field example

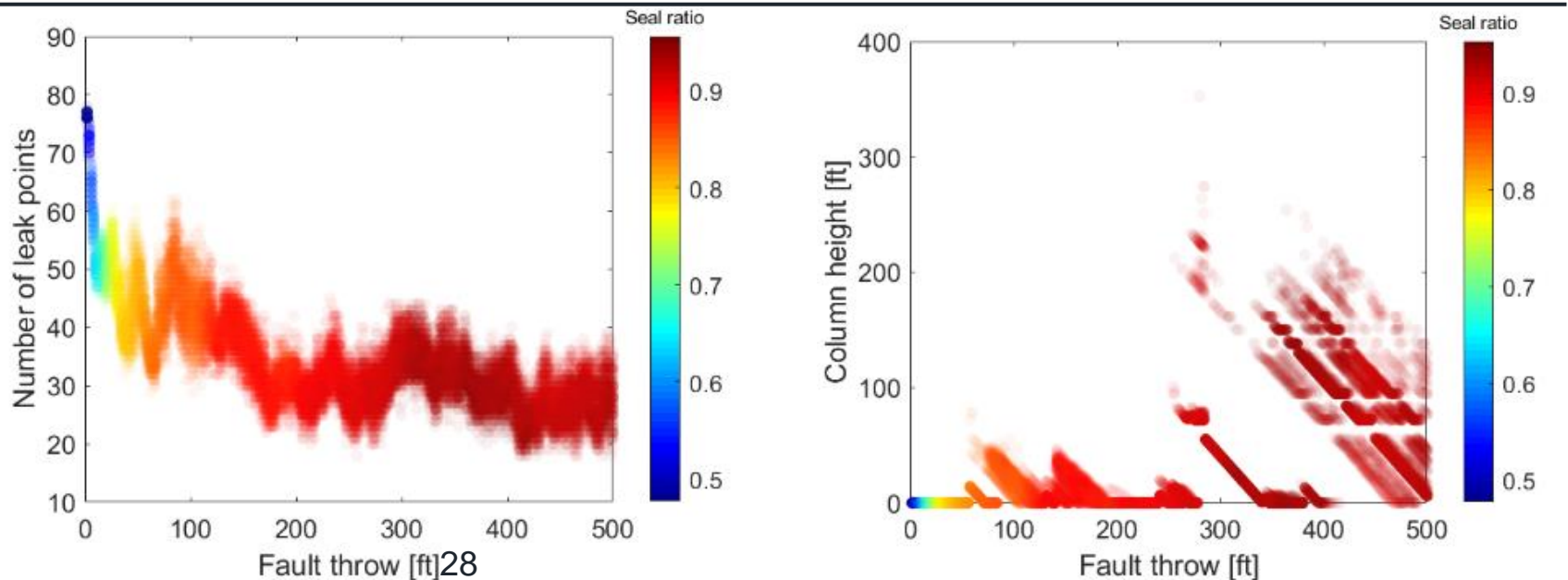
**Run one time**

$$Seal\ Ratio = \frac{L_{total} - \sum_i^N L_{gap}}{L_{total}}$$

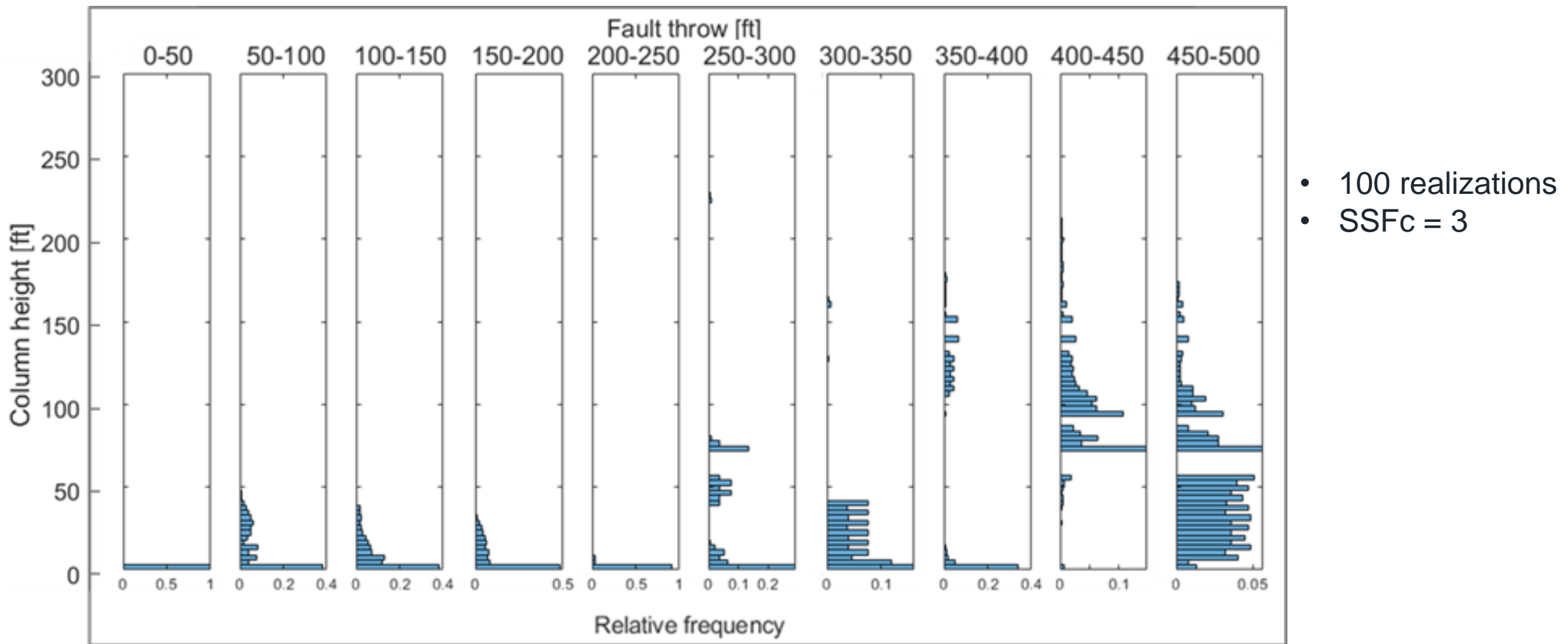


**Run 100 times**

The presence of leak points in faults leads to the large variability of the potential sealing capacity.



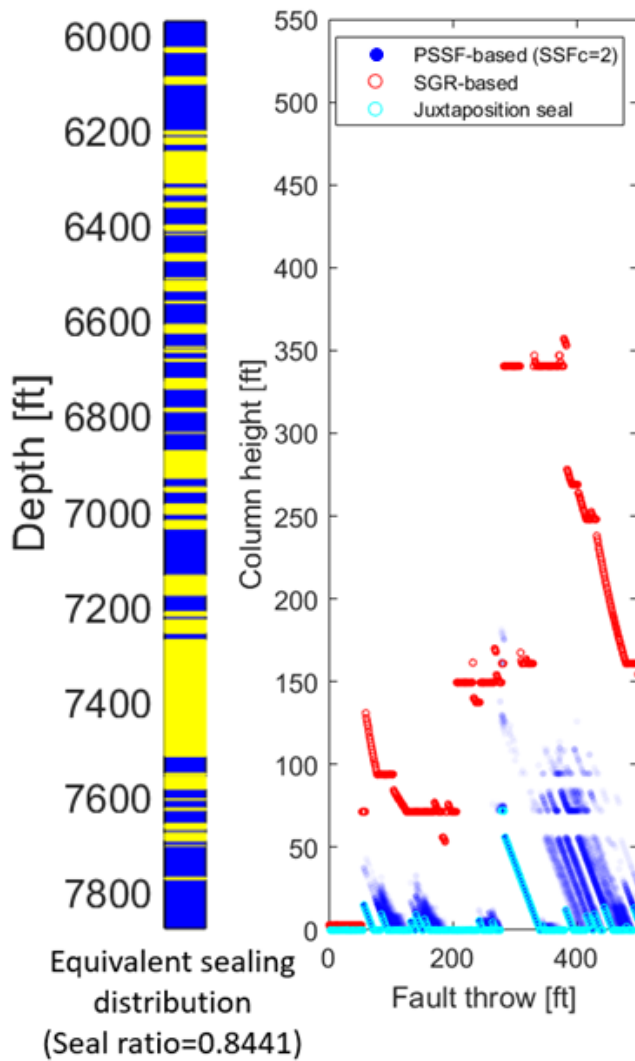
# Statistical analysis on CO<sub>2</sub> column height



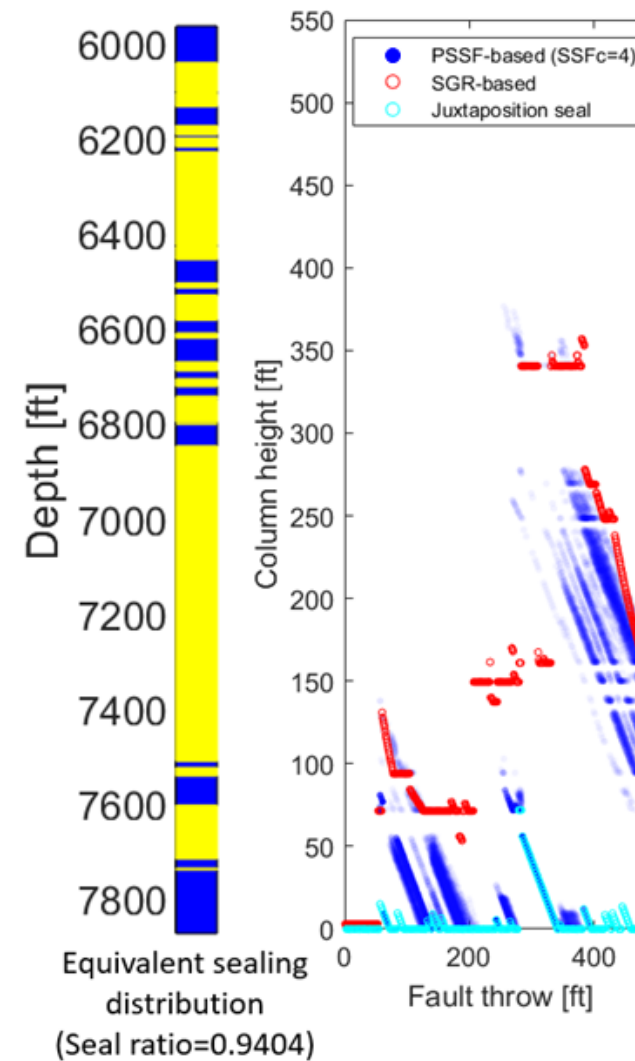
- There is no fault sealing capacity for fault throw smaller than 50 ft.
- It is very unlikely to have a CO<sub>2</sub> column higher than 200 ft in the High Island field at any fault throw.

# $\text{CO}_2$ column height prediction

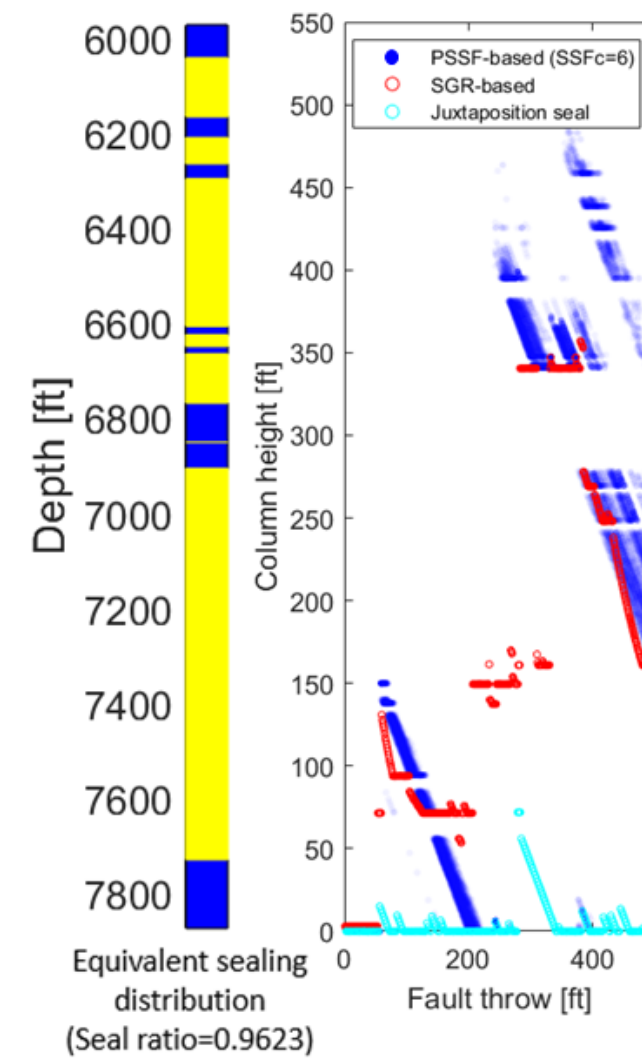
(a) Brittle case ( $\text{SSFc}=2$ )



(b) Intermediate case ( $\text{SSFc}=4$ )



(c) Ductile case ( $\text{SSFc}=6$ )



# Summary

## Reservoir injectivity

- How to manage CO<sub>2</sub> injection pressure in the reservoir?

## Reservoir sealing capacity

- Can CO<sub>2</sub> migrate through a fault?
- What is the height of CO<sub>2</sub> column?

## Subsurface monitoring

- How to monitor subsurface leakages?

- Large fault throws (>275 ft) present many smear discontinuities and therefore large variability in the potential trapped CO<sub>2</sub> column height.
- Ductile clays have the potential to produce continuous smears and result in significantly large column heights.

# Contents

## Reservoir injectivity

- How to manage CO<sub>2</sub> injection pressure in the reservoir?

## Reservoir sealing capacity

- How much CO<sub>2</sub> can go through a fault?
- What is the height of CO<sub>2</sub> column?

## Subsurface monitoring

- How to monitor subsurface leakages?

### Chapter 1

**Measurement of Unloading Pore Volume Compressibility of Frio Sand under Uniaxial-strain Stress Path and Implications on Reservoir Pressure Management**

### Chapter 2

**Multiphase CO<sub>2</sub>-brine Transport Properties of Synthetic Fault Gouge**

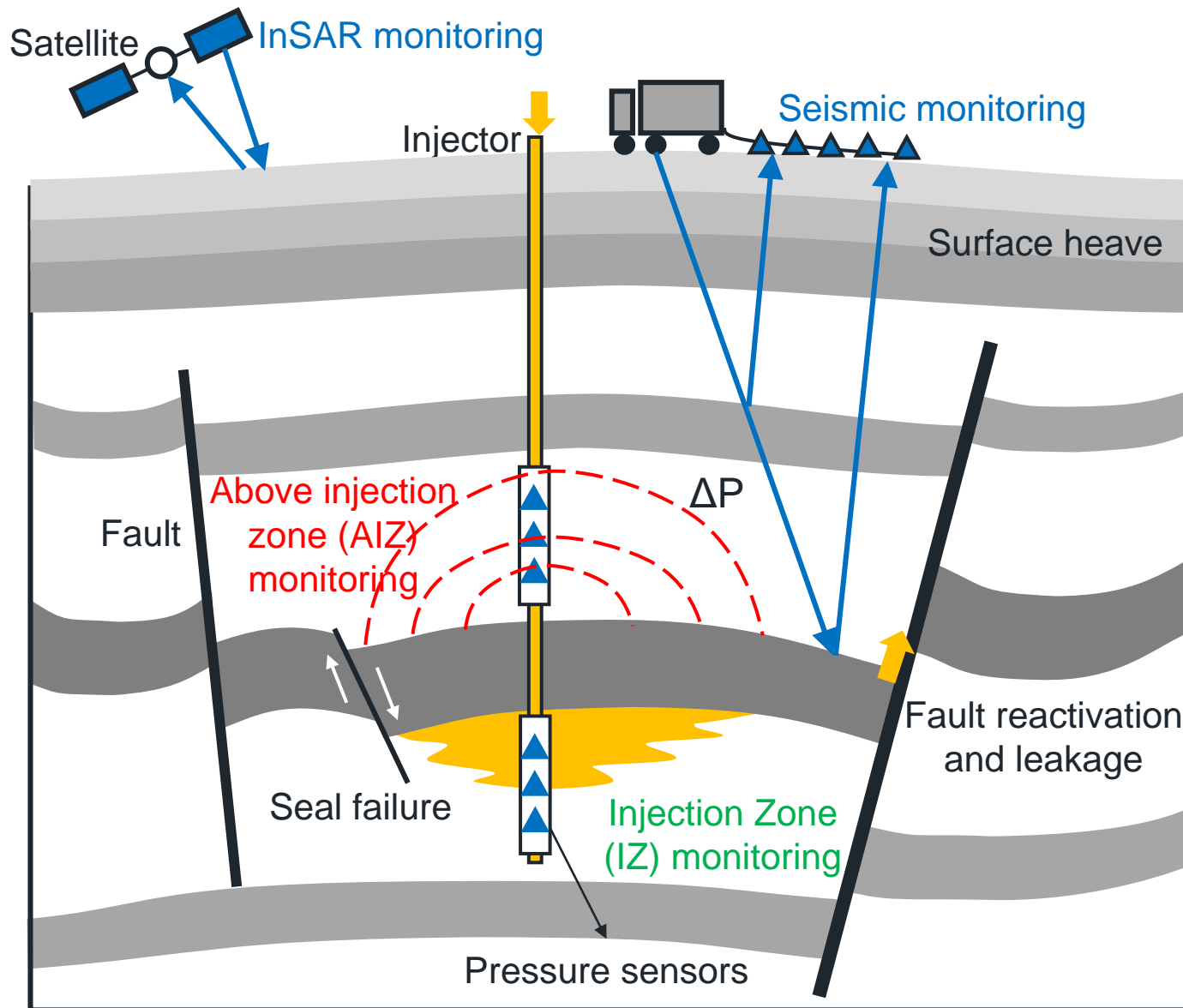
### Chapter 3

**Stochastic Quantification of CO<sub>2</sub> Fault Sealing Capacity in Sand-Shale Sequences**

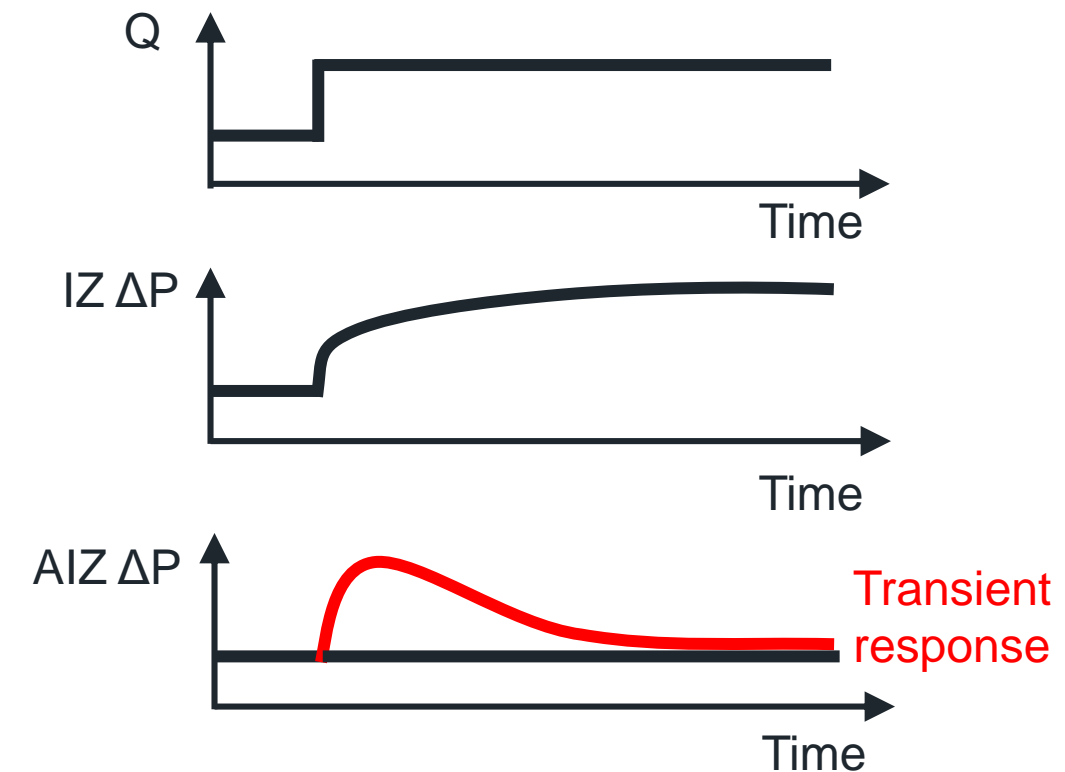
### Chapter 4

**Poroelastic Monitoring above the Injection Zone for CO<sub>2</sub> Geological Storage**

# Monitoring above the injection zone

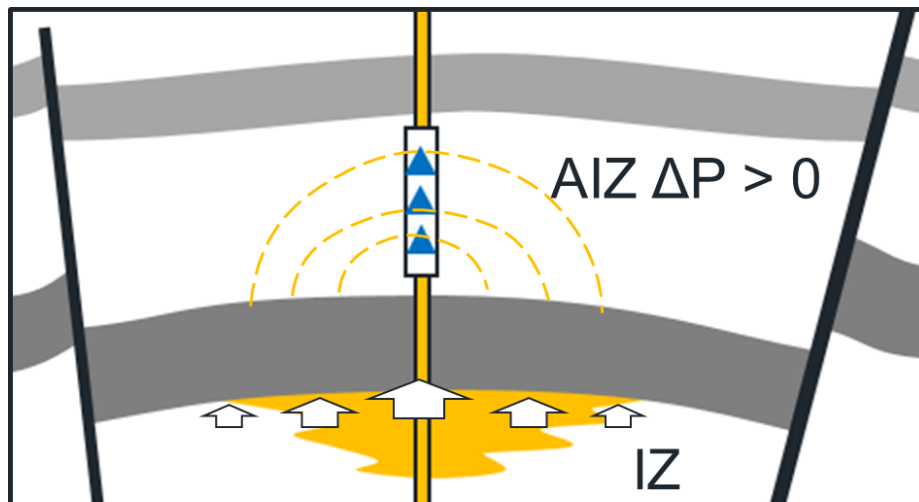


- On surface monitoring
- Monitoring in the injection zone (IZ)
- Monitoring above the injection zone (AIZ)



# Pore pressure change due to undrained loading

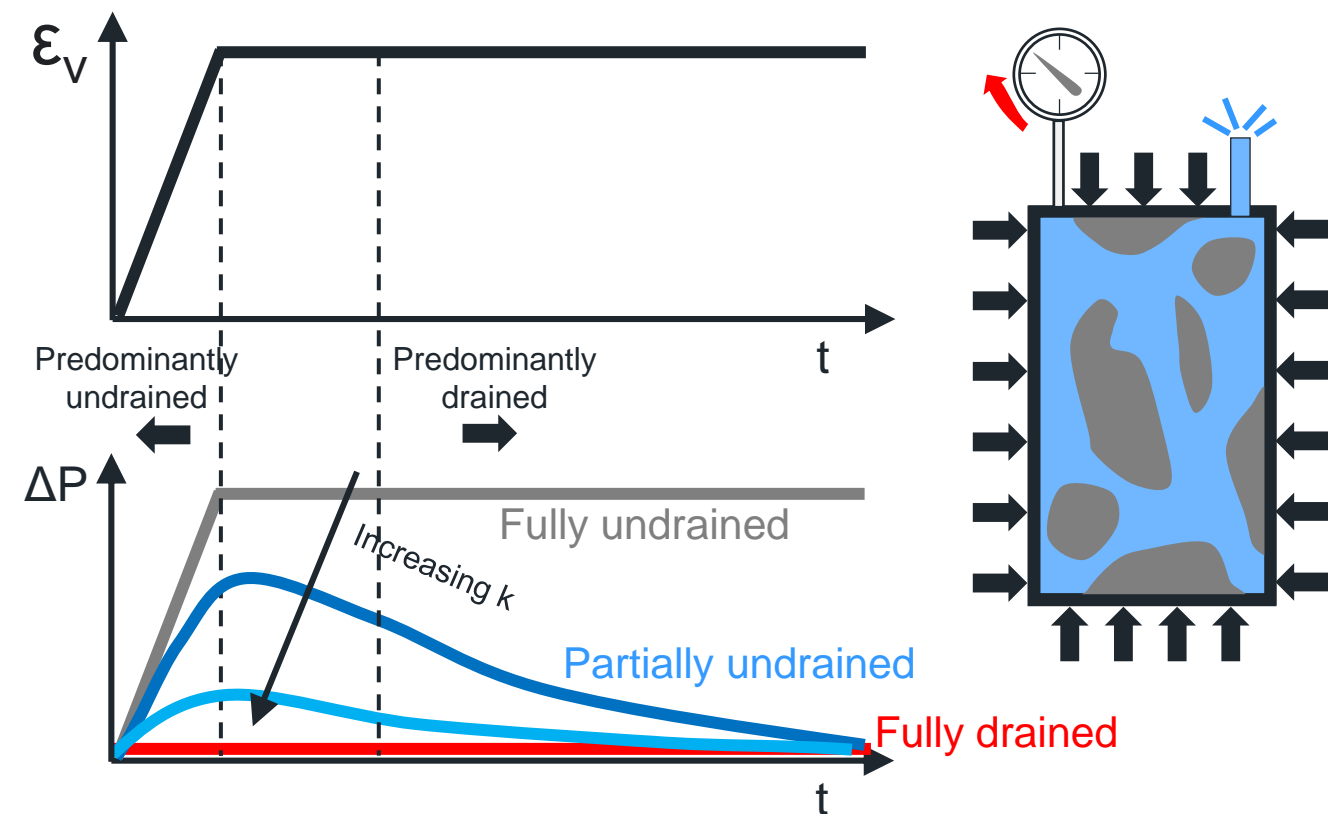
Pore pressure increase due to undrained loading during CO<sub>2</sub> injection (Kim & Hosseini, 2014)



For a linear elastic isotropic porous solid, a change of volumetric strain under undrained loading imparts a change of pore pressure equal to (Coussy, 2004)

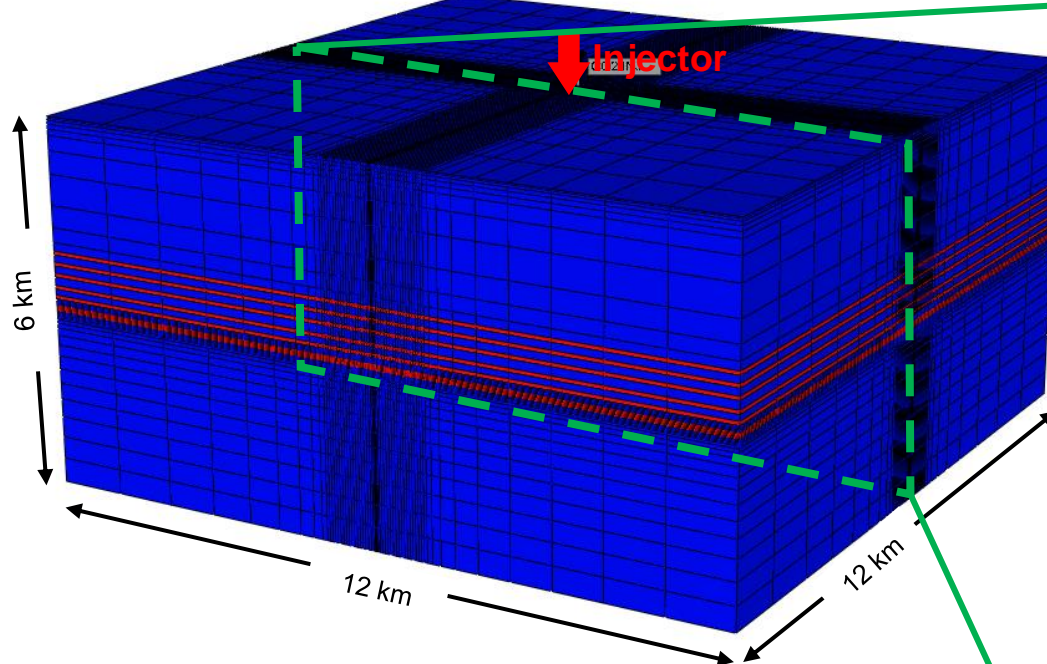
$$\Delta P = - \left( \frac{\phi_0}{K_f} + \frac{b - \phi_0}{K_m} \right)^{-1} b \Delta \varepsilon_V$$

Drained, undrained, and partially undrained conditions

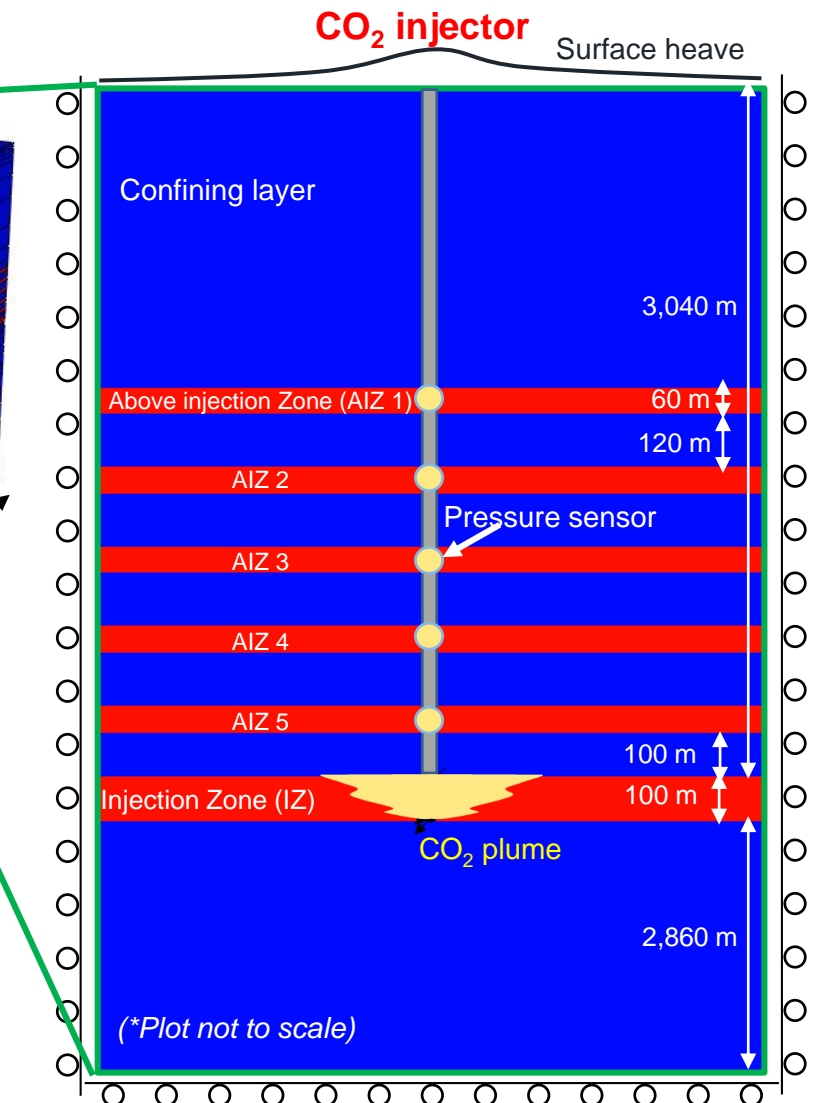


# Reservoir model

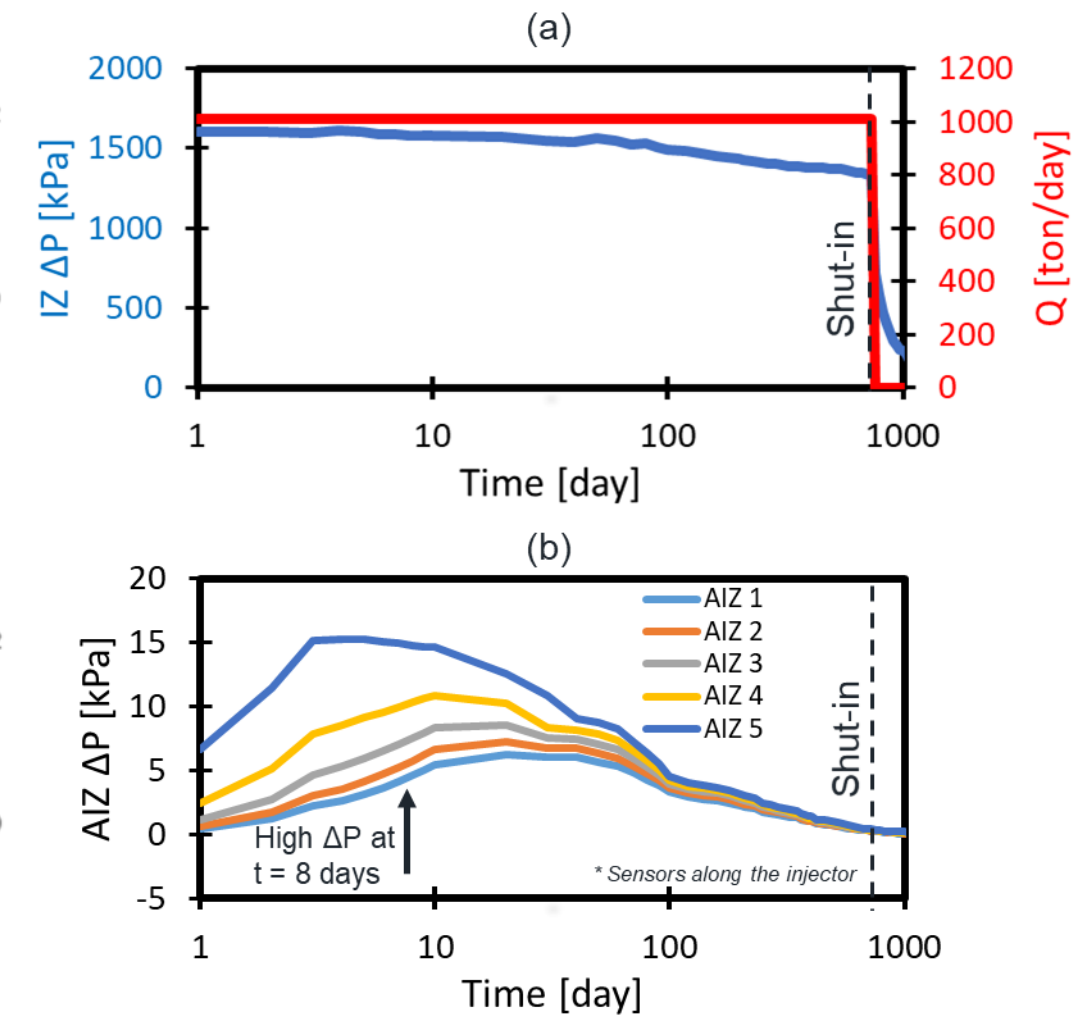
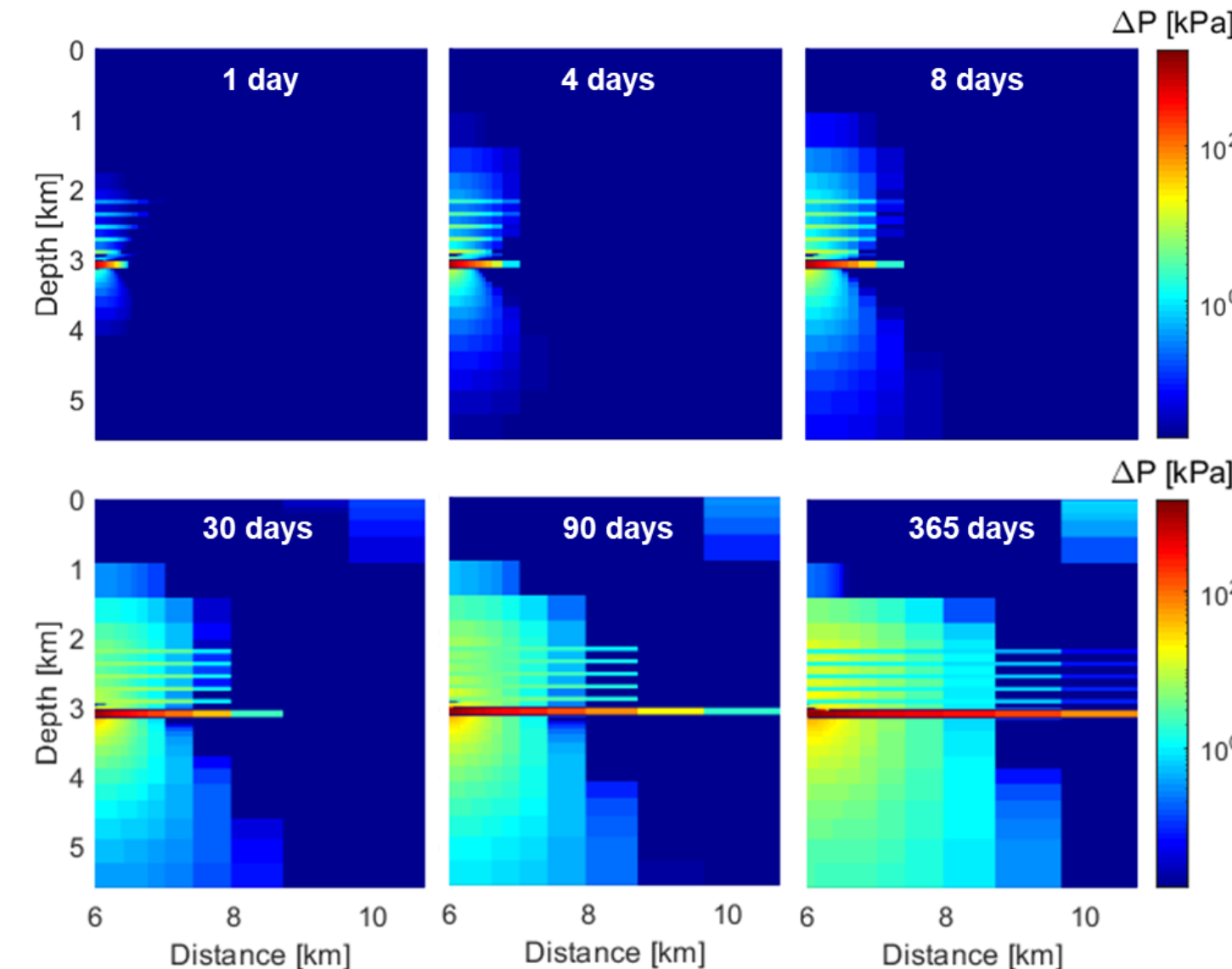
- Two years injection + one year shut-in
- Injection rate: 1008 tons/day (0.37 Mt/year)



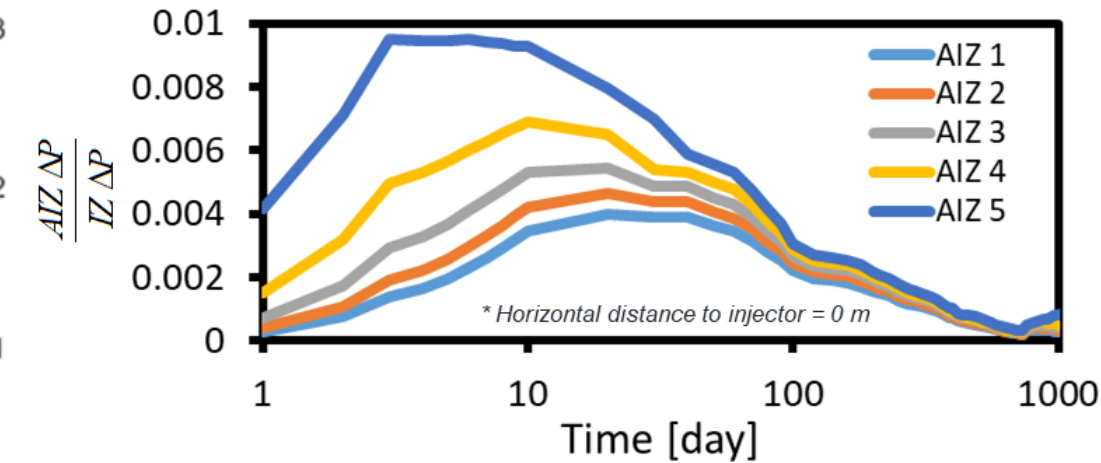
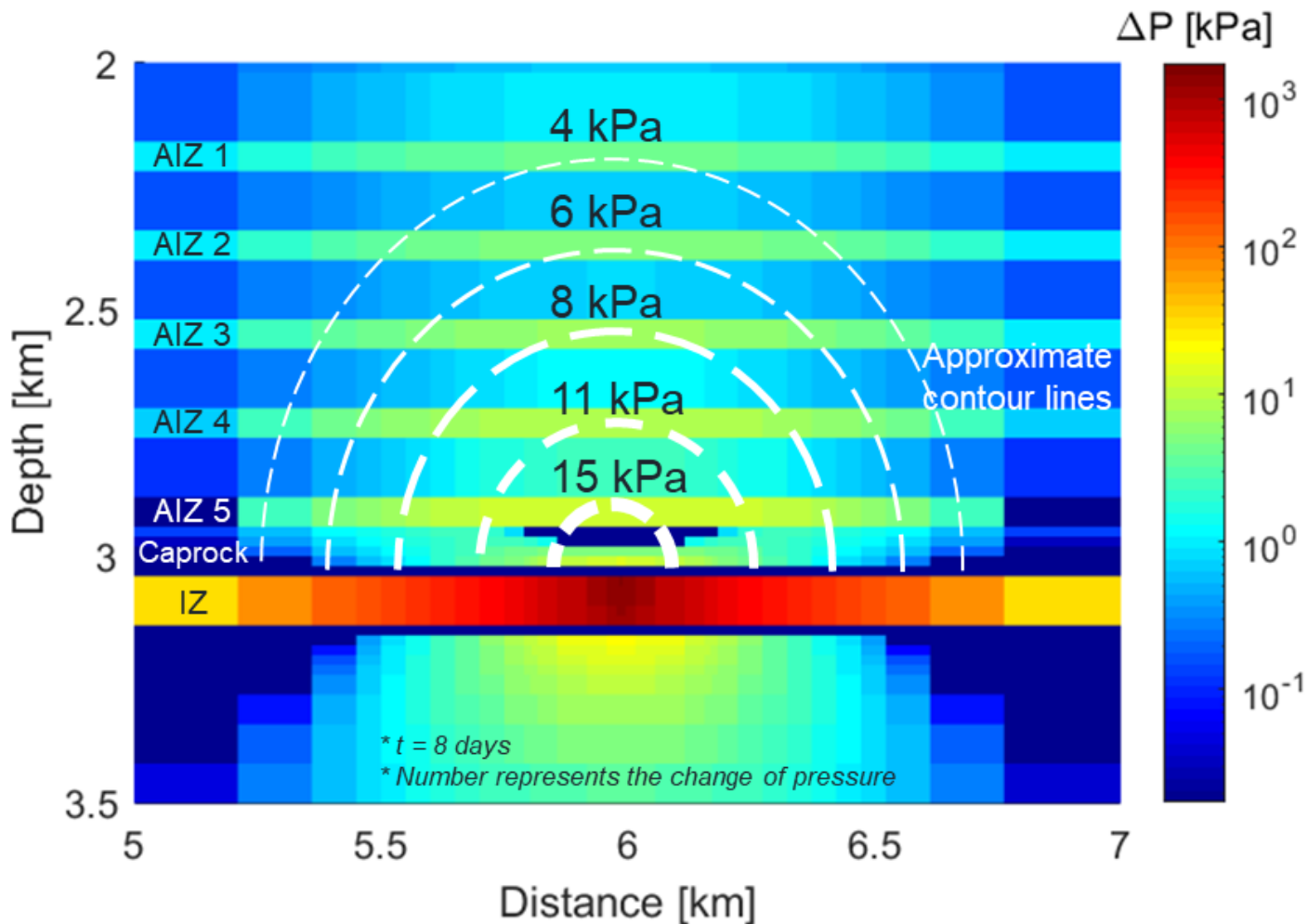
Property	Symbol	IZ/AIZ (Sand)	Caprock (Shale)
Initial porosity [-]	$\phi$	0.22	0.1
Permeability [mD]	$k$	300	0.0001
Young's modulus [GPa]	$E$	5	20
Poisson's ratio [-]	$\nu$	0.2	0.3
Bulk modulus of brine [GPa]	$K_f$	2.2	
Bulk modulus of rock matrix [GPa]	$K_m$	36	



# Pressure changes with time



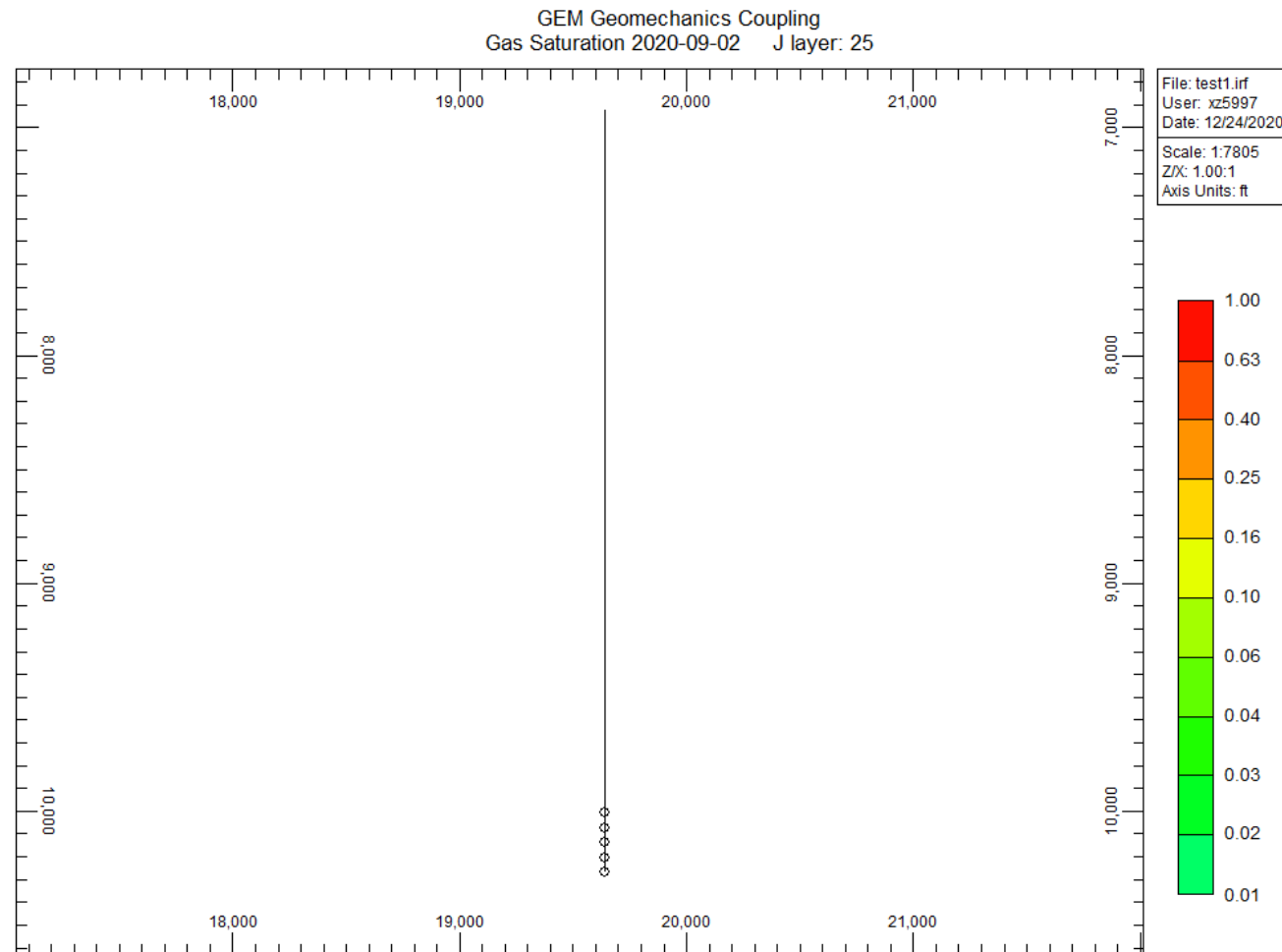
# Pressure front and the magnitude of AlZ $\Delta P$



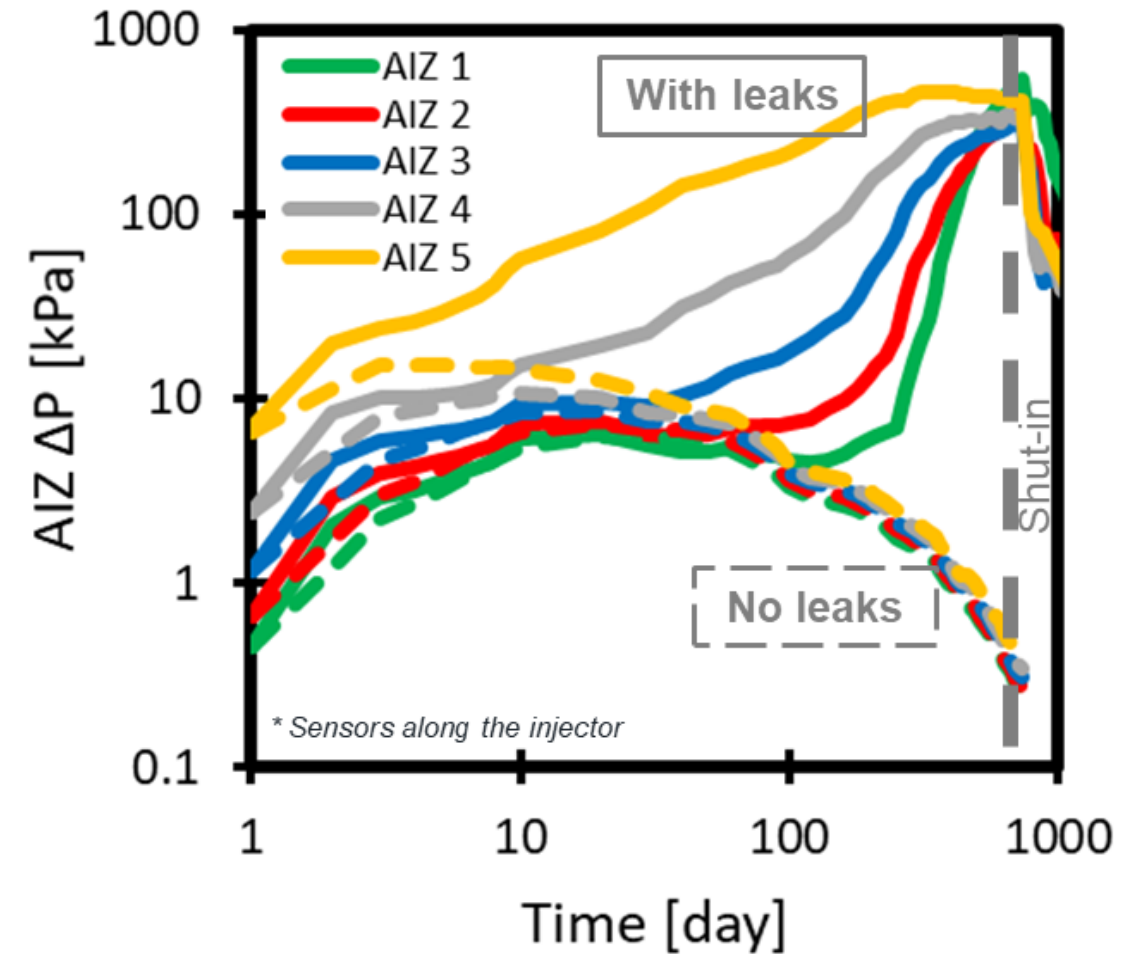
- The AlZ  $\Delta P$  decays nonlinearly with the increase of distance to the injector.
- The AlZ pressure increase can be as large as  $\sim 1\%$  of the IZ pressure increase for this selected model.

# AIZ $\Delta P$ with the presence of a leaky fault

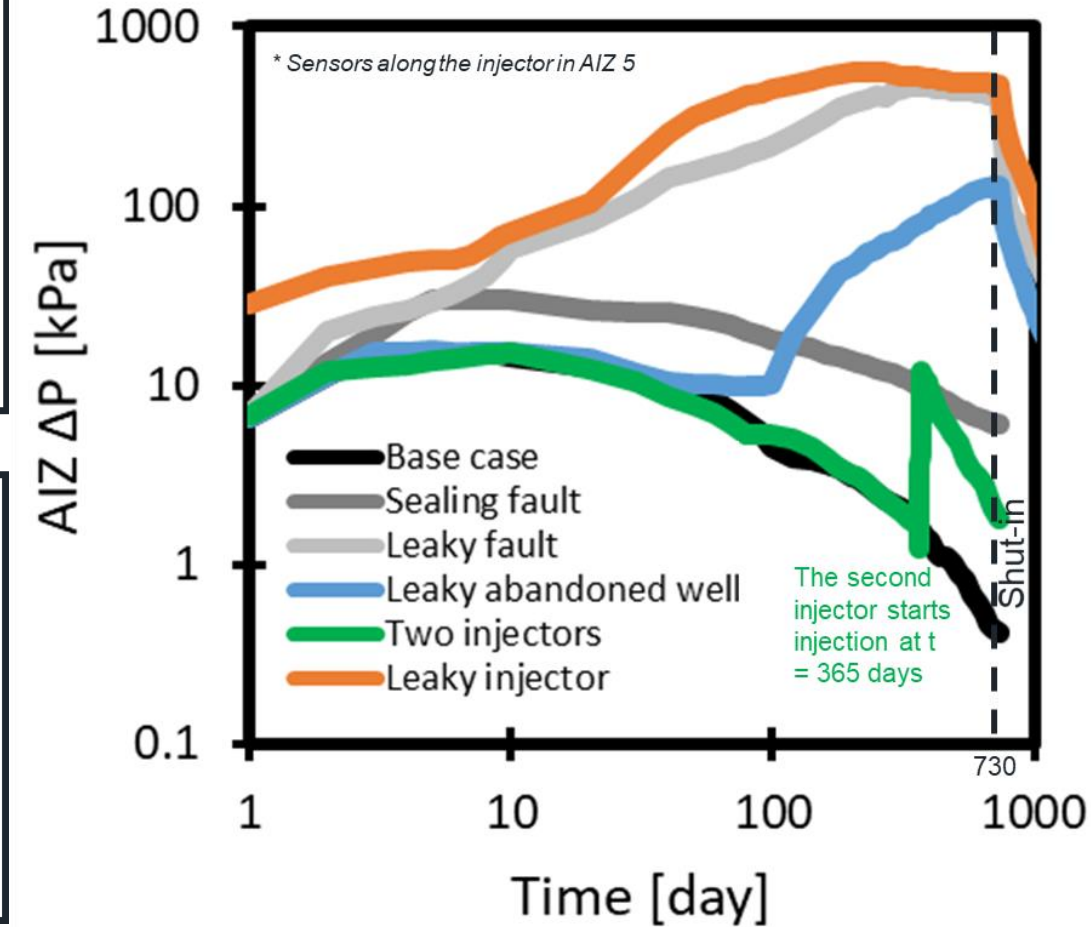
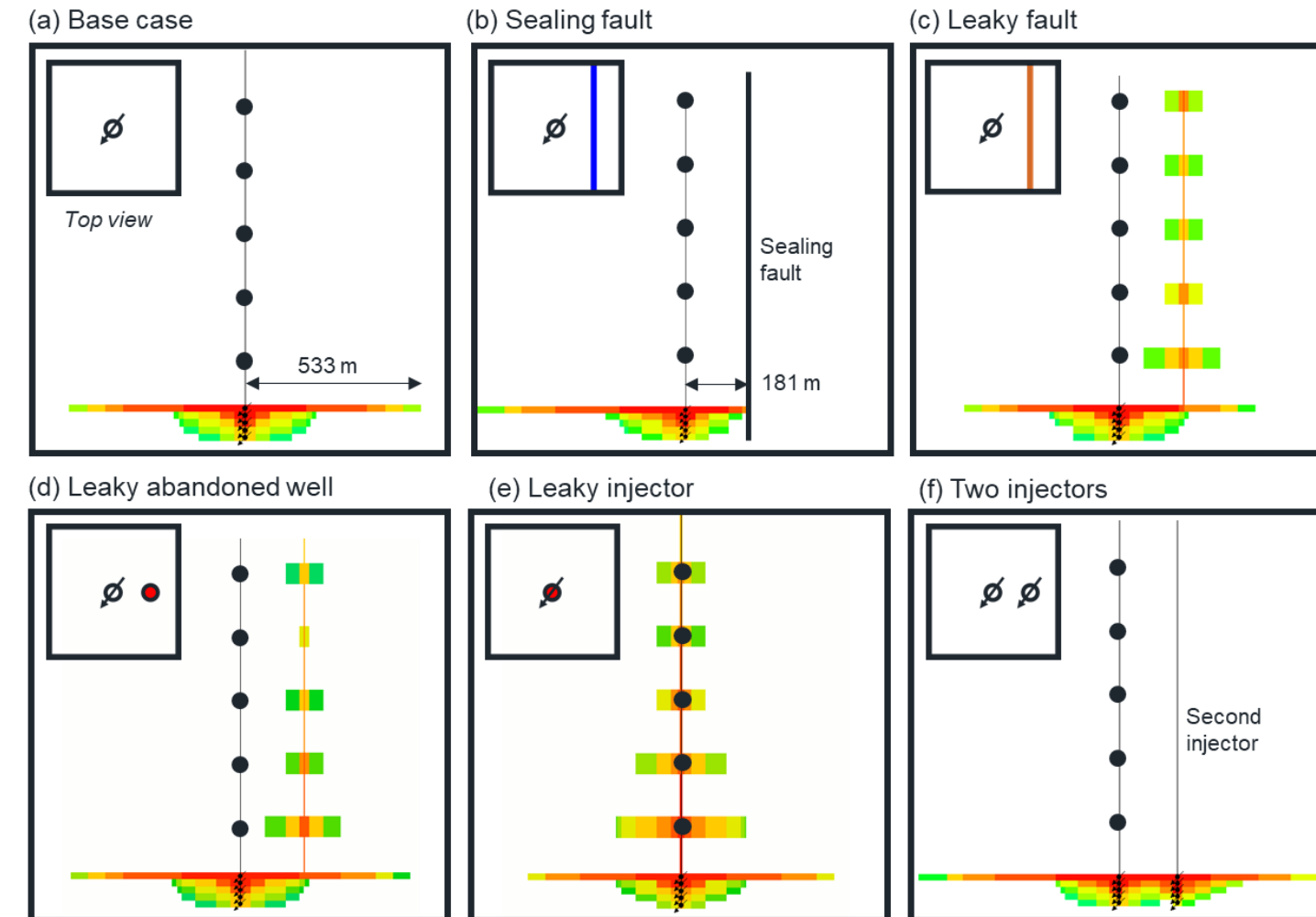
## CO<sub>2</sub> plume Distribution



- Distance = 181 m
- Fault perm = 1 D
- Fault thickness = 10 ft



# AIZ $\Delta P$ in different subsurface conditions



# Summary

## Reservoir injectivity

- How to manage CO<sub>2</sub> injection pressure in the reservoir?

## Reservoir sealing capacity

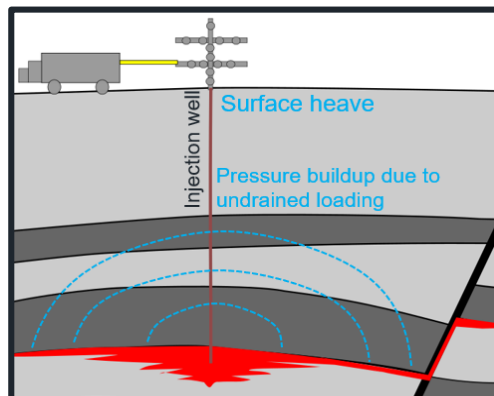
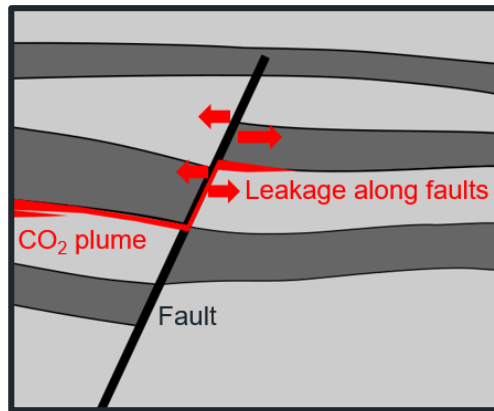
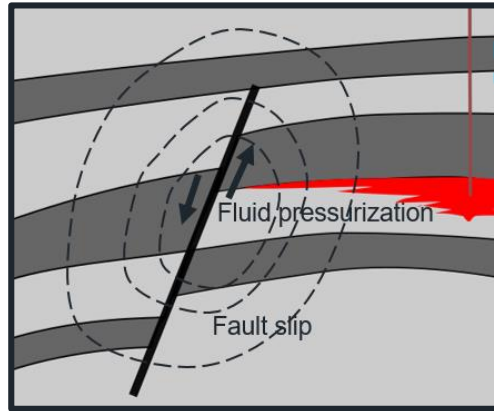
- Can CO<sub>2</sub> migrate through a fault?
- What is the height of CO<sub>2</sub> column?

## Subsurface monitoring

- How to monitor subsurface leakages?

- The AIZ pressure increase due to undrained loading is up to 1% of the injection zone (IZ) pressure increase for the chosen reservoir model.
- The AIZ ΔP with leaks can be one order of magnitude larger than the case without leaks. Understanding distinct features of pressure increase with or without leaks can help identify potential leaks into the AIZ.

# Conclusions



## To reduce risk in CO<sub>2</sub> geological storage:

- It is critical to use a correct compressibility input for CO<sub>2</sub> storage projects to avoid underestimating the risk of fault reactivation.
- Determination of fault properties is important for making realistic predictions on CO<sub>2</sub> leakage because clay content has a large influence on fault gouge sealing capacity.
- Evolution and distribution of clay smear in faults explain uncertainties and variabilities in the estimation of CO<sub>2</sub> column height.
- The pressure monitoring above injection zone is an effective technique to detect potential leaks.

# Acknowledgments

## Advisor

D. Nicolas Espinoza

## Dissertation Committee

Kamy Sepehrnoori

Matthew Balhoff

Tip Meckel

Hugh Daigle

## Funding

ExxonMobil

DeWitt-Morette France-UT Endowed Excellence Grants

## Collaborators

Ganeswara Dasari, Gary Teletzke, Martin Lacasse, Steve Davis, and Rodrick Myers  
Matthieu Vandamme, and Jean-Michel Pereira

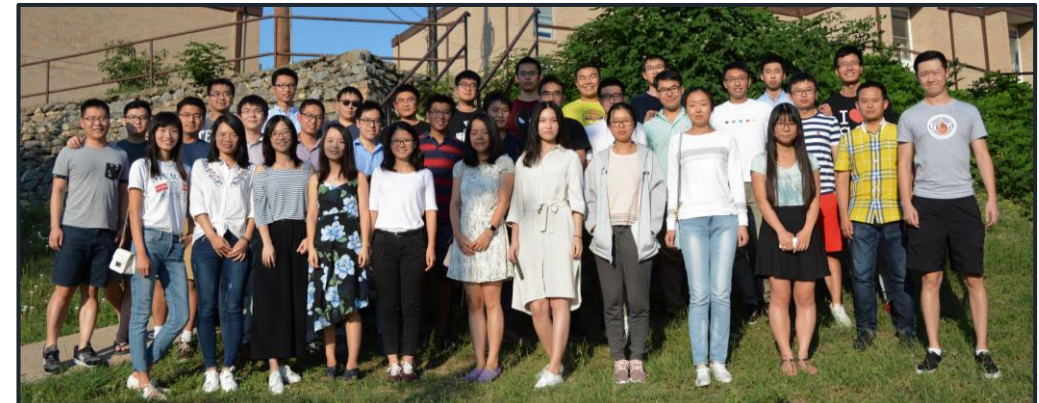
## PGE staff

Glen Baum, Gary Miscoe, Daryl Nygaard, Diane Landeros, Traci Laird,  
Leah Freeman, and Amy Stewart

## Energy Geomechanics Laboratory



## PGE Chinese Students Alumni



# Publications

---

## Journal papers

- **Xiaojin Zheng** and D. Nicolas Espinoza. Multiphase CO<sub>2</sub>-brine Transport Properties of Synthetic Fault Gouge, *Marine and Petroleum Geology*, accepted, 2021.
- **Xiaojin Zheng** and D. Nicolas Espinoza. Measurements of Unloading Compressibility of Frio Sand under Uniaxial-Strain Stress Path and Implications on Reservoir Pressure Management, *Rock Mechanics and Rock Engineering*, under review, 2021.
- **Xiaojin Zheng** and D. Nicolas Espinoza. Stochastic Quantification of CO<sub>2</sub> Fault Sealing Capacity in Sand-Shale Sequences, *Marine and Petroleum Geology*, under review, 2021.
- **Xiaojin Zheng**, D. Nicolas Espinoza, Matthieu Vandamme, and Jean-Michel Pereira. CO<sub>2</sub> Plume and Pressure Monitoring through Pressure Sensors above the Injection Zone, under internal review, 2021.

## Conference papers

- **Xiaojin Zheng**, D. Nicolas Espinoza, Matthieu Vandamme, and Jean-Michel Pereira. Feasibility of Poroelastic Monitoring above Injection Zone for CO<sub>2</sub> Geological Storage, *55<sup>th</sup> US Rock Mechanics/Geomechanics Symposium*. Houston, 20-23, June, 2021.
- **Xiaojin Zheng**, Zhuang Sun, and D. Nicolas Espinoza. Uniaxial Strain Unloading Compressibility of Frio Sand: Measurements and Implications on Reservoir Pressure Management for CO<sub>2</sub> Storage, *53<sup>rd</sup> US Rock Mechanics/Geomechanics Symposium*. New York City, 23-26, June, 2019.



# Geomechanical and Petrophysical Studies to Reduce Risk in CO<sub>2</sub> Geological Storage

---

**Xiaojin (Andy) Zheng**

Ph.D. candidate

Hildebrand Department of Petroleum and Geosystems Engineering

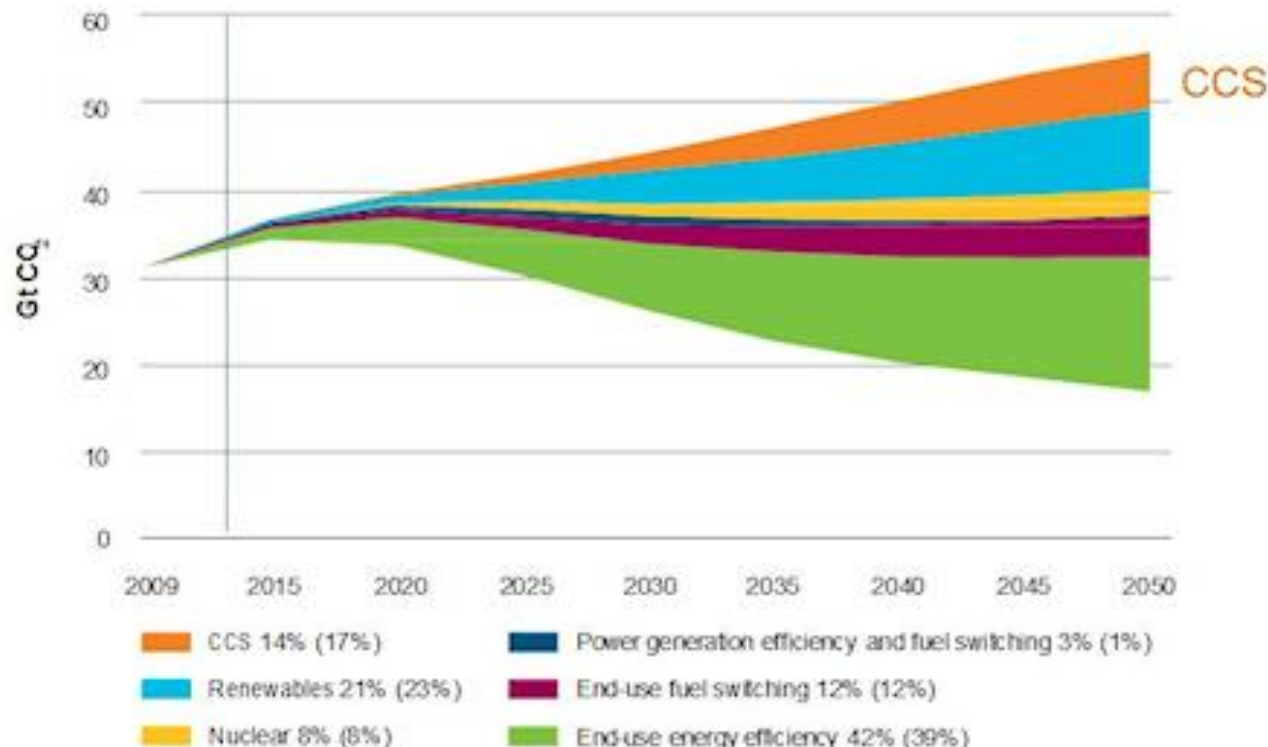
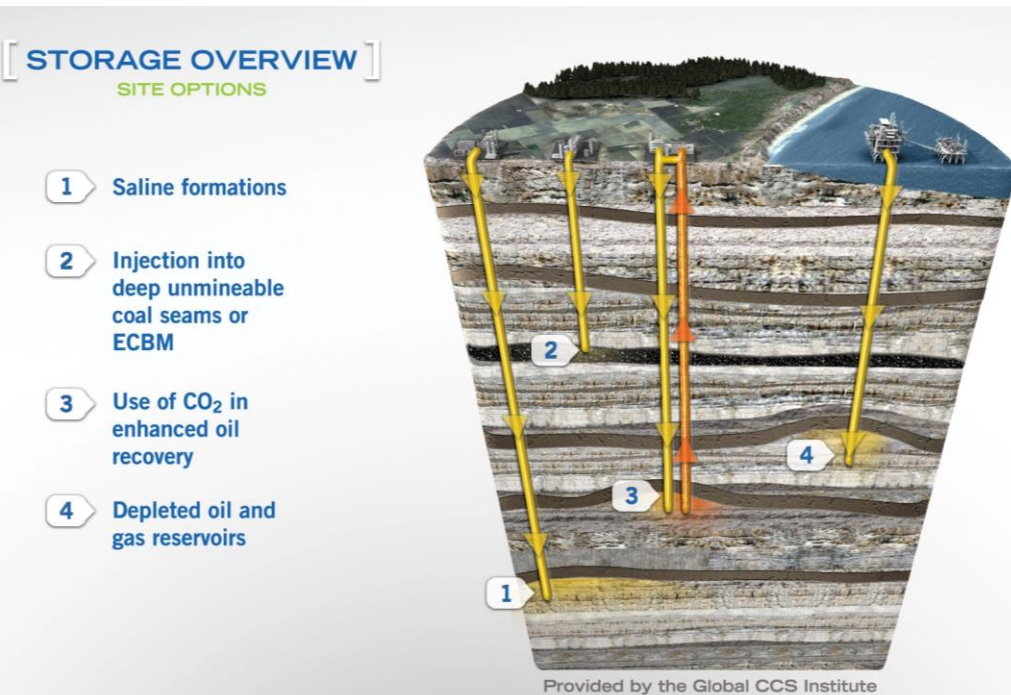
The University of Texas at Austin

[xiaojin.zheng@utexas.edu](mailto:xiaojin.zheng@utexas.edu)

# Backup slides

# CCS

## The mitigation wedges required to meet 2050 emission target



Percentages represent share of cumulative emissions reductions to 2050.

Percentages in brackets represent share of emissions reductions in the year 2050.

(Source: [CCS Image Library](#), Global CCS Institute)

IEA 2012, GCCSI 2012

# Overview of CO<sub>2</sub> storage project

	Formation	Caprock	Sedimentary environment	Geological settings	Injection rate	Injectivity	Pressure increase	References
<b>Sleipner CO<sub>2</sub> storage project in Norway by Statoil</b>	Utsira sandstone	Nordland shale	Shallow to deep marine	large aquifer with few barriers to flow; average porosity is 0.35-0.4, permeability in the range 1-3Darcy; little evidence of faulting	0.9 Mt/year, (start in 1996, cumulative injected 15.5Mt by 2015)	Excellent	Negligible (0.2 MPa in 8 years)	Verdon et al., 2013; Eiken et al., 2011
<b>Snohvit CO<sub>2</sub> storage project in Norway by Statoil</b>	Tubaen sandstone	Nordmela mudrock	Deltaic, fluvial/coastal plane	deeply buried with low porosity and permeability; with sealing faults(fault throw>200m)	0.7 Mt/year (start in 2008)	Poor	5-6.5MPa in 15 months	Eiken et al., 2011; Hansen et al., 2013; Grude et al., 2013; Shi et al., 2013
<b>Quest CO<sub>2</sub> project by Shell in Canada</b>	Basal Cambrian sandstone	Deadwood shale	Tidal marine	45m average thickness sandstone with locally thin- to very thin-bedded mudstones; Porosities and permeabilities average about 17% and 1,000mD respectively	1 Mt/year (up to 1.2Mt/year), (start in 2015, cumulative 4Mt)	Good	0.8MPa in three years	Tawiah et al., 2020; Tucker et al., 2016
<b>Decatur CO<sub>2</sub> project by Midwest Geological Sequestration Consortium</b>	Mount Simon Sandstone	Eau Claire shale	Marine, fluvial aeolian/marine	highly porous and permeable (0.1mD-1D, porosity up to 30%); influenced by pre-existing planes of weakness	0.33 Mt/year (1000 tonnes/day), (2011-2014, cumulative 1Mt)	Good	<1.14Mpa in three years	Bauer et al., 2016; Bui & Dowell, 2019; Frailey et al., 2011

# Compressibility theory

$$\boxed{C_{bc}^{iso} = -\frac{1}{V_b} \left( \frac{\partial V_b}{\partial P_c} \right)_{P_p=cst} \quad C_{bp}^{iso} = \frac{1}{V_b} \left( \frac{\partial V_b}{\partial P_p} \right)_{P_c=cst} \quad C_{pc}^{iso} = -\frac{1}{V_p} \left( \frac{\partial V_p}{\partial P_c} \right)_{P_p=cst} \quad C_{pp}^{iso} = \frac{1}{V_p} \left( \frac{\partial V_p}{\partial P_p} \right)_{P_c=cst}}$$

Derivation for the isotropic compressibility

$$K = \frac{\Delta \sigma_m^{eff}}{\Delta \varepsilon_v} \quad \sigma_m^{eff} = \frac{\sigma_1 + \sigma_2 + \sigma_3}{3} - p_p = \frac{\sigma_D}{3} + P_c - P_p$$

Case 1:  $\sigma_D = cst$

$$\rightarrow \boxed{K \Big|_{P_p} = \frac{\Delta P_c}{\Delta \varepsilon_v} \Big|_{P_p}} \rightarrow \begin{cases} C_{bc}^{iso} = \frac{-1}{V_b} \left( \frac{\partial V_b}{\partial P_c} \right)_{P_p} = \frac{\Delta \varepsilon_v}{\Delta P_c} \Big|_{P_p} = \frac{1}{K \Big|_{P_p}} \\ C_{pc}^{iso} = \frac{-1}{V_p} \left( \frac{\partial V_p}{\partial P_c} \right)_{P_p} = \frac{1}{\phi} \frac{\Delta \varepsilon_v}{\Delta P_c} \Big|_{P_p} = \frac{1}{\phi K \Big|_{P_p}} \end{cases}$$

Case 2:  $\sigma_D = cst$

$$\rightarrow \boxed{K \Big|_{P_c} = \frac{\Delta P_p}{\Delta \varepsilon_v} \Big|_{P_c}} \rightarrow \begin{cases} C_{bp}^{iso} = \frac{1}{V_b} \left( \frac{\partial V_b}{\partial P_p} \right)_{P_c} = \frac{\Delta \varepsilon_v}{\Delta P_p} \Big|_{P_c} = \frac{1}{K \Big|_{P_c}} \\ C_{pp}^{iso} = \frac{1}{V_p} \left( \frac{\partial V_p}{\partial P_p} \right)_{P_c} = \frac{1}{\phi} \frac{\Delta \varepsilon_v}{\Delta P_p} \Big|_{P_c} = \frac{1}{\phi K \Big|_{P_c}} \end{cases}$$

# Compressibility theory

$$C_{bc}^{uni} = \frac{1}{V_b} \left( \frac{\partial V_b}{\partial \sigma_{zz}^{eff}} \right)_{\varepsilon_{xx}, \varepsilon_{yy}, P_p = cst} \quad C_{bp}^{uni} = -\frac{1}{V_b} \left( \frac{\partial V_b}{\partial P_p} \right)_{\varepsilon_{xx}, \varepsilon_{yy}, \sigma_{zz} = cst} \quad C_{pc}^{uni} = \frac{1}{V_p} \left( \frac{\partial V_p}{\partial \sigma_{zz}^{eff}} \right)_{\varepsilon_{xx}, \varepsilon_{yy}, P_p = cst} \quad C_{pp}^{uni} = -\frac{1}{V_p} \left( \frac{\partial V_p}{\partial P_p} \right)_{\varepsilon_{xx}, \varepsilon_{yy}, \sigma_{zz} = cst}$$

Derivation for the uniaxial strain compressibility

$$M = \left( \frac{\Delta \sigma_{zz}^{eff}}{\Delta \varepsilon_{zz}} \right)_{\varepsilon_{xx}, \varepsilon_{yy} = cst}$$

$$C_{bc}^{uni} = \frac{1}{V_b} \left( \frac{\partial V_b}{\partial \sigma_{zz}^{eff}} \right) = \frac{\Delta \varepsilon_b}{\Delta \sigma_{zz}^{eff}} = \frac{\Delta \varepsilon_{zz}}{\Delta \sigma_{zz}^{eff}} = \frac{1}{M}$$

$$\downarrow \quad \sigma_{zz} = \sigma_{zz}^{eff} + \alpha P_p$$

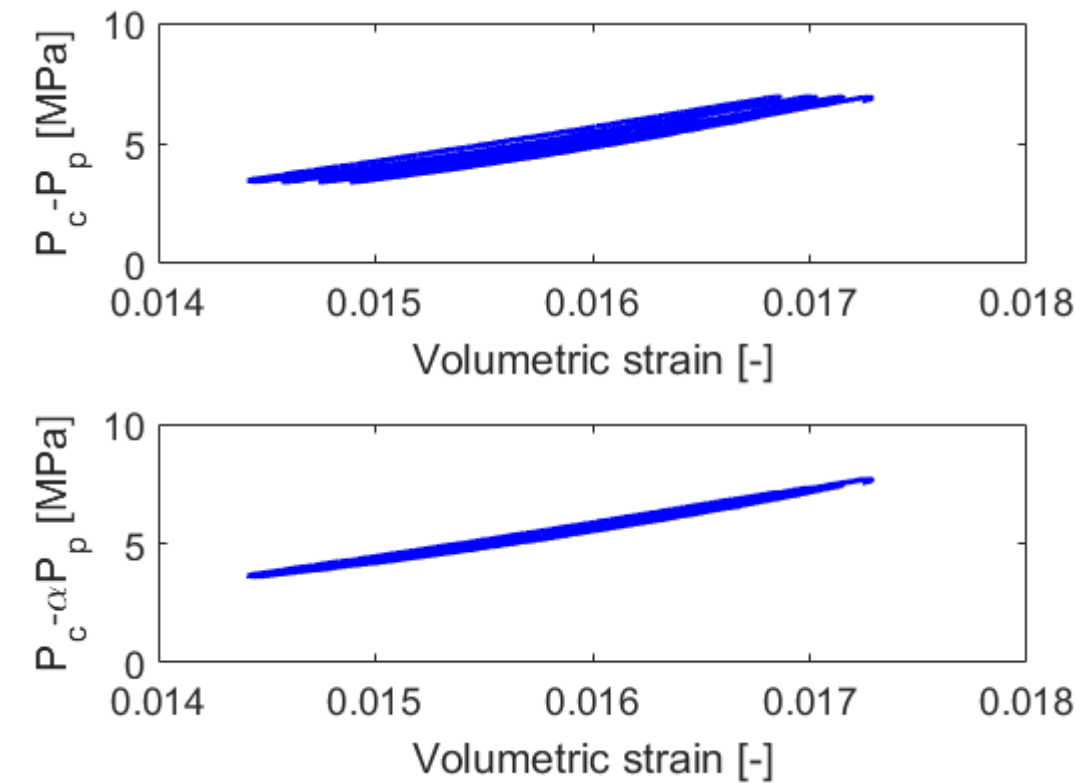
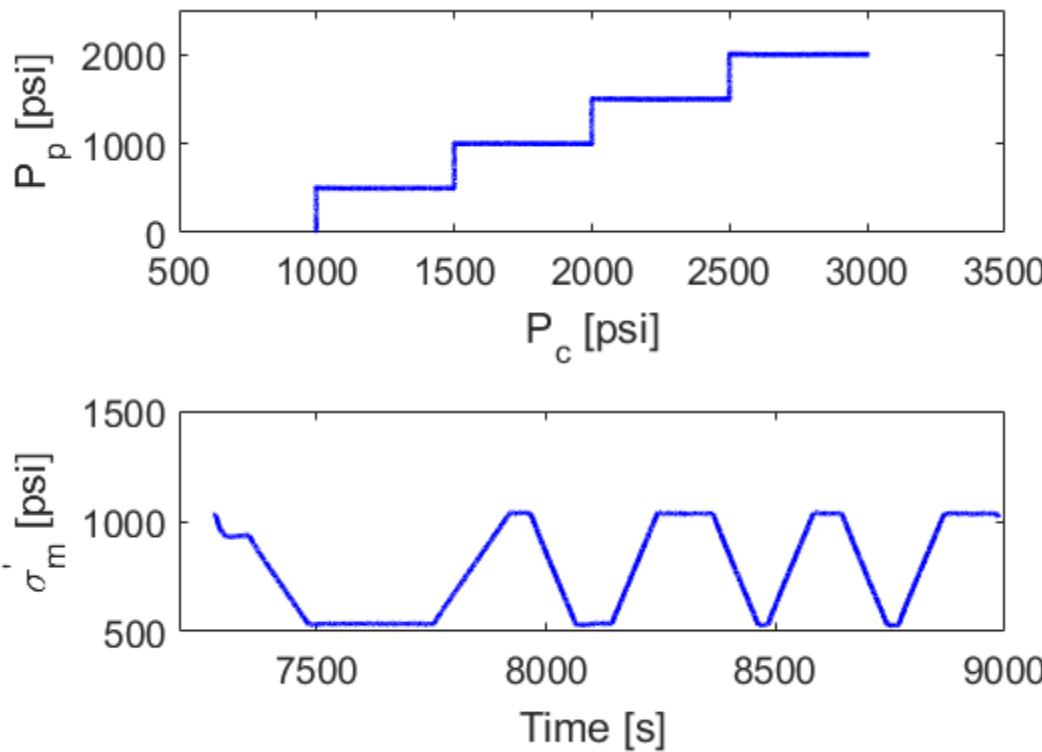
$$C_{bp}^{uni} = -\frac{1}{V_b} \left( \frac{\partial V_b}{\partial P_p} \right) = \frac{\Delta \varepsilon_b}{\Delta P_p} = \frac{\Delta \varepsilon_{zz}}{\Delta P_p} = \frac{\alpha \Delta \varepsilon_{zz}}{\Delta \sigma_{zz}^{eff}} = \frac{\alpha}{M}$$

$$C_{pc}^{uni} = \frac{\alpha}{\phi M}$$

$$C_{pp}^{uni} = \frac{-2(1-2\nu)\alpha^2 + 3(1-\nu)[\alpha(1+\phi)-\phi]}{\phi(1+\nu)M}$$

(Zimmerman, 1990; Zimmerman, 2000)

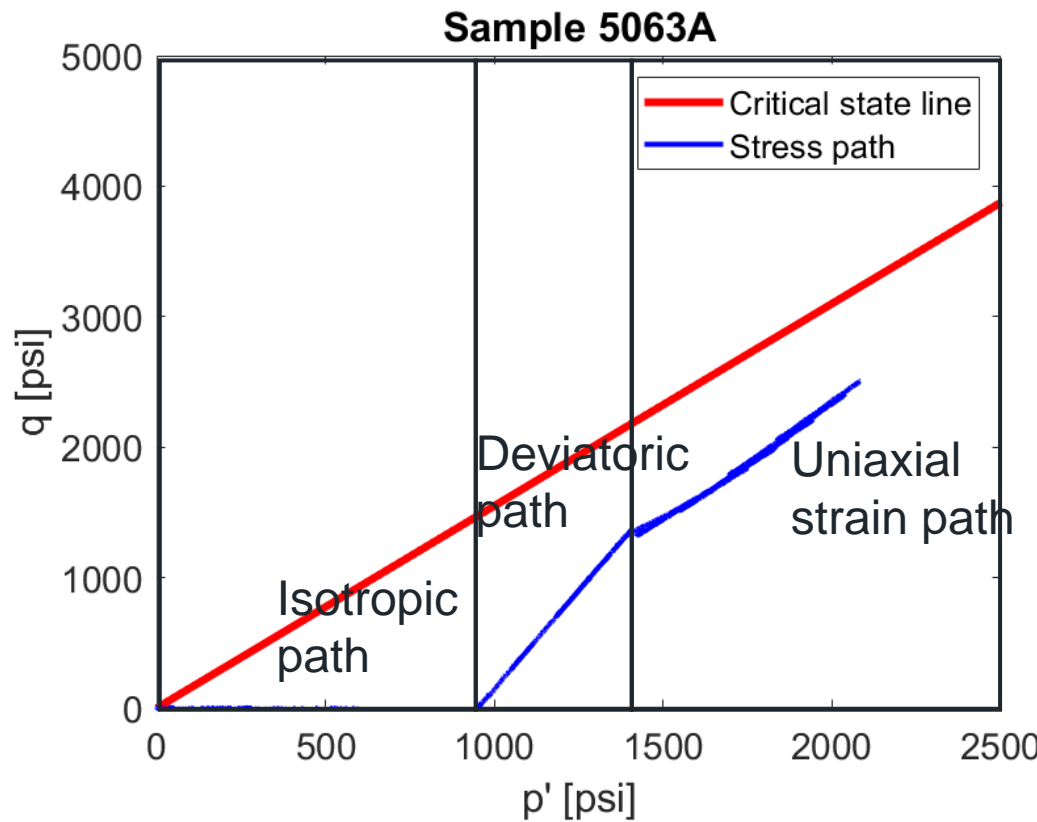
# Biot coefficient measurement



$$\boxed{\begin{aligned}\sigma_m^{eff} &= \sigma_m - p_u \\ \sigma_m^{eff} &= \sigma_m - \alpha p_u\end{aligned}}$$

$$\alpha = 1 - \frac{K}{K_s} \quad \alpha = 0.944$$

# Effects of stress path on rock failure

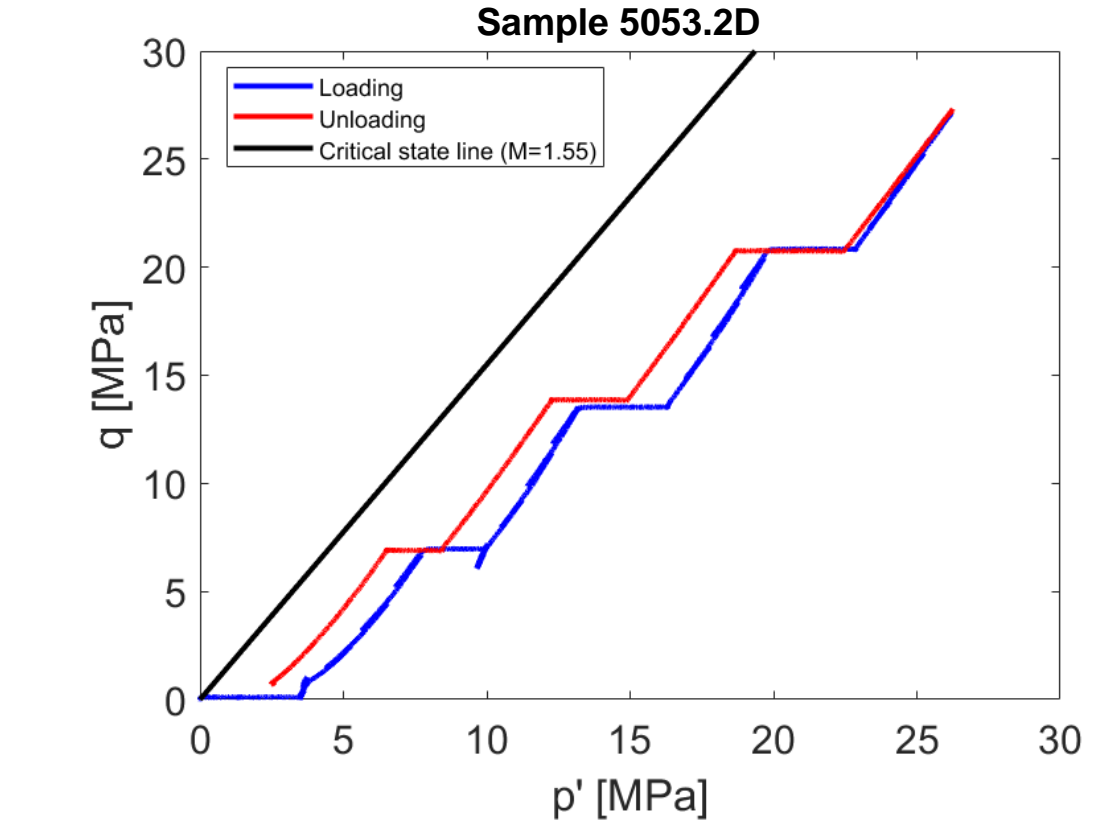


$$M = \frac{q}{p} \Big|_{CSL} = \frac{\sigma_a - \sigma_r}{\sigma_a + 2\sigma_r}$$

$$\frac{\sigma_a}{\sigma_r} = \frac{1 + \sin \varphi}{1 - \sin \varphi}$$

$$\varphi = 38^\circ$$

$$M = 1.55$$

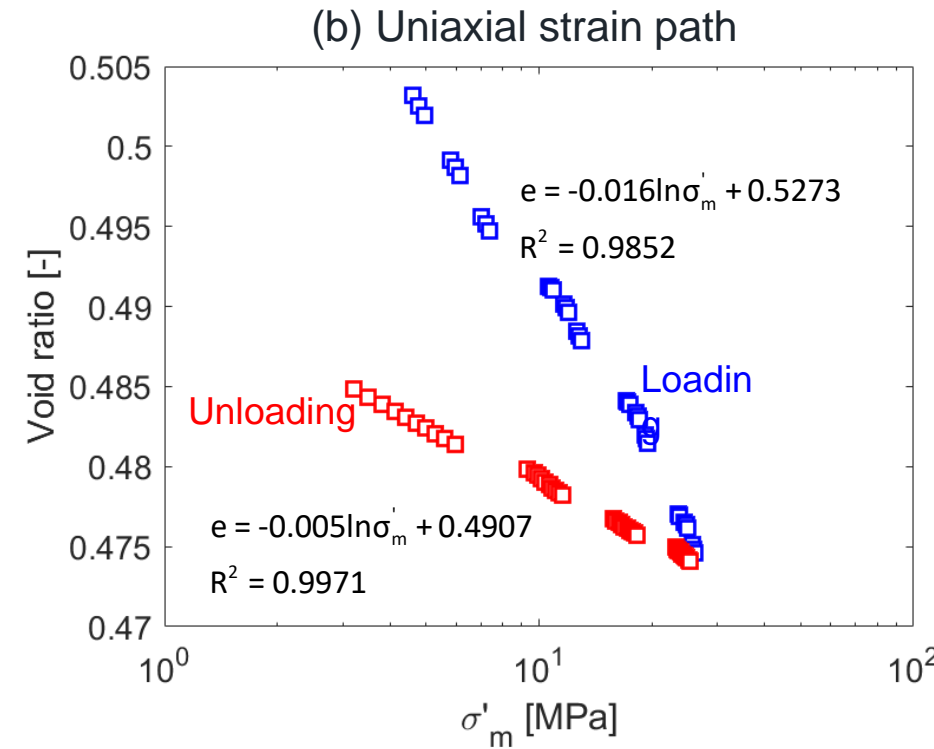
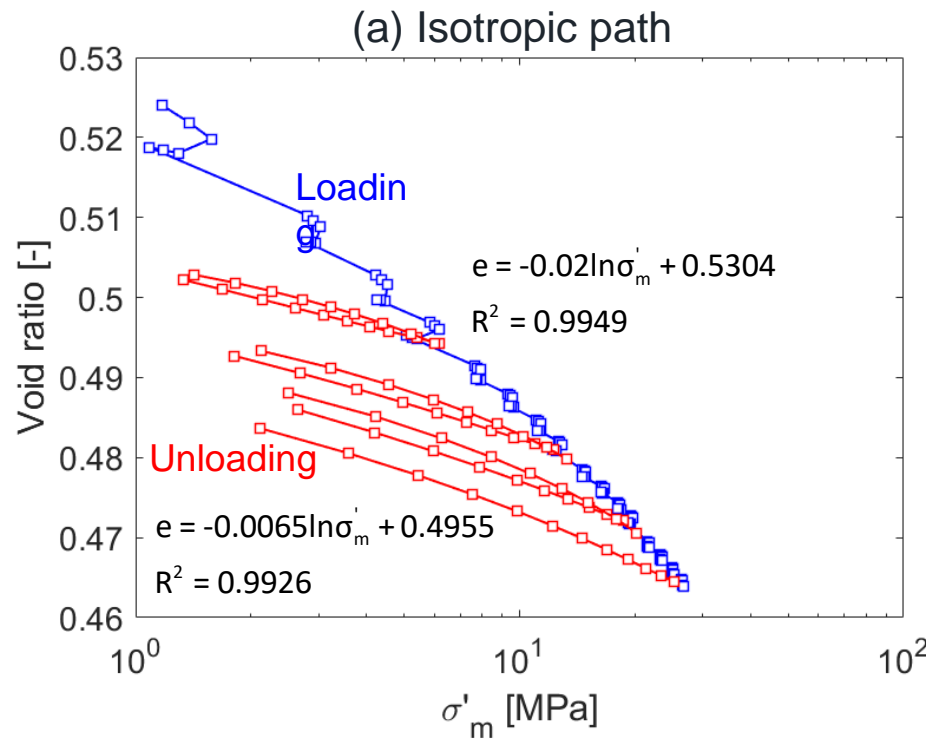


$$p' = \frac{2\sigma_r + \sigma_a}{3} = \frac{2\left(\frac{\nu}{1-\nu}\sigma_a\right) + \sigma_a}{3} = \frac{1+\nu}{3(1-\nu)}\sigma_a$$

$$q = \sigma_a - \sigma_r = \sigma_a - \left(\frac{\nu}{1-\nu}\sigma_a\right) = \frac{1-2\nu}{1-\nu}\sigma_a$$

$$\frac{dq}{dp'} = \frac{3(1-2\nu)}{(1+\nu)} = N$$

# Void ratio and mean effective stress

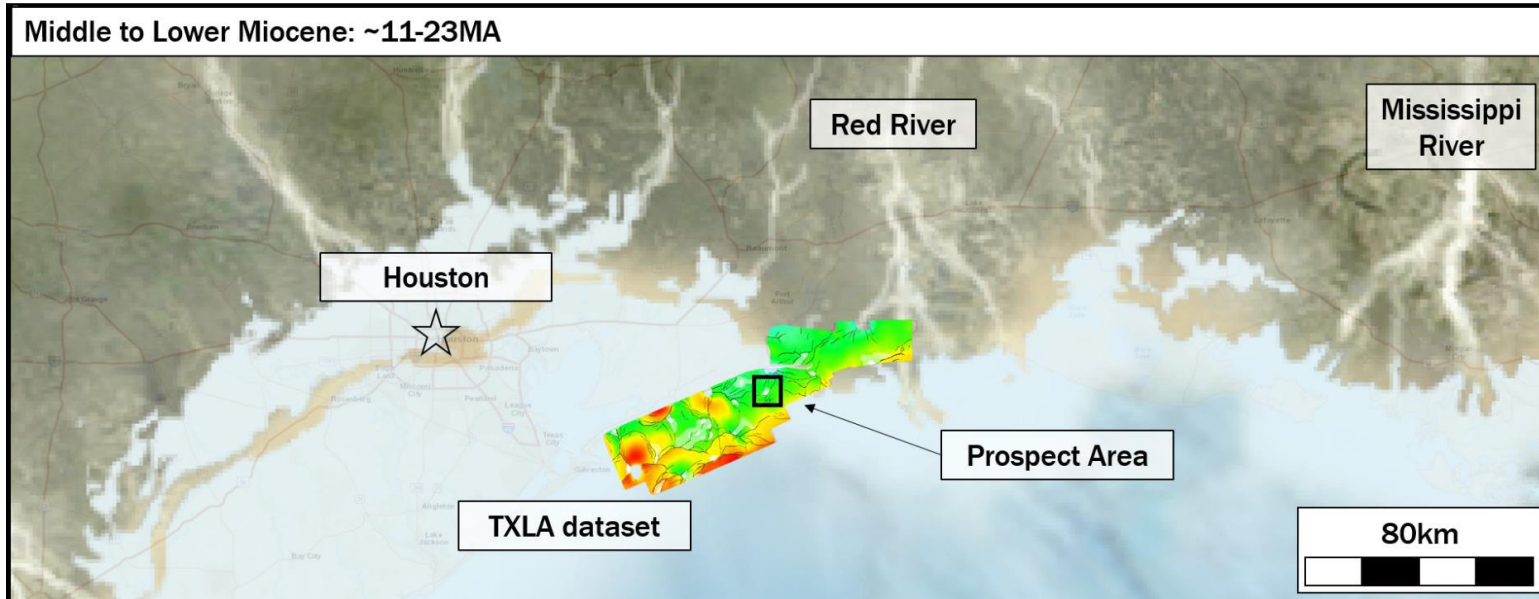


$$\text{Void ratio } e = \frac{\phi}{1-\phi}$$

$$\text{(loading)} \quad \Delta e = \lambda \ln \frac{\sigma'_m}{\sigma'_{m0}}$$

$$\text{(unloading)} \quad \Delta e = \kappa \ln \frac{\sigma'_m}{\sigma'_{m0}}$$

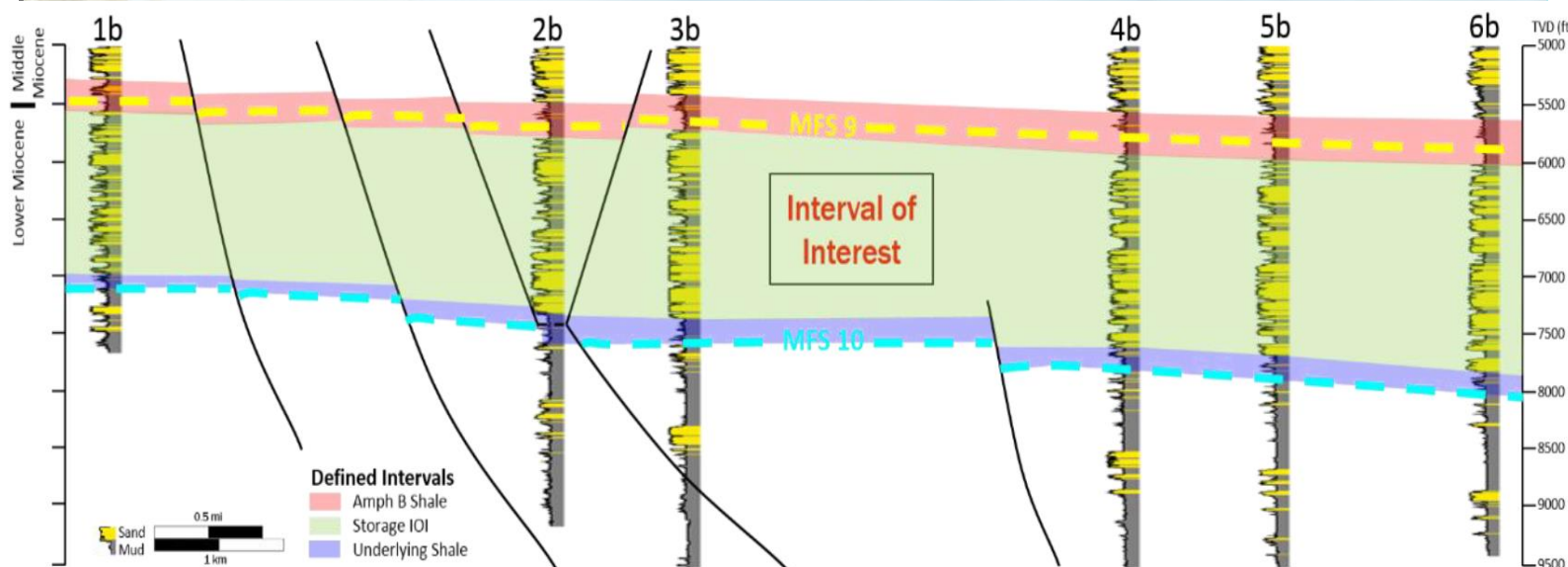
# Sample site



## GOM fault

- High Island oil filed

(Emily Beckham, MS thesis, 2018)



(Credit to Prasanna and Dr. Meckel)

# How fault gouge forms

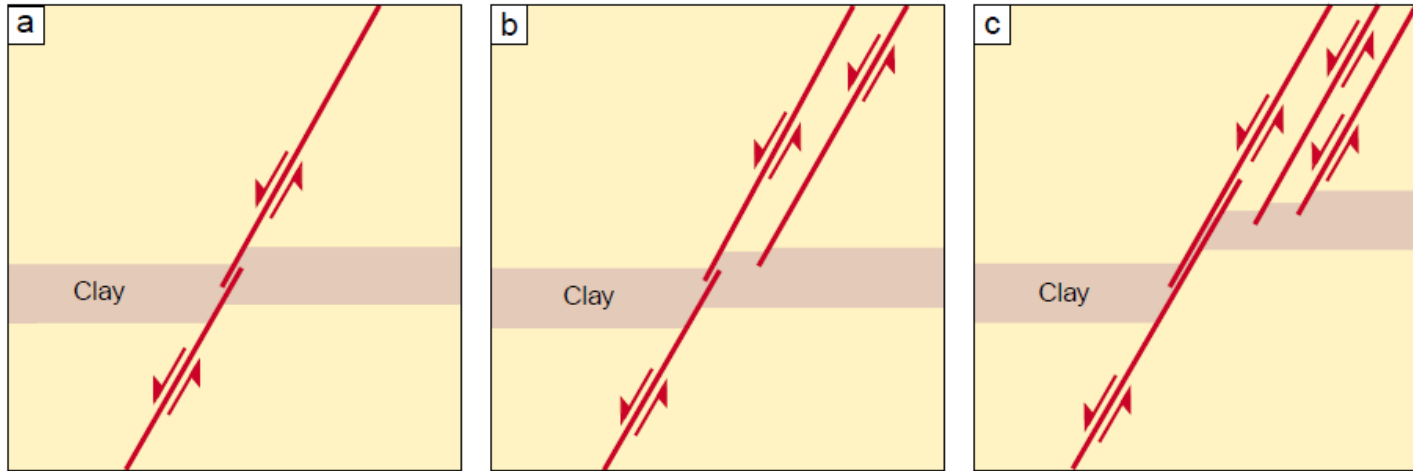
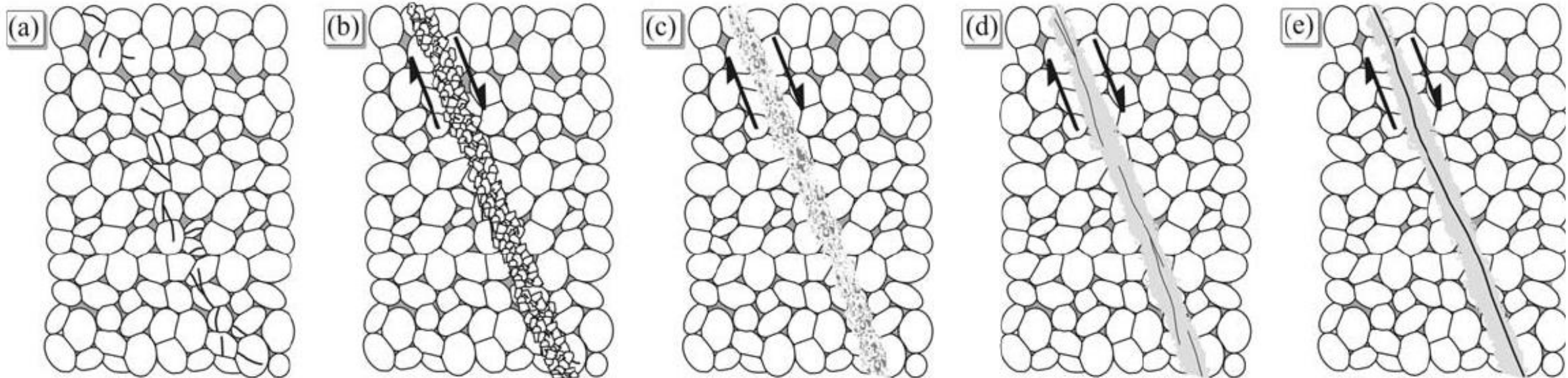


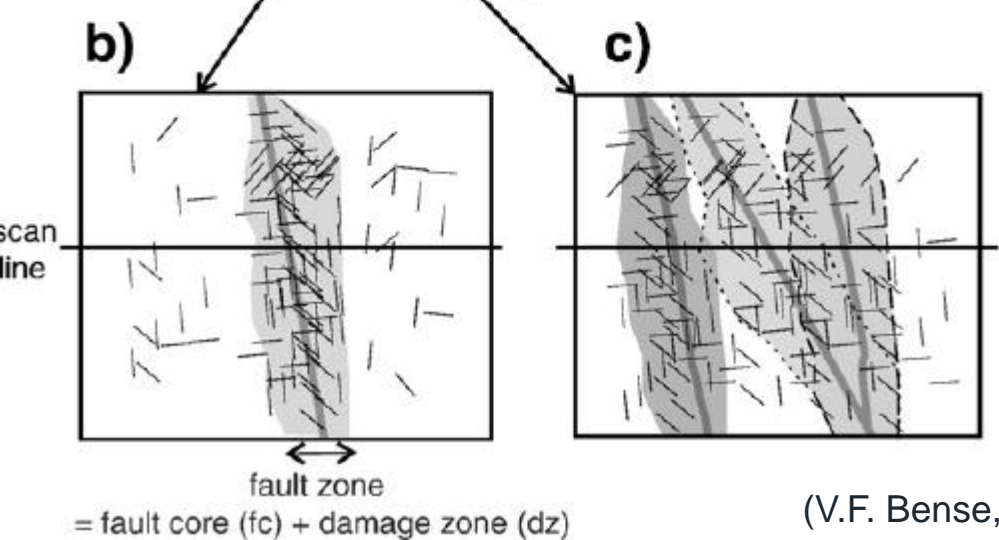
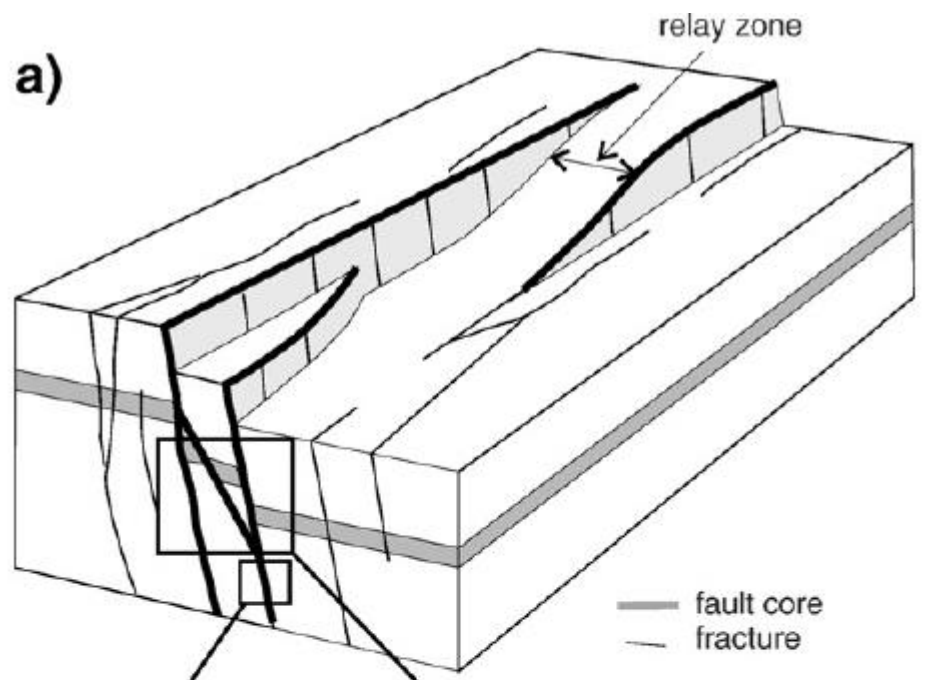
Figure 10: Kinematic model of lateral clay injection based on the kinematics shown in Figure 5.

(Wouter van der Zee, 2003)

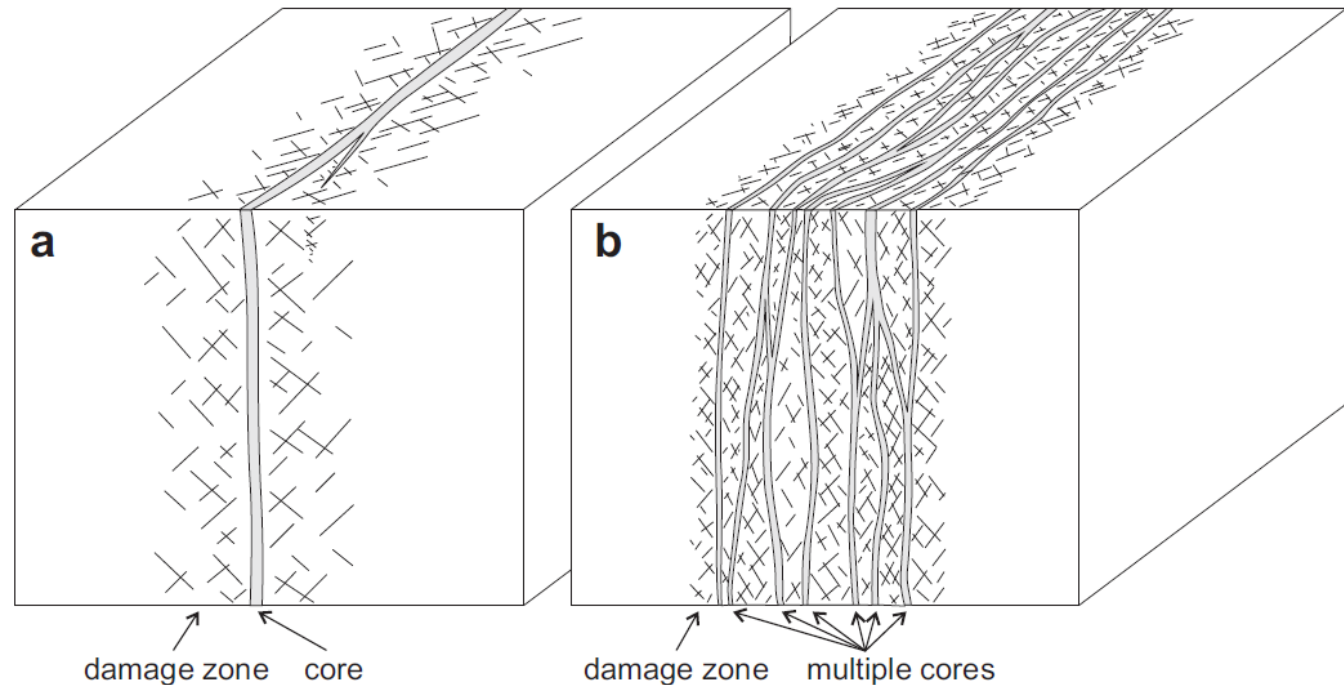


(Tord Erlend Skeie Johansen, 2005)

# Multiple strain localizations

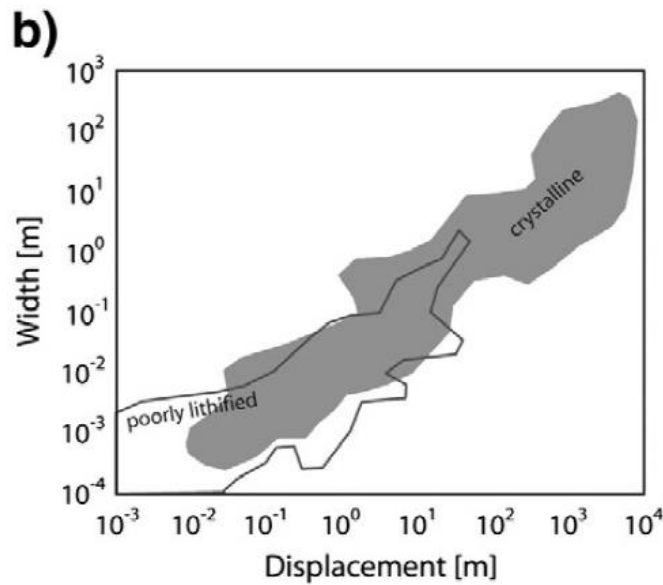
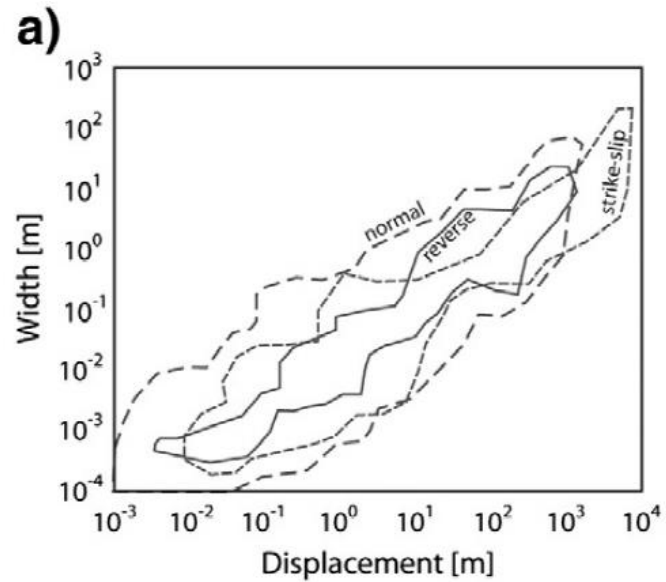


(V.F. Bense, 2013)

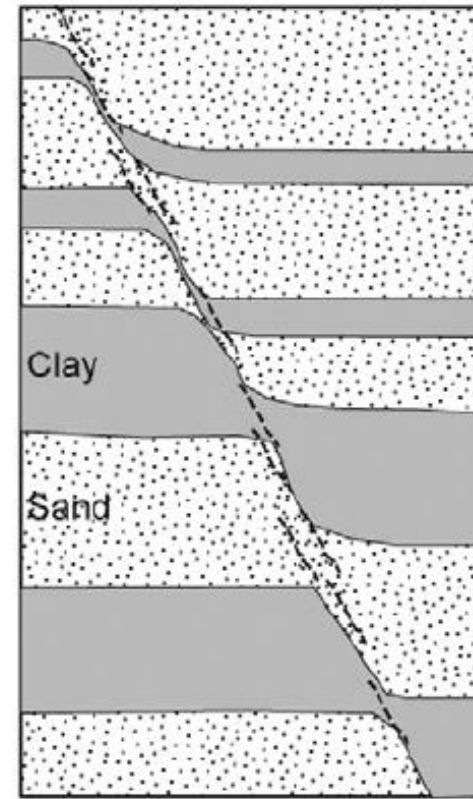


(D.R. Faulkner, 2010)

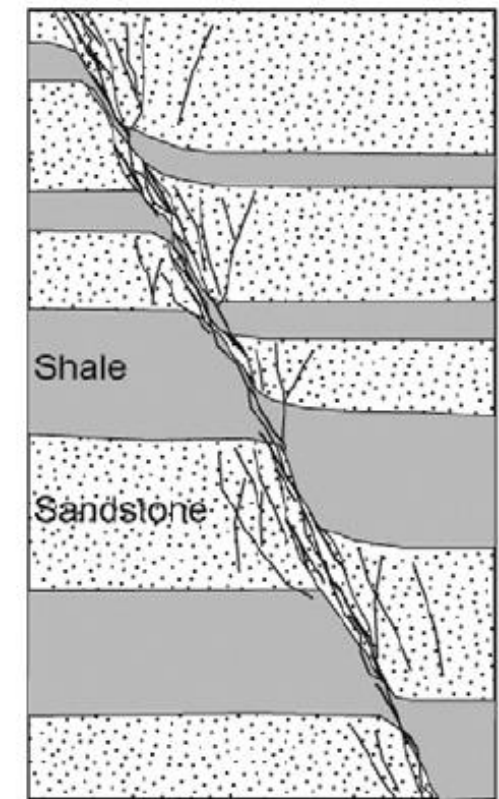
# Effects of lithifications on faults



Unlithified siliciclastic rock



Lithified siliciclastic rock



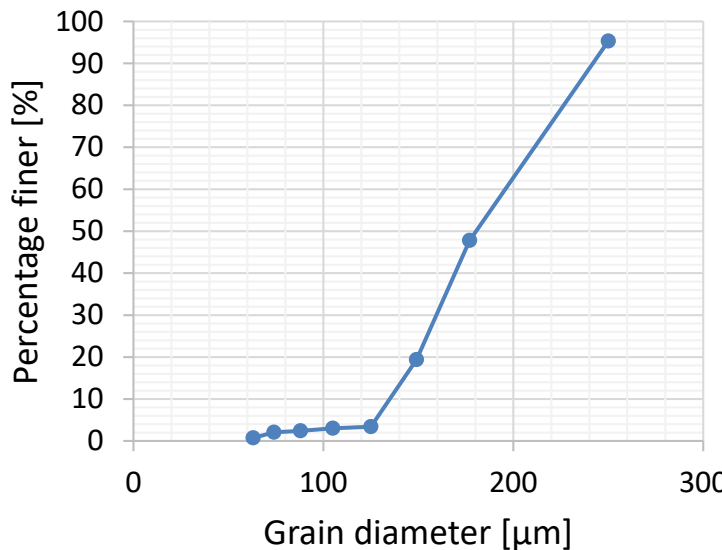
- Depth (confining pressure, porosity, cataclasis)
- Lithification and cementation (cohesive strength)
- Fault throw
- Fault type
- Property contrast between sand and shale

(Fault zone hydrogeology, V.F. Bense, 2013)

# Grain size distribution of synthetic fault gouge

## Frio sand core

Sieve layer	Mesh number		Grain diameter [um]		Grain diameter [um]	Weight [g]	Weight percentage [%]	Percentage finer [%]
	Lower one	Upper one	Mininum (stopped on the lower one)	Maximum (pass the upper one)				
1	60		250		d>250	32.62	4.69	100.00
2	80	60	177	250	177< d < 250	330.65	47.51	95.31
3	100	80	149	177	149< d < 177	197.63	28.40	47.80
4	120	100	125	149	125< d < 149	111.32	16.00	19.40
5	140	120	105	125	105< d < 125	2.73	0.39	3.40
6	170	140	88	105	88< d < 105	4.11	0.59	3.01
7	200	170	74	88	74< d < 88	2.46	0.35	2.42
8	230	200	63	74	63< d < 74	9.22	1.32	2.07
9		230		63	d<63	5.16	0.74	0.74



## Silty sand particles:

- Sands with small amounts of silt and clay.
- $D_{10} = 134 \mu\text{m}$ ,  $D_{50} = 180 \mu\text{m}$ ,  $D_{90} = 240 \mu\text{m}$

## Pure sand particles:

- Remove all the silts. All the grains are larger than  $125 \mu\text{m}$

## Anahuac shale core



### Clay particles:

- The clay components are particles from the Anahuac shale passing  $88 \mu\text{m}$  sieve (mostly clay with minor amounts of silt).

- Silty Sand (SS) sample:** Use silty sand particles
- Pure Sand (PS) sample:** Use pure sand particles
- Clayey Sand (CS) sample:** Mix pure sand particles and clay particles

# Consolidation theory

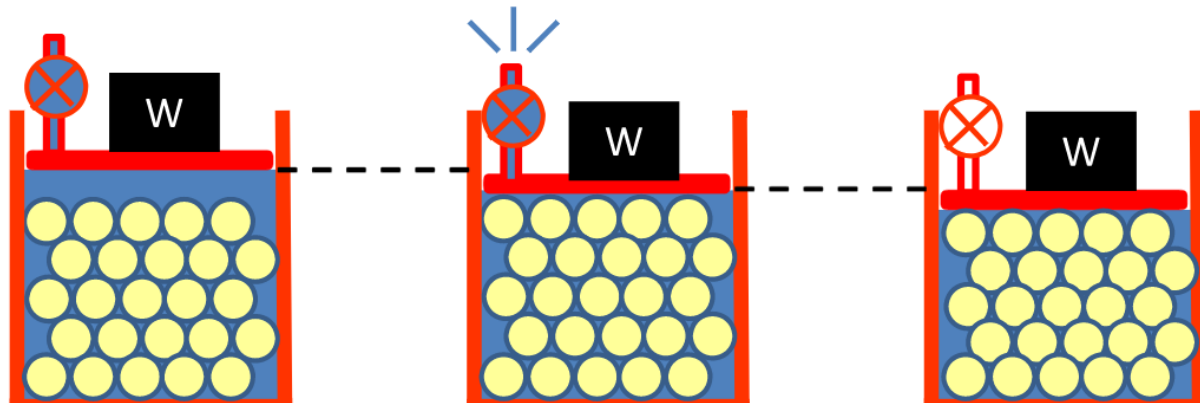
## Terzaghi consolidation theory

$$c \frac{\partial^2 u_e}{\partial z^2} = \frac{\partial u_e}{\partial t} - \frac{\partial \sigma}{\partial t}$$

(Germaine and Germaine, 2009)

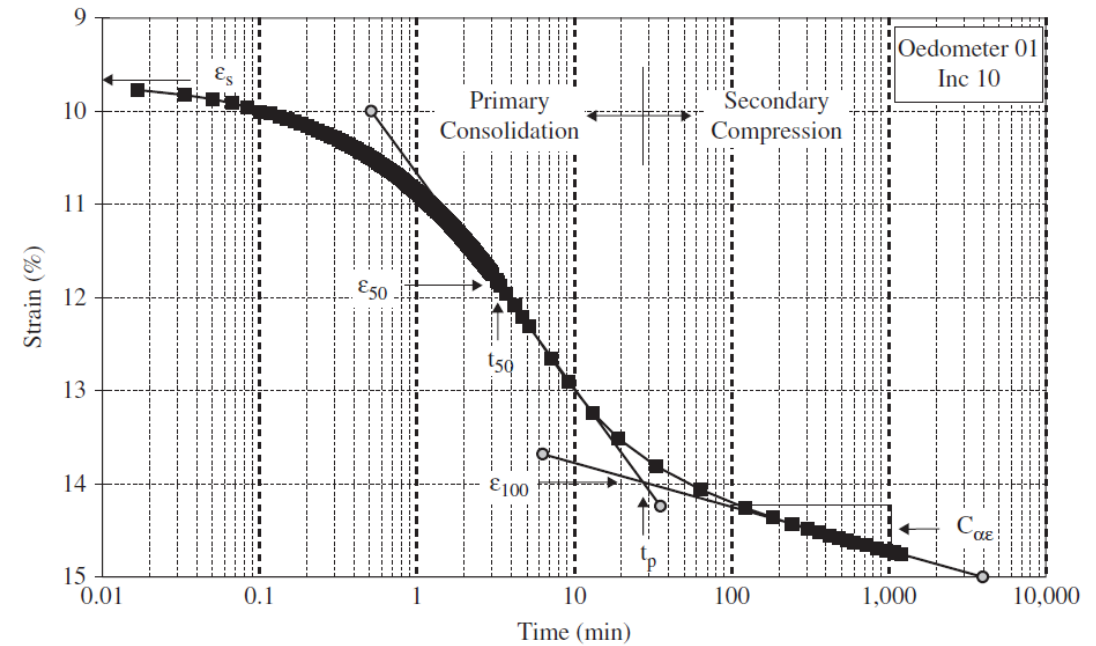
Consolidation is a coupled process between flow and volume change:

- **Disequilibrium compaction:** Primary consolidation is the process of progressive volume change due to dissipation of excess pore pressure.
- **Tectonic compression:** Compression characterizes the movement of the particles due to the reaction in inter-particle forces. Secondary compression is time - dependent volume change at constant effective stress (creep).



(Introduction to Energy Geomechanics, Espinoza, 2020)

## Log of time method



Strain at 50% consolidation

$$\varepsilon_{50} = \frac{\varepsilon_{100} + \varepsilon_s}{2}$$

Drainage height

$$H_d = \left(1 - \frac{\varepsilon_{50}}{100}\right) \times \frac{H_0}{f}$$

Coefficient of consolidation

$$c_v = \frac{0.197 H_d^2}{t_{50}}$$

Bulk volume compressibility

$$C_b = \frac{\Delta \varepsilon_a}{\Delta \sigma_a^{eff}}$$

Constrained modulus

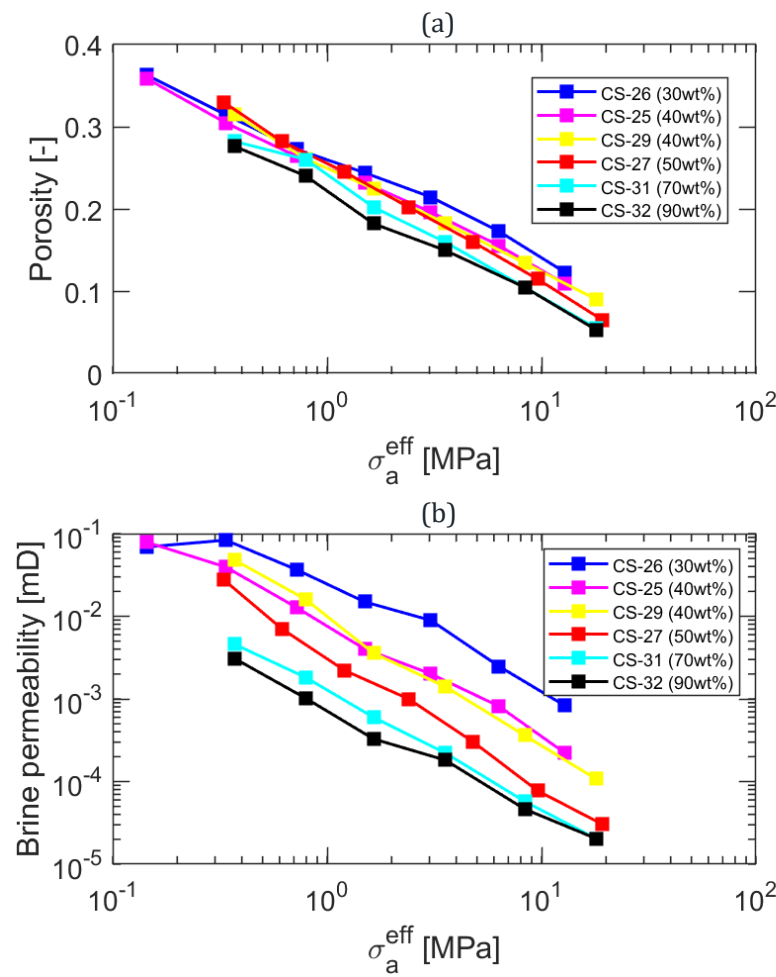
$$M = \frac{\Delta \sigma_a^{eff}}{\Delta \varepsilon_a}$$

Permeability

$$k = c_v C_b \mu_f$$

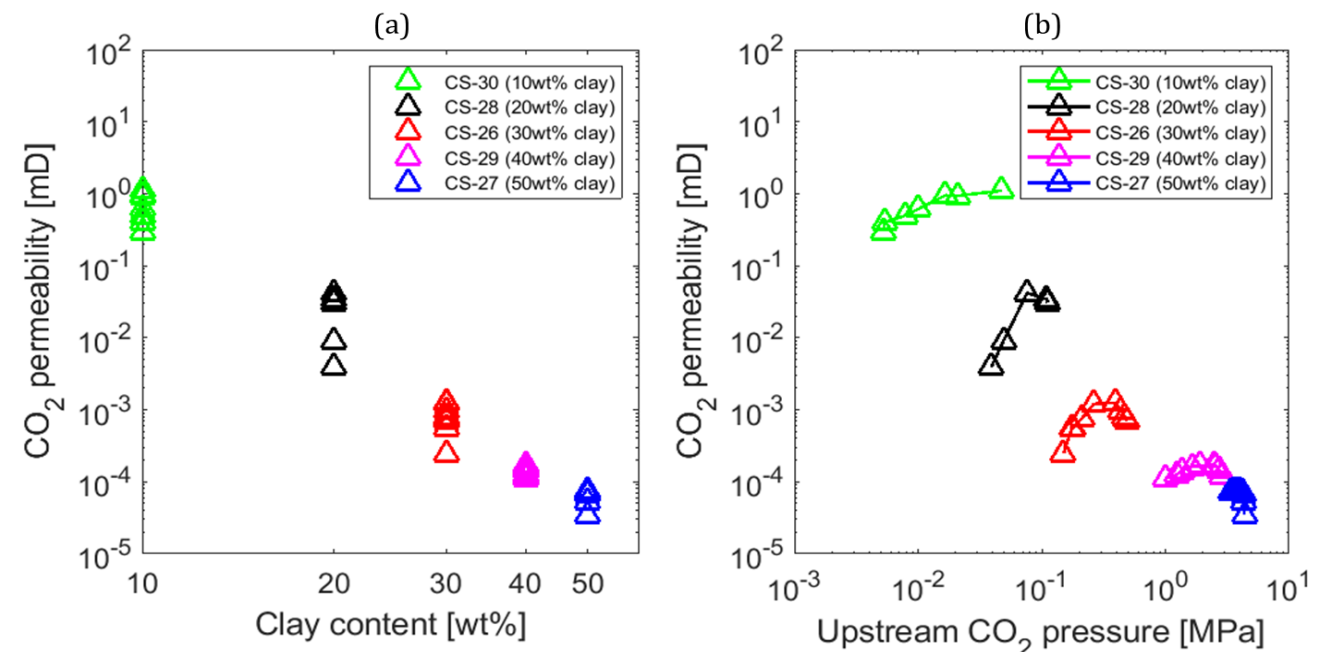
# Permeability measurements

Effects of axial stress on brine permeability

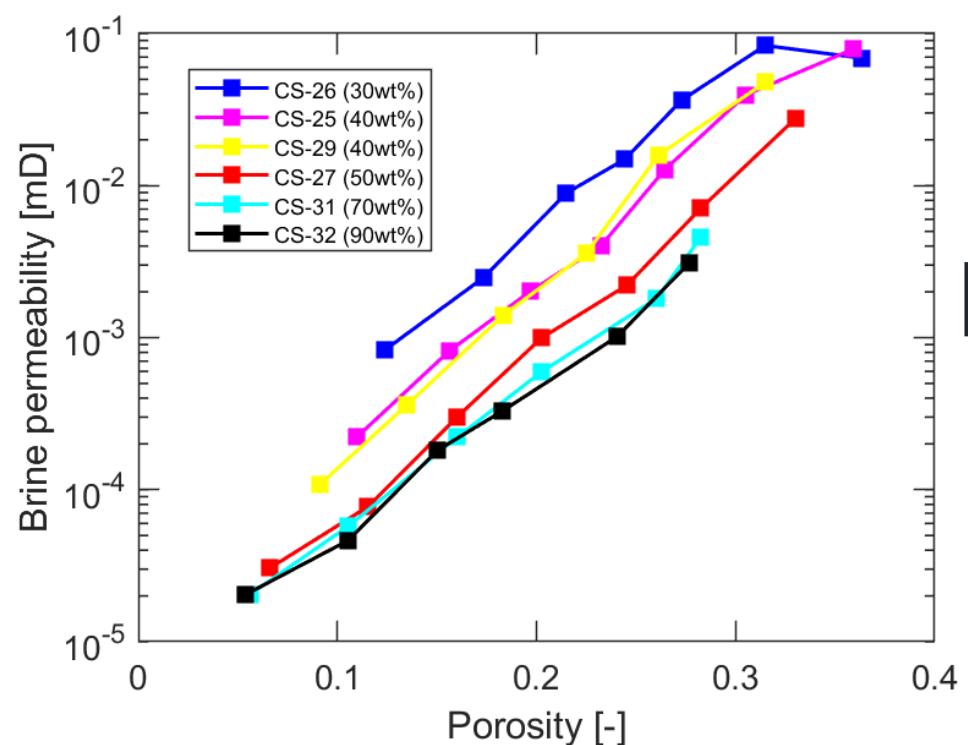
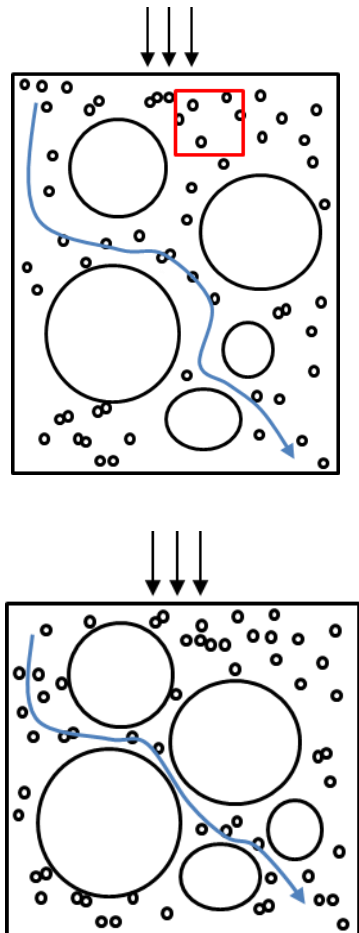


Combining Boyle's law, Darcy's law, and the equation of state for a real gas,  $\text{CO}_2$  gas permeability after breakthrough is

$$k_{\text{CO}_2} = \frac{2q_{\text{down}}\bar{\mu}LP_{\text{down}}Z_{\text{up}}}{A(P_{\text{up}}^2 - P_{\text{down}}^2)Z_{\text{down}}}$$



# Fine-grain void ratio

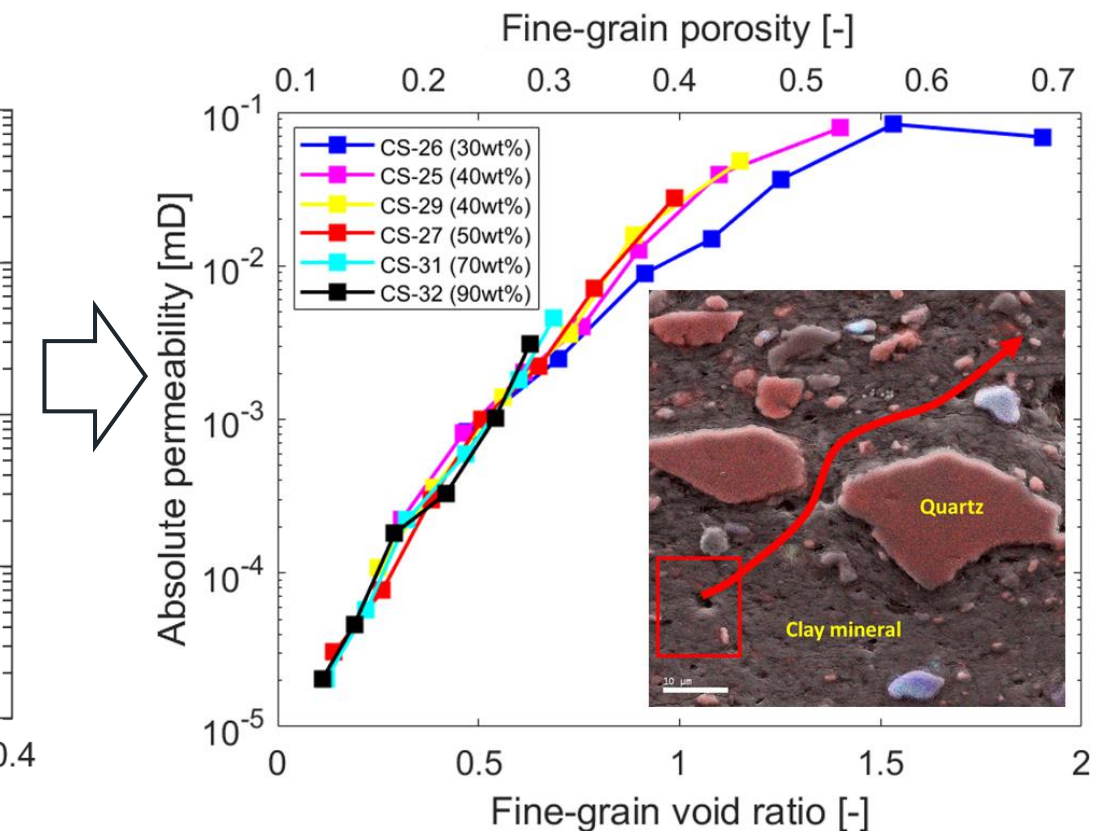


Void ratio

$$e = \frac{V_p}{V_s} = \frac{\phi}{1-\phi}$$

Fine-grain  
void ratio

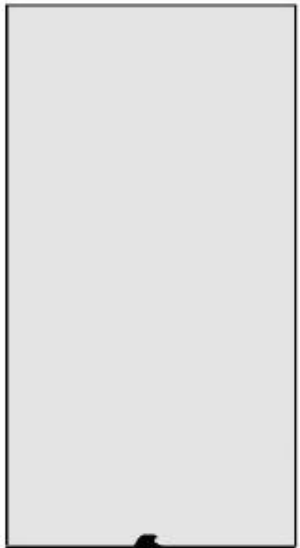
$$e_f = \frac{V_p}{V_{sf}} = \frac{\phi}{(1-\phi)y_f}$$



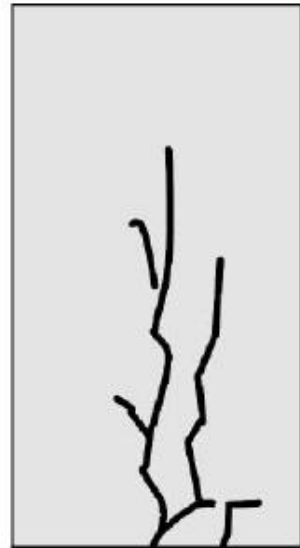
Permeability is mainly controlled by fine-grain void ratio.

# $\text{CO}_2$ breakthrough pressure

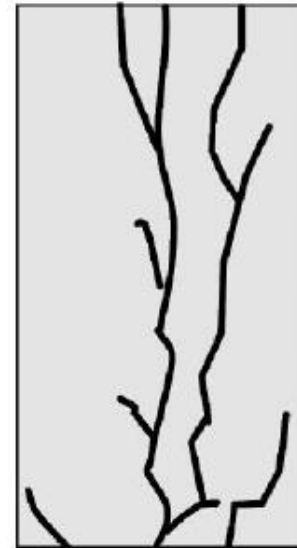
- **Breakthrough pressure:** It refers to the pressure in  $\text{CO}_2$  at which the  $\text{CO}_2$  is displaced to an extent that the percolation threshold is exceeded and continuous flowpaths of  $\text{CO}_2$  form across the core.



$P_{c, \text{entry}}$



$P_{c, \text{entry}} < P_c < P_{c, \text{threshold}}$



$P_{c, \text{threshold}}$   
 $P_{c, \text{breakthrough}}$

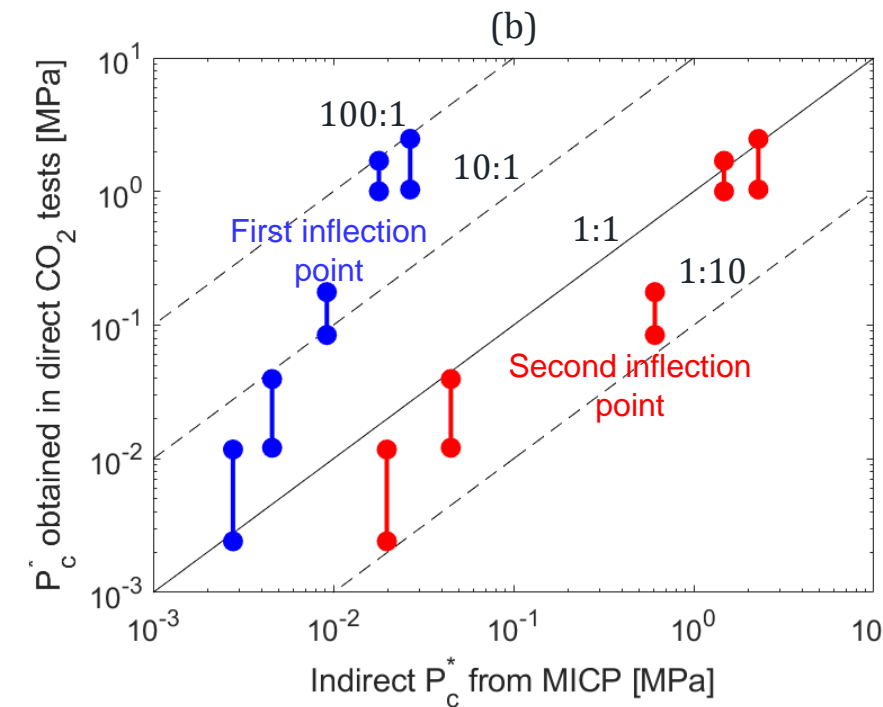
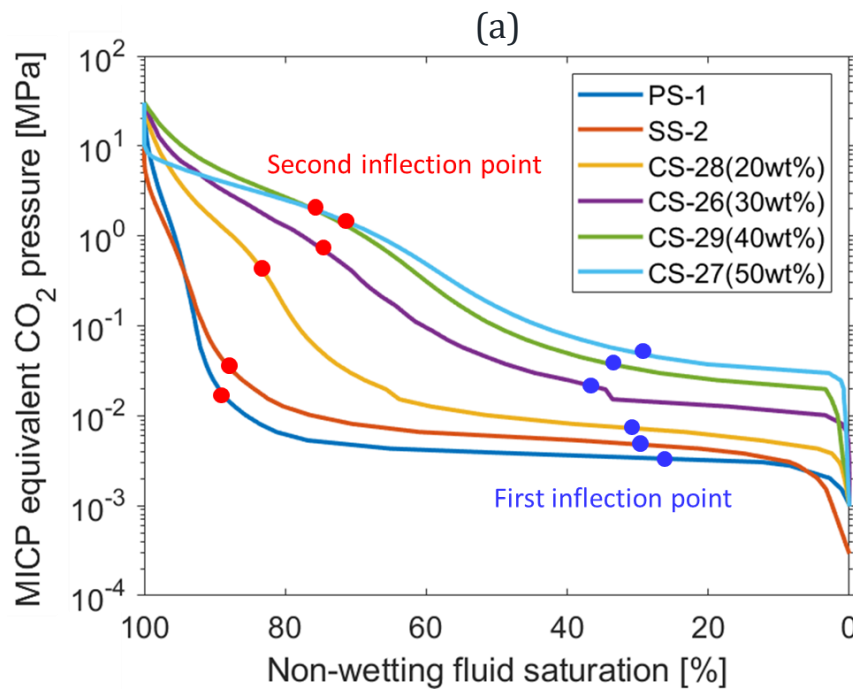


$P_c \gg P_{c, \text{threshold}}$

(Hildenbrand, 2002)

Unlike permeability, breakthrough pressure is not a simple volume average because breakthrough pressure represents the displacement resistance in the **largest interconnected pores** rather than in the overall pore space.

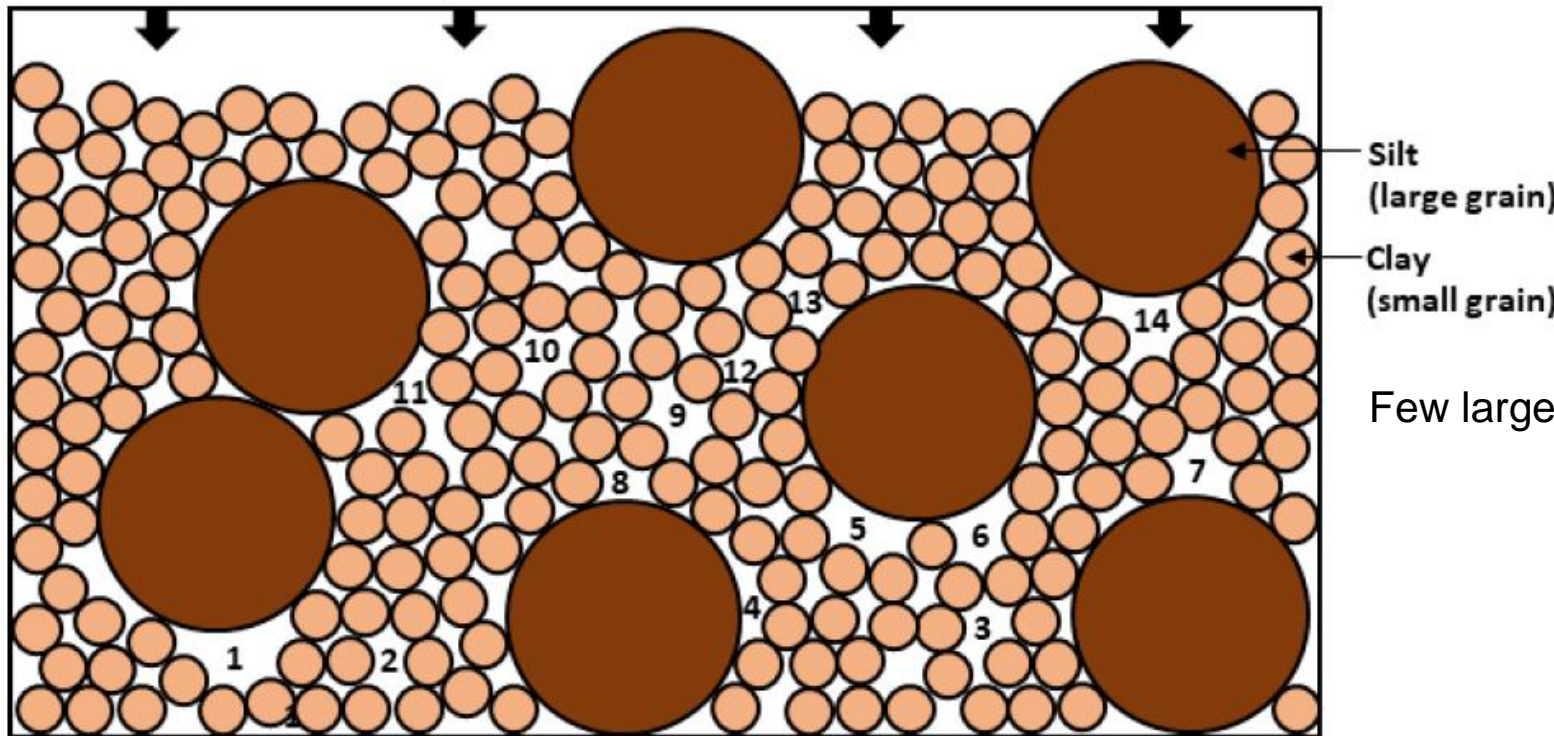
# MICP measurements



$$P_{c \text{ system}2}^* = P_{c \text{ system}1}^* \frac{\sigma_{\text{system}2} \cos \theta_{\text{system}2}}{\sigma_{\text{system}1} \cos \theta_{\text{system}1}}$$

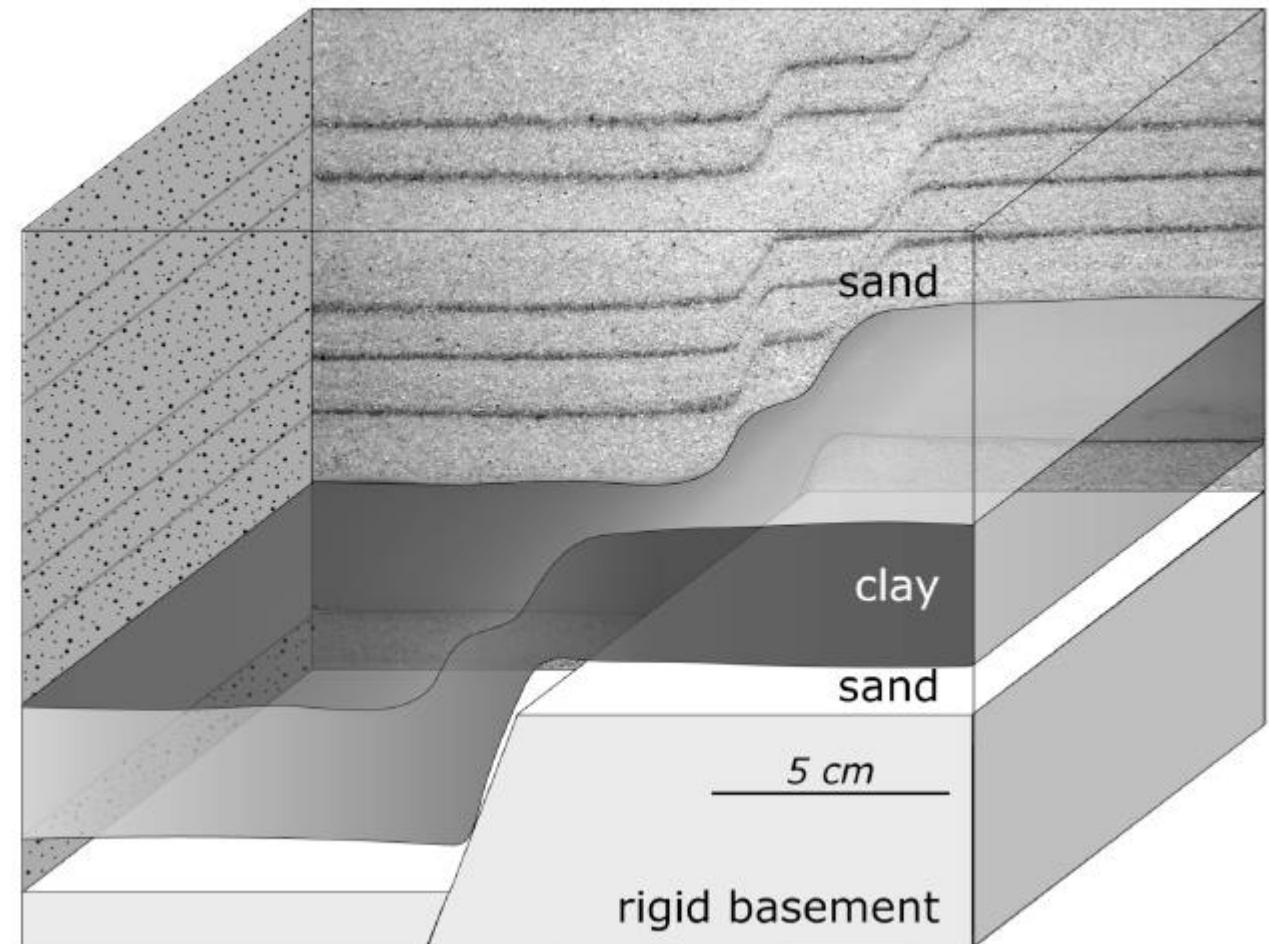
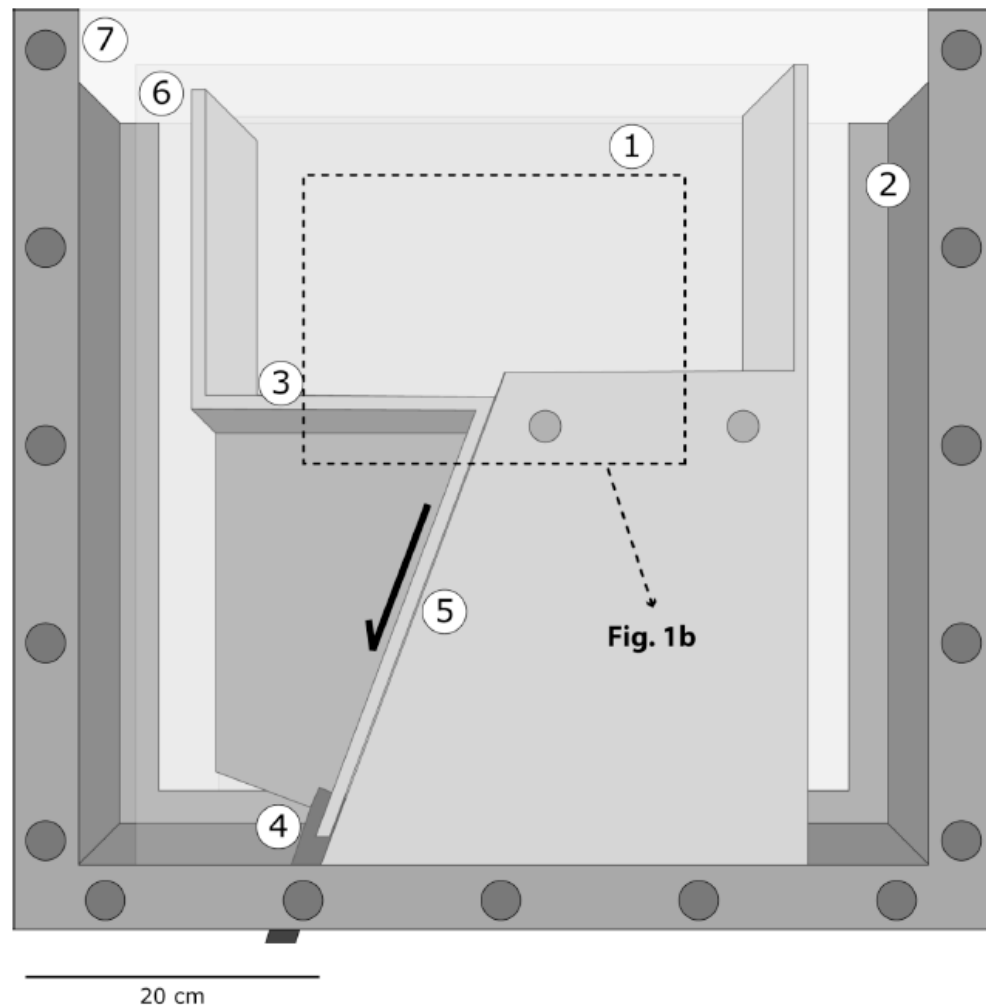
- **Displacement pressure:** the pressure when the non-wetting phase saturation reaches approximately 10% of the rock pore volume; a tangent line fitted to the inflection point of the cumulative intrusion curve and extrapolate the trend to the logarithmic pressure axis to find the displacement pressure.
- **Threshold pressure (first inflection):** the inflection point of the cumulative intrusion curve, or the pressure at which the first derivative of the intrusion curve reaches a local maximum; the pressure corresponding to the largest increase on the first derivative of the capillary pressure curve.
- **Measured breakthrough pressure:**
- **Threshold pressure (second inflection):**

# Silt bridging



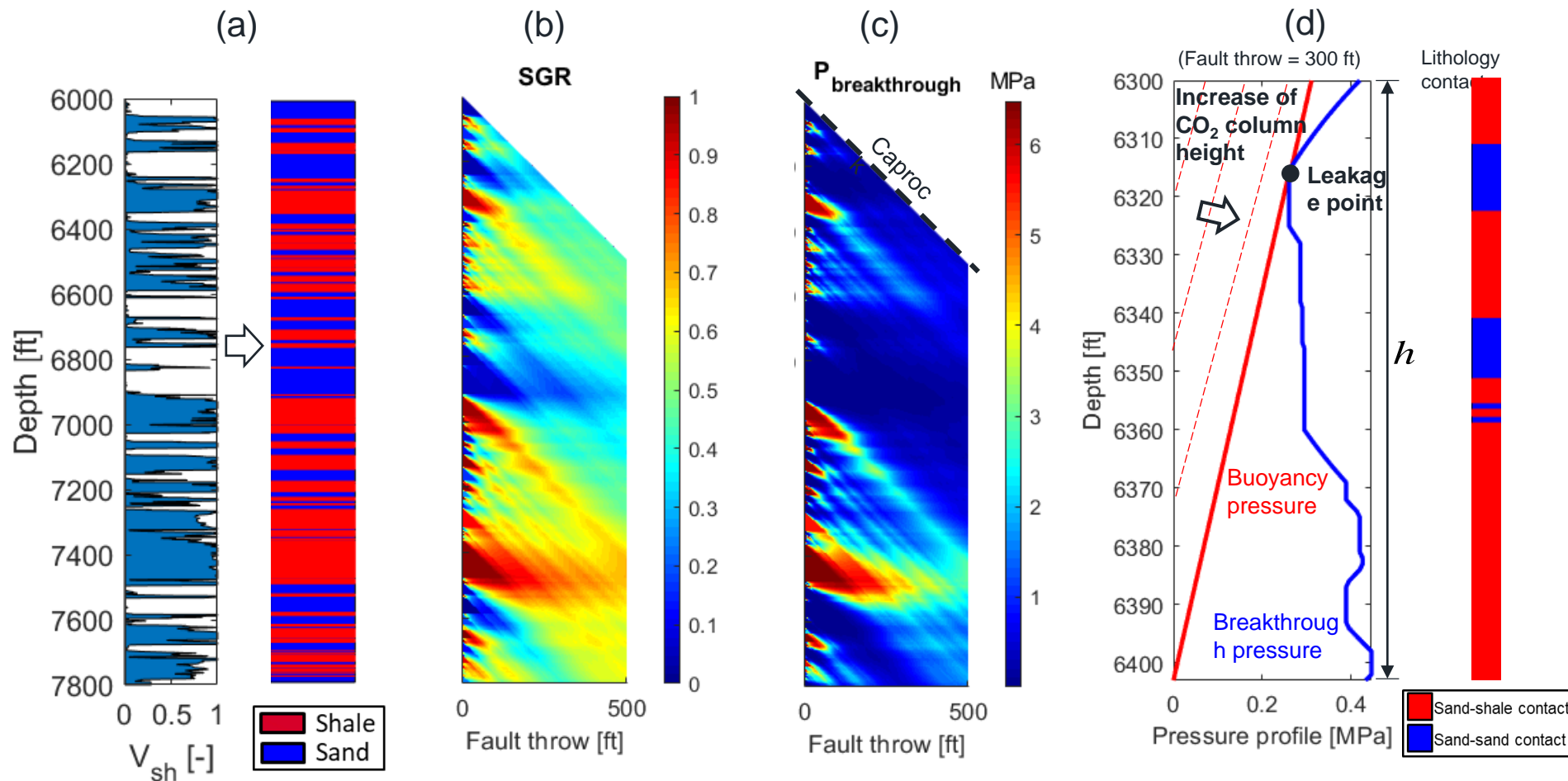
- High silt content in mudrocks helps preserve large pore throats and lowers percolation threshold due to silt bridging (with strong force chains), which may cause sealing failure in a mudrock.
- The capillary pressure curves displayed two percolation thresholds, probably due to larger pore throats being sheltered adjacent to larger grains because of silt bridging.

# Sandbox experiments

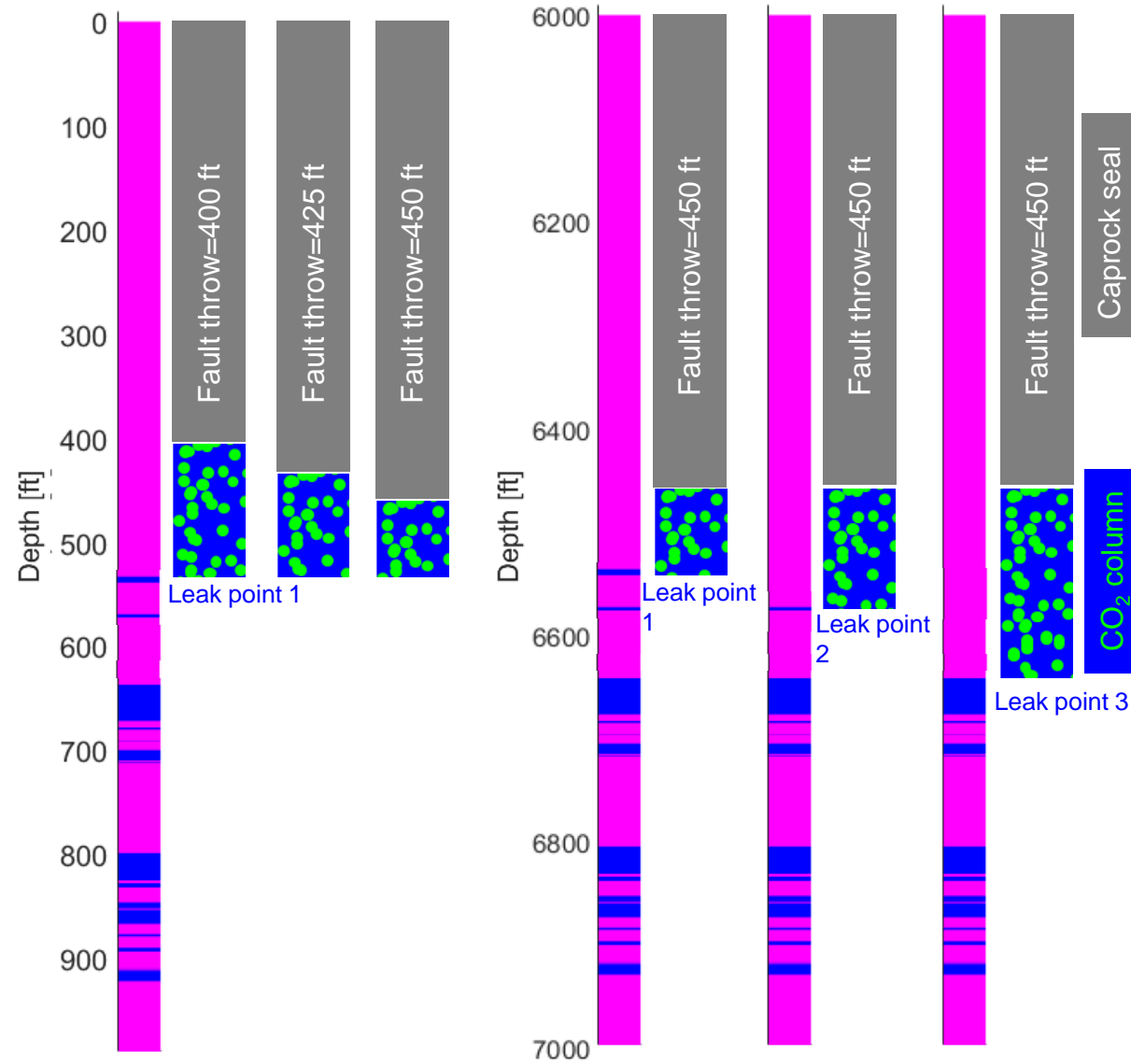
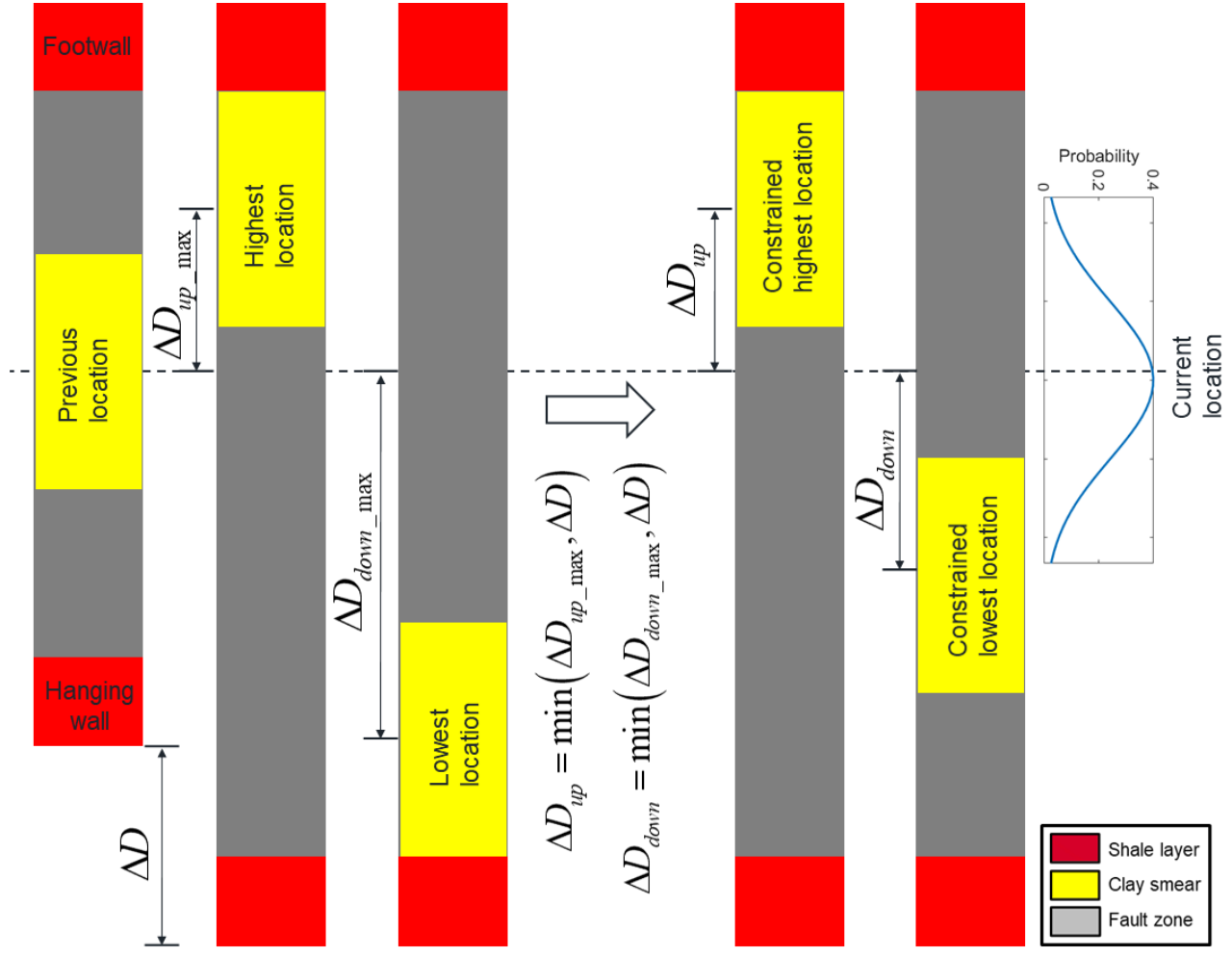


(Joyce Schmatz, 2010, Clay smear processes in mechanically layered sequences  
— Results of water-saturated model experiments with free top surface)

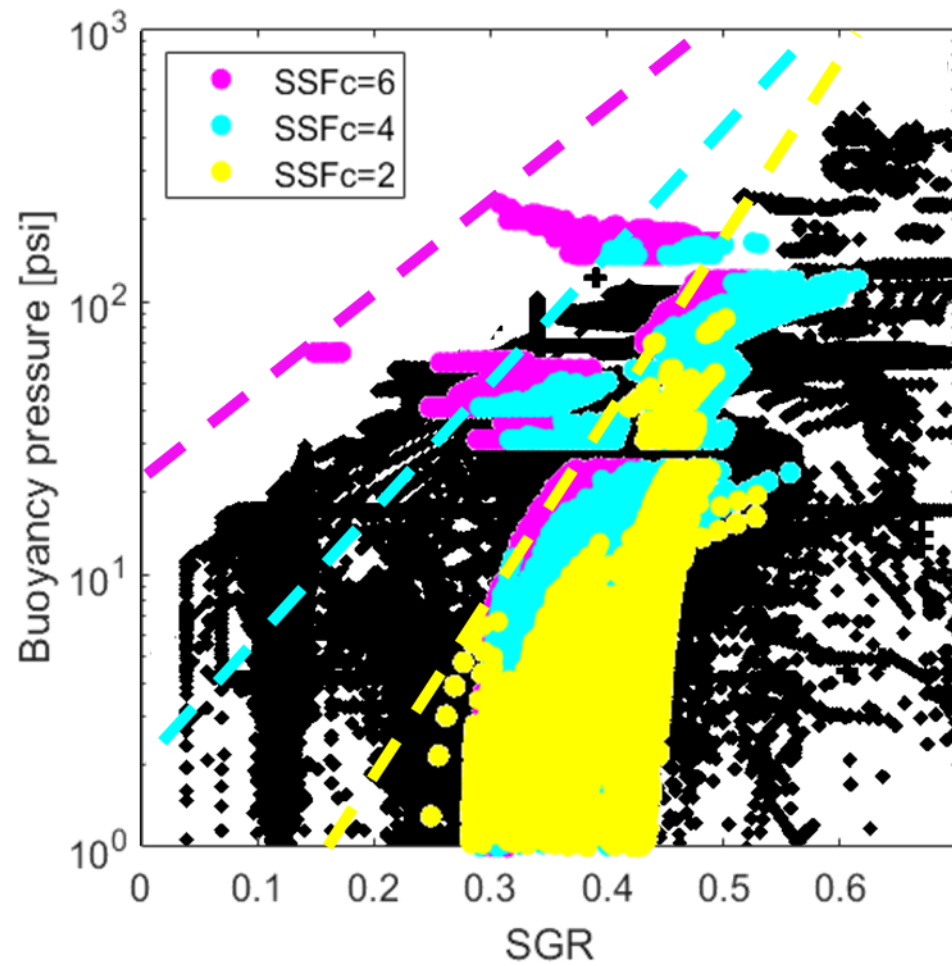
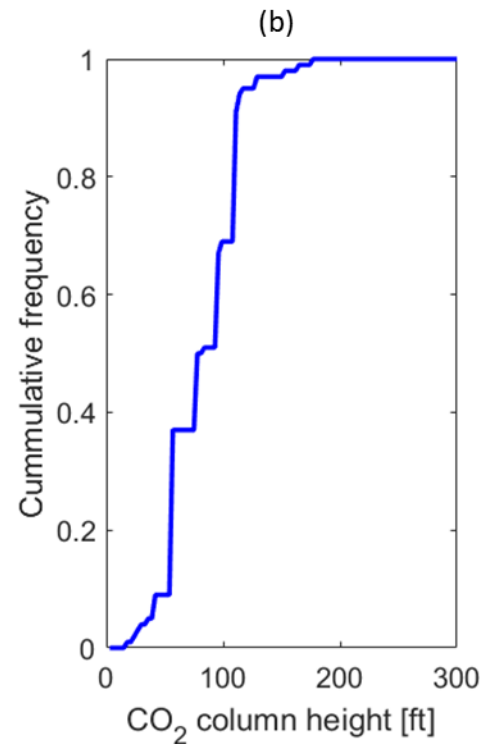
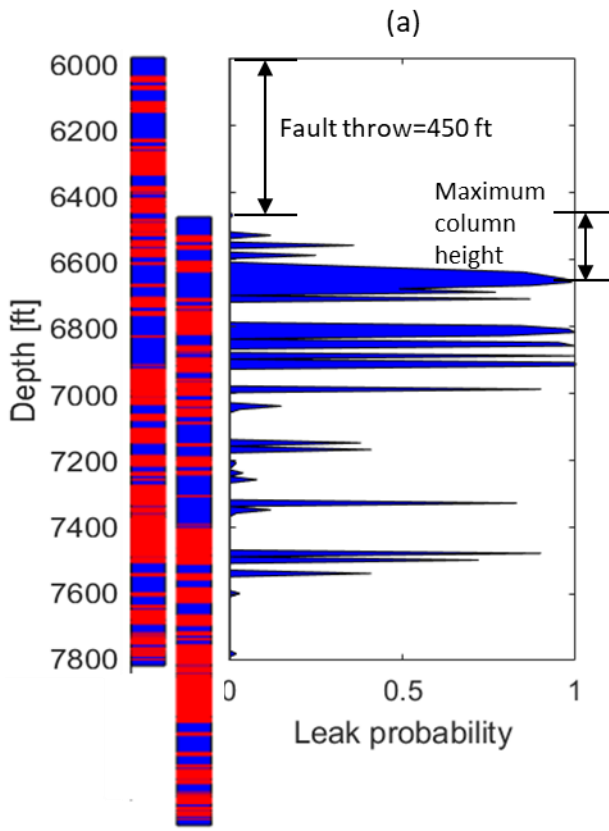
# CO<sub>2</sub> height prediction based on SGR method



# Smear distribution and impacts



# PSSF-based method



(Yielding, 2002)

# Fault gouge permeability predictor

$$PSSF = 1 - \frac{T(SSF_c - 1)}{D - T} \quad (\text{Childs, 2007; Yields, 2012})$$

## PSSF permeability

- Arithmetic permeability
- Upper bound (SSFc is small)

$$k = PSSF \cdot k_s + (1 - PSSF) \cdot k_c$$

## Shear zone model permeability

- Harmonic permeability
- Lower bound (SSFc=infinity)

$$k = \frac{1}{\frac{PSSF}{k_s} + \frac{(1 - PSSF)}{k_c}}$$

## SGR permeability

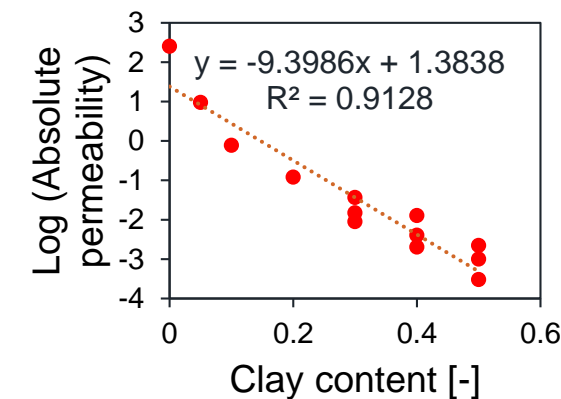
- Geometric permeability
- Mediate value

(Gutjahr, 1978)

$$k = k_c^{\varphi_v} k_s^{1-\varphi_v}, \log k = \varphi_v \log \frac{k_c}{k_s} + \log k_s$$

$$\log k = SGR \log \frac{k_c}{k_s} + \log k_s$$

$$k_s = 4mD, k_c = 3.31 \times 10^{-4} mD$$



$$k_{harmonic} < k_{geometric} < k_{arithmetic}$$

(Childs, 2007)

# Fluid-mechanics two-way coupling

The geomechanical deformation response is expressed in the fluid flow calculation through changing parameters in the porosity function. Porosity is a function of pressure, temperature and total mean stress formula and has the form:

$$\phi_{n+1} = \phi_n + (c_0 + c_2 a_1)_n (p - p_n) + (c_1 + c_2 a_2)_n (T - T_n) + \omega^{(k)} (\phi_n^c - \phi_n)$$

where:

$$\phi_n^c = \frac{V_n^p}{V_0^b} : \text{Actual porosity based on the definition}$$

$V_n^p$  : Pore volume at time step n

$V_0^b$  : Initial bulk volume

$$c_0 = \frac{1}{V_0^b} \left( \frac{dV_p}{dp} + V_b \alpha c_b \frac{d\sigma_m}{dp} - V_p \beta \frac{dT}{dp} \right)$$

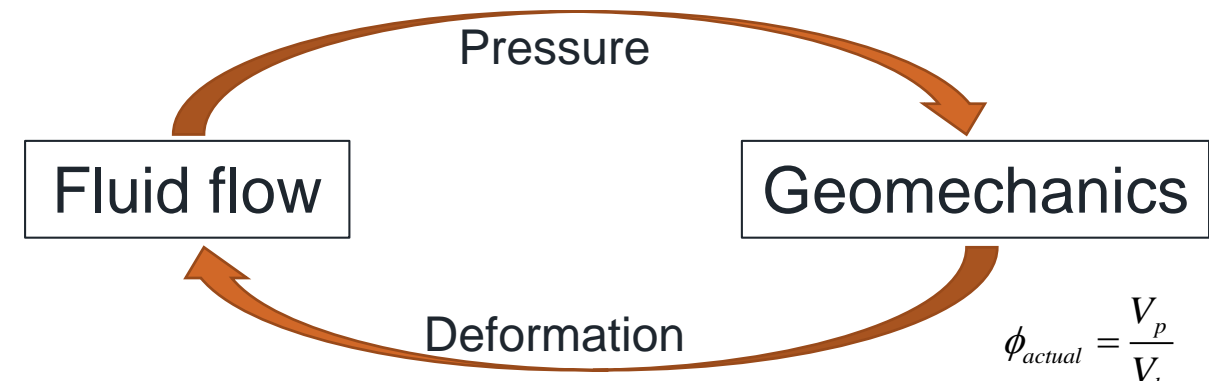
$$c_1 = \frac{V_p}{V_0^b} \beta$$

$$c_2 = -\frac{V_b}{V_0^b} \alpha c_b$$

$$a_1 = \text{factor} \left\{ \frac{2}{9} \frac{E}{(1-\nu)} \alpha c_b \right\}$$

$$a_2 = \text{factor} \left\{ \frac{2}{9} \frac{E}{(1-\nu)} \beta \right\}$$

$\omega^{(k)}$ : Weighting function at k<sup>th</sup> iteration is expressed as:  
 $\omega^{(k)} = \alpha_p f(\varepsilon_p^k) + \alpha_T f(\varepsilon_T^k)$

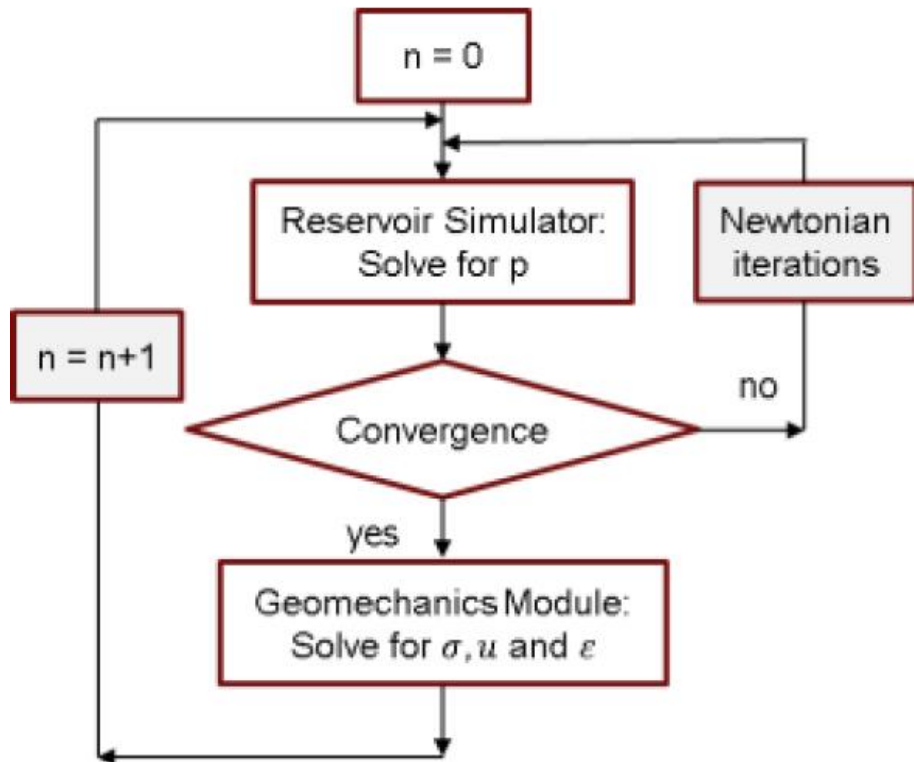


In terms of modularity, the fluid flow and geomechanics modules can be discretized in different ways including finite difference volume based grids and finite element nodal-based grids.

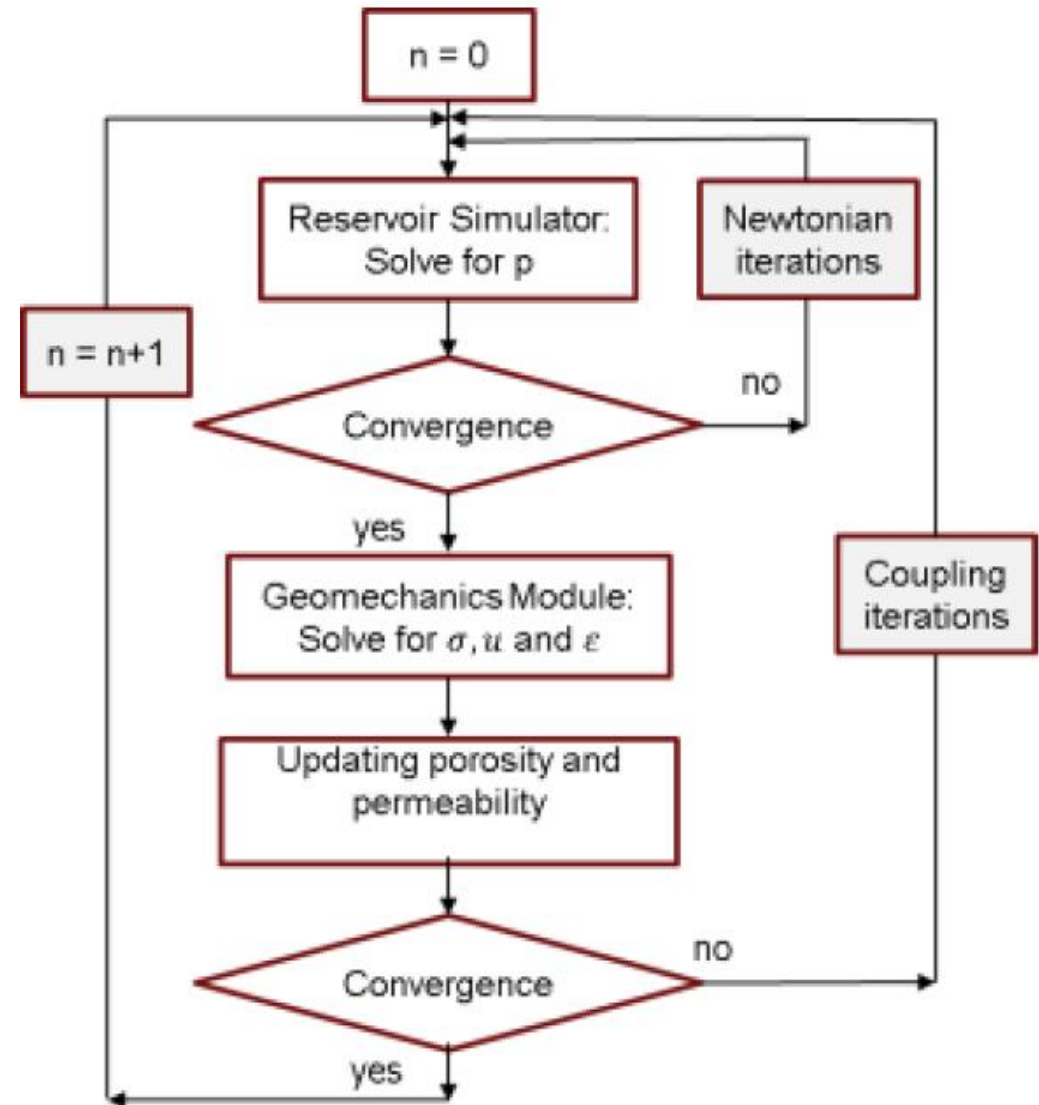
$$\phi_{actual} = \frac{V_p}{V_b}$$

# One-way vs two-way coupling

Explicit (One-Way) Coupling Schematic



Iterative (Two-Way) Coupling Schematic



# Fluid-mechanics two-way coupling

## Fluid flow equations:

- Darcy's law
- Mass conservation
- Equation of state

$$\begin{aligned} v &= -\frac{k}{\mu_f} \nabla p \\ \frac{\partial(\phi\rho)}{\partial t} &= \nabla \cdot (\rho v) + q \\ c_R &= \frac{\left( \frac{\phi}{\phi_i} - 1 \right)}{p - p_i} \end{aligned}$$

The mass conservation equation needs to be modified in order to account for geomechanical deformations.

$$\frac{\partial}{\partial t} [\phi^* \rho_f] - \nabla \cdot \left( \rho_f \frac{k}{\mu_f} \cdot [\nabla p - \rho_f b] \right) = Q_f$$

## Geomechanics equations:

- Force equilibrium equation
- Strain-displacement relationship
- Constitutive stress-strain relationship

$$\begin{aligned} \nabla \cdot \vec{\sigma} - B &= 0 \\ \vec{\sigma} &= \frac{1}{2} [\nabla \vec{u} + (\nabla \vec{u})^T] \\ \vec{\sigma} &= \vec{C} : \vec{\delta} + \alpha p I \end{aligned}$$

Substituting the strain-displacement relationship and the constitutive stress-strain relationship into the force equilibrium equations, the final geomechanics combined formulation becomes

$$\nabla \left[ \vec{C} : \left( \frac{1}{2} (\nabla \vec{u} + (\nabla \vec{u})^T) \right) \right] = -\nabla \alpha p I + \rho g$$

# Pressure increased due to undrained loading

These coupled mechanical deformation–pore pressure diffusion processes are captured by the pressure diffusivity equation for fluid flow coupled with poroelasticity (Cheng, 2016; Detournay & Cheng, 1993)

$$\frac{dP}{dt} = \frac{kM^*}{\mu} \nabla^2 P - \alpha M^* \frac{d\varepsilon_v}{dt}$$

The Biot modulus is

$$M^* = \left( \frac{\phi_0}{K_f} + \frac{\alpha - \phi_0}{K_m} \right)^{-1} \quad \alpha = 1 - \frac{K}{K_m}$$

For a linear elastic isotropic porous solid, the expected pore pressure change  $\Delta P$  under undrained loading is directly proportional to the volumetric strain (Coussy, 2004):

$$\Delta P = -M^* \alpha \Delta \varepsilon_v$$

The characteristic pressure diffusion time captures the time when ~2/3 of the pore pressure is relieved and indicates the rate of pore pressure change (Cheng, 2016):

$$T_{ch} = \frac{L^2}{D_h}$$

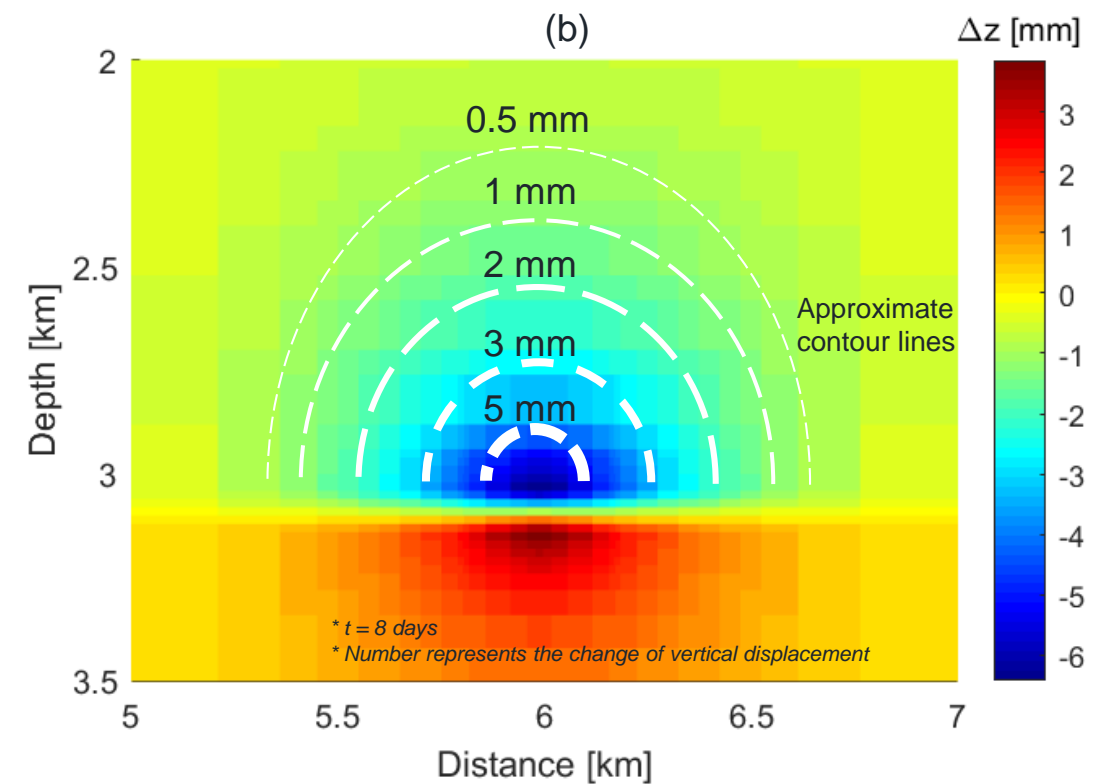
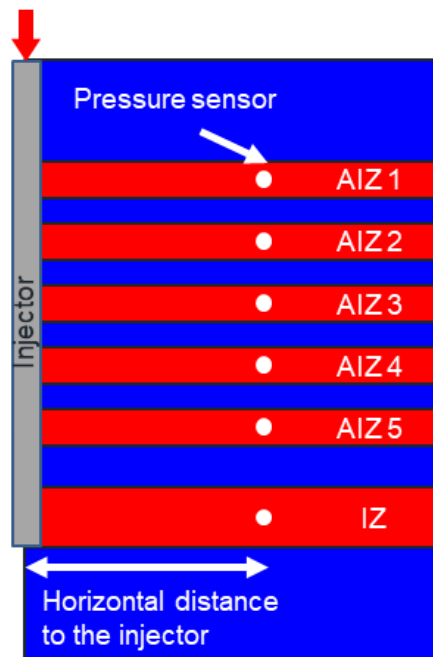
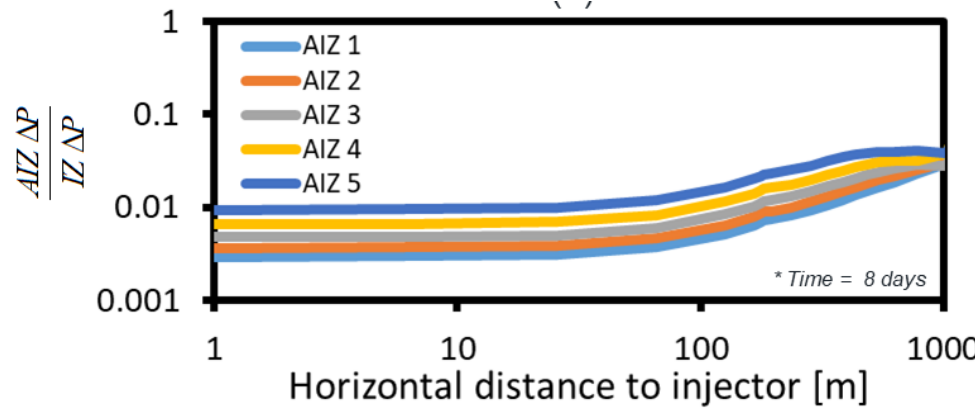
The hydraulic diffusivity parameter is

$$D_h = \frac{kM^*}{\mu}$$

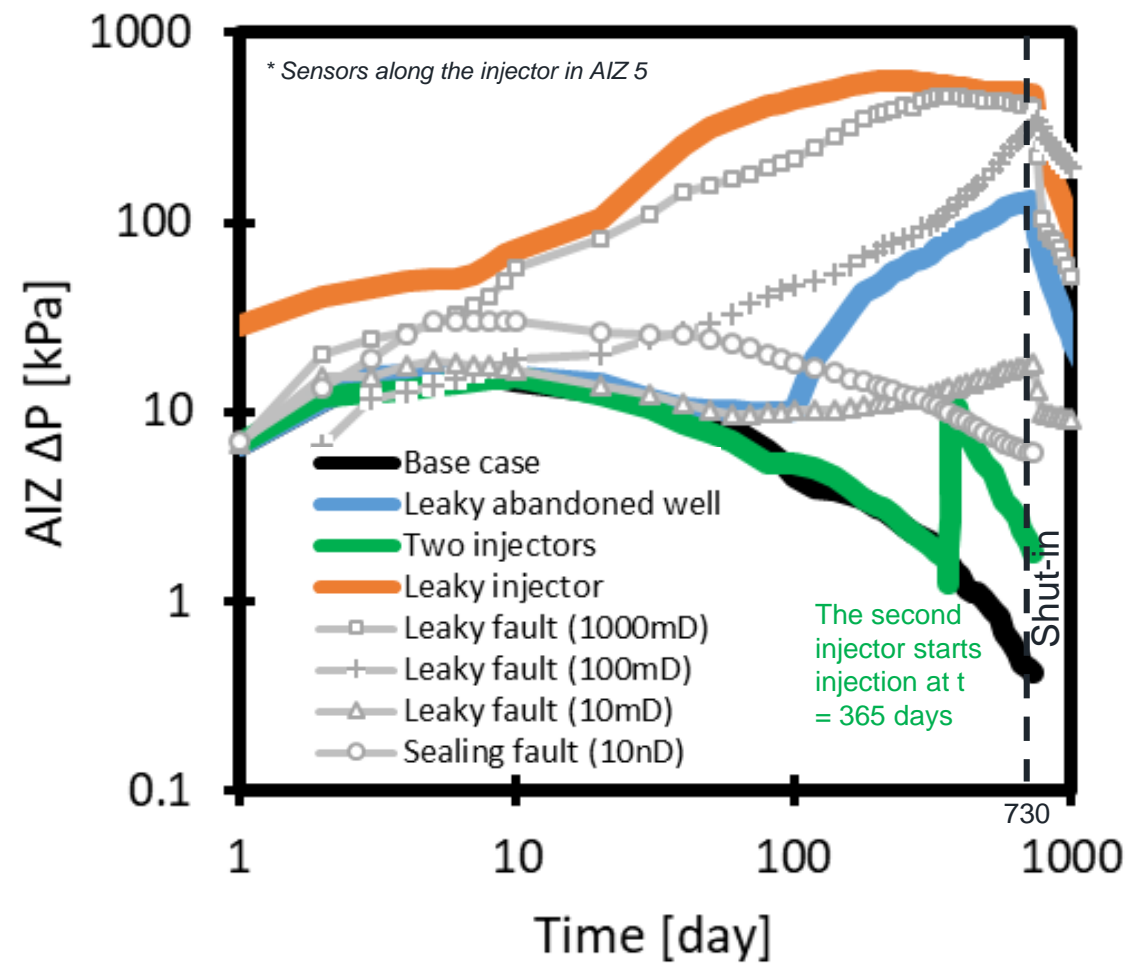
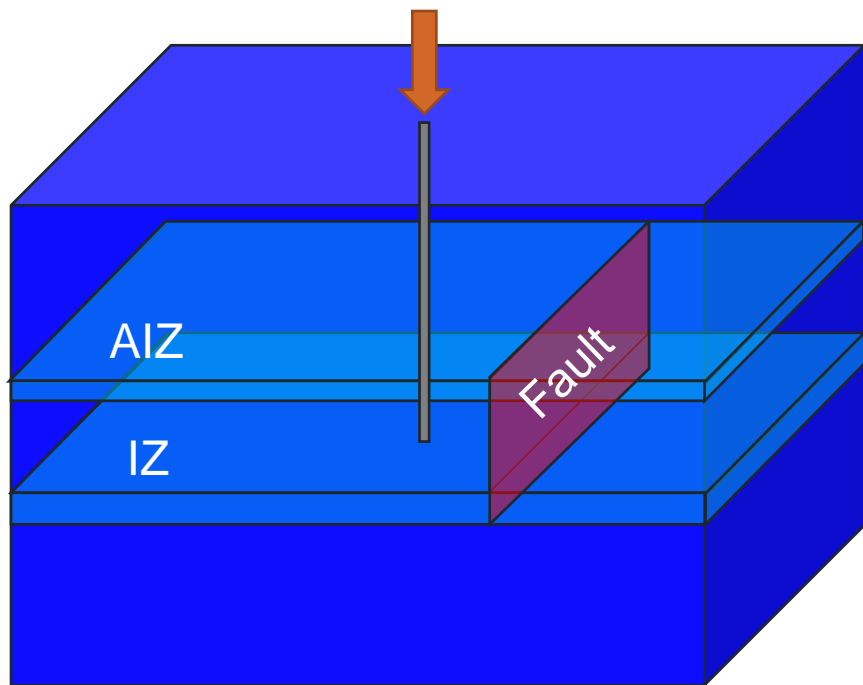
The sand with a lower bulk modulus and higher permeability experiences a larger volumetric strain, and thus a higher pressure increase, than the shale. The sand also drains more quickly than the shale because of its larger hydraulic diffusivity.

Therefore, pore pressure in AI2Z sands increases in the first 10 days to a peak value and then decreases with time, while pore pressure in shale exhibits more gradual and long-lasting changes than in pervious sands.

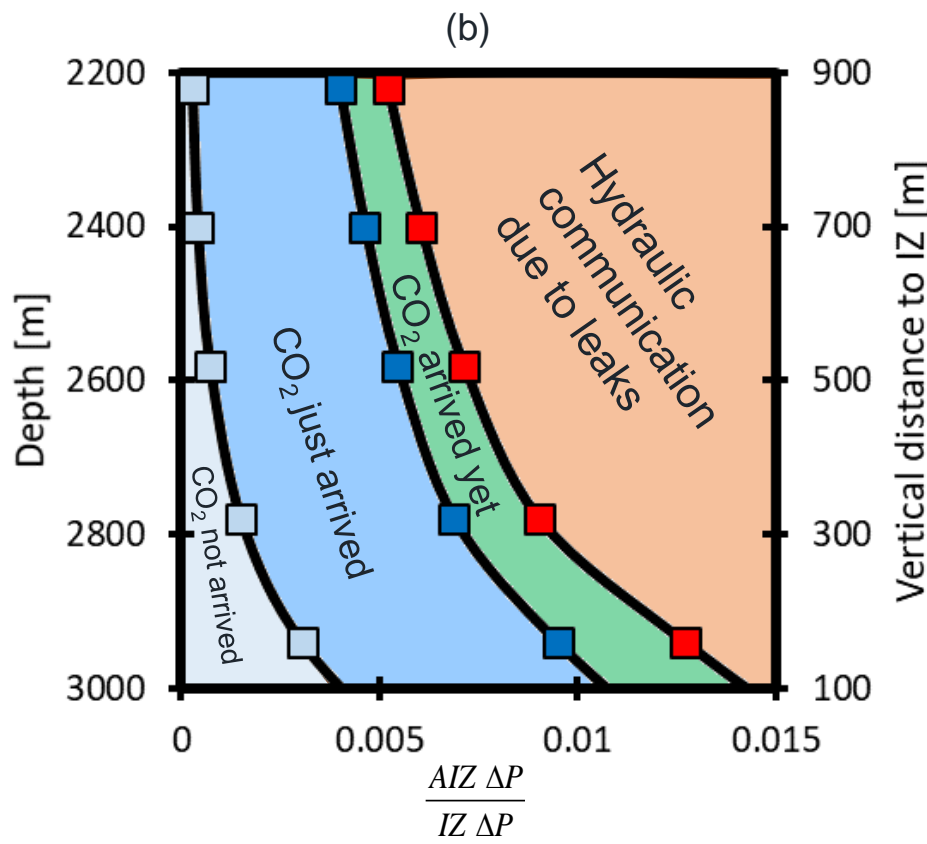
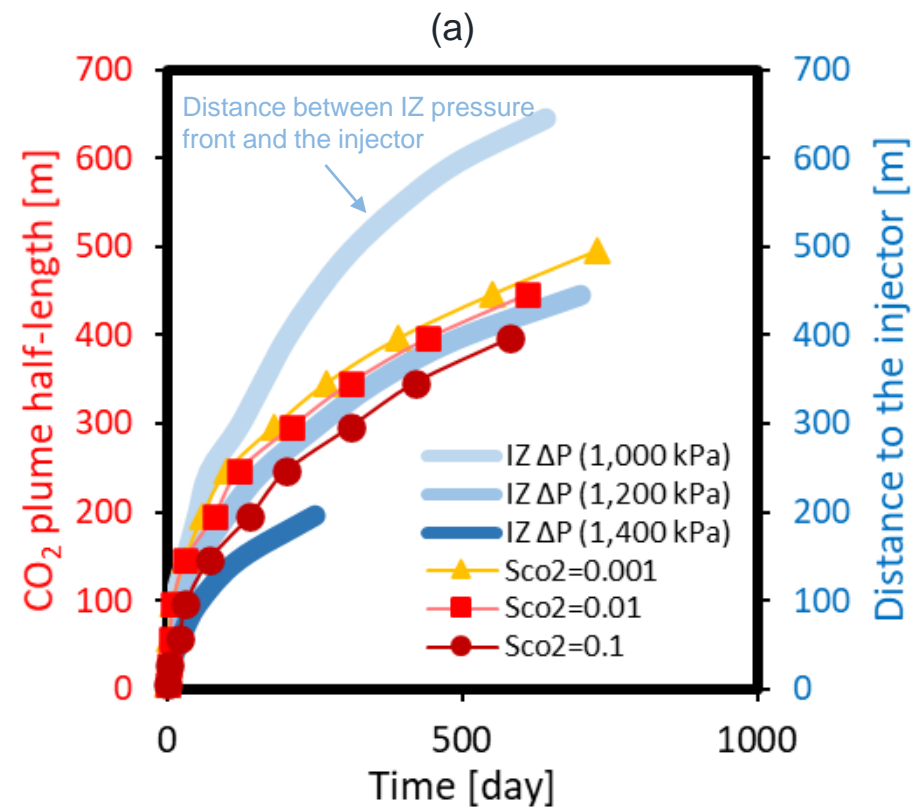
# Effects of location and vertical displacement



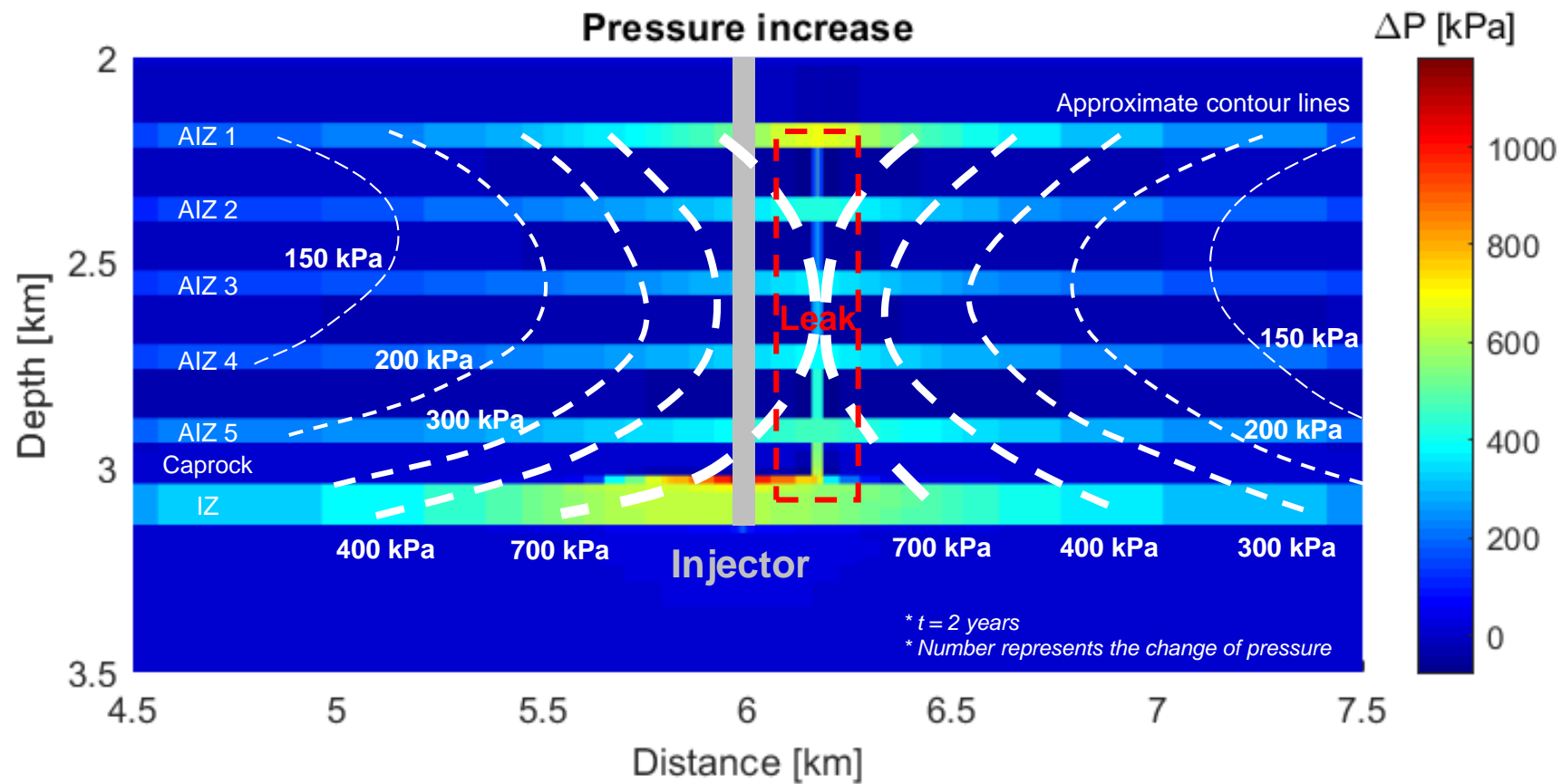
# Effects of fault permeability on AlZ $\Delta P$



# Prediction of CO<sub>2</sub> plume migration

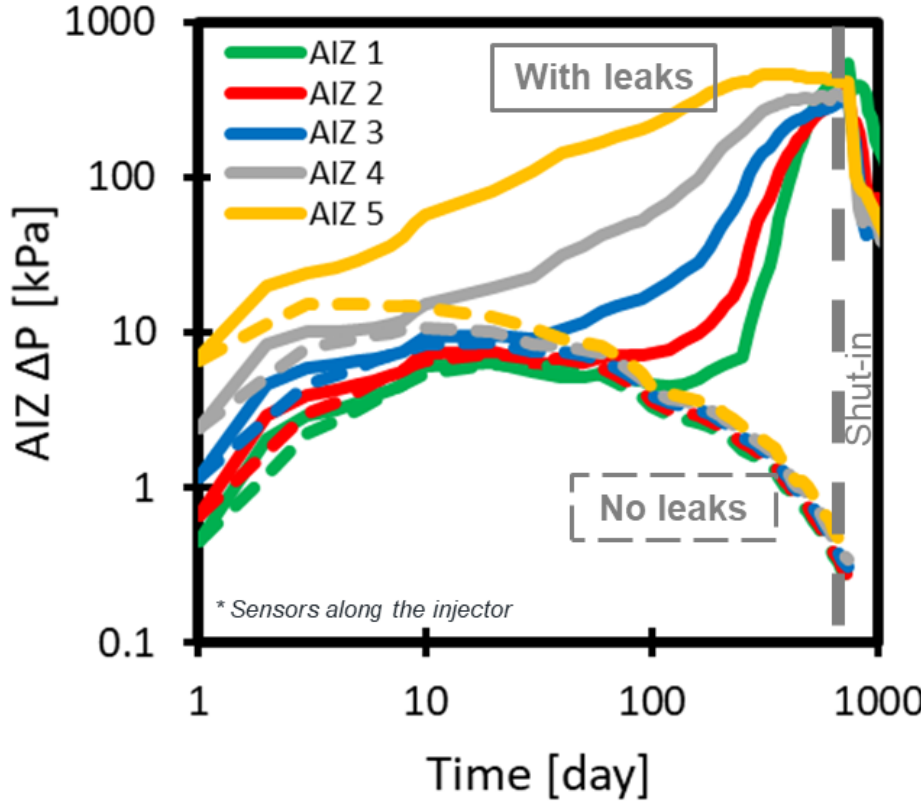


# Pressure front with the presence of a leaky fault

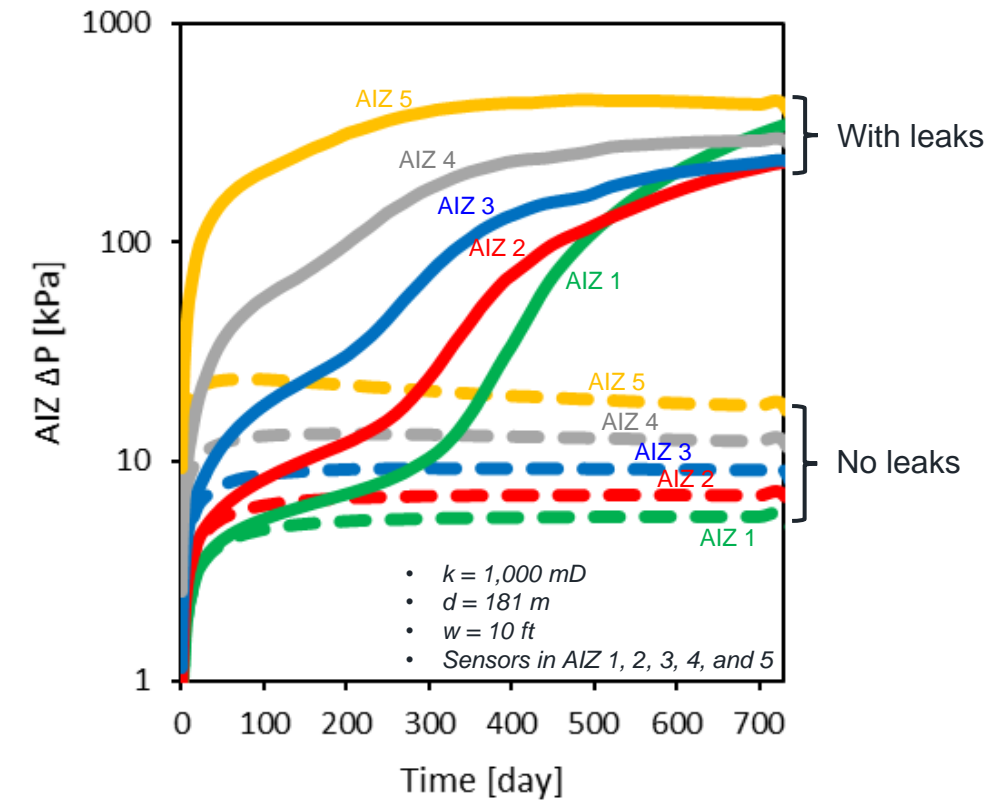


# Analytical estimation on poroelastic response

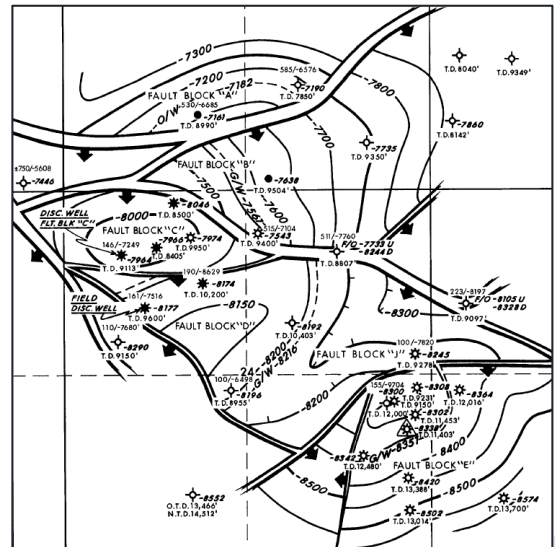
Direct output of the system



Analytical estimation  $\Delta P = -\left(\frac{\phi_0}{K_f} + \frac{b-\phi_0}{K_m}\right)^{-1} b \Delta \varepsilon_v$

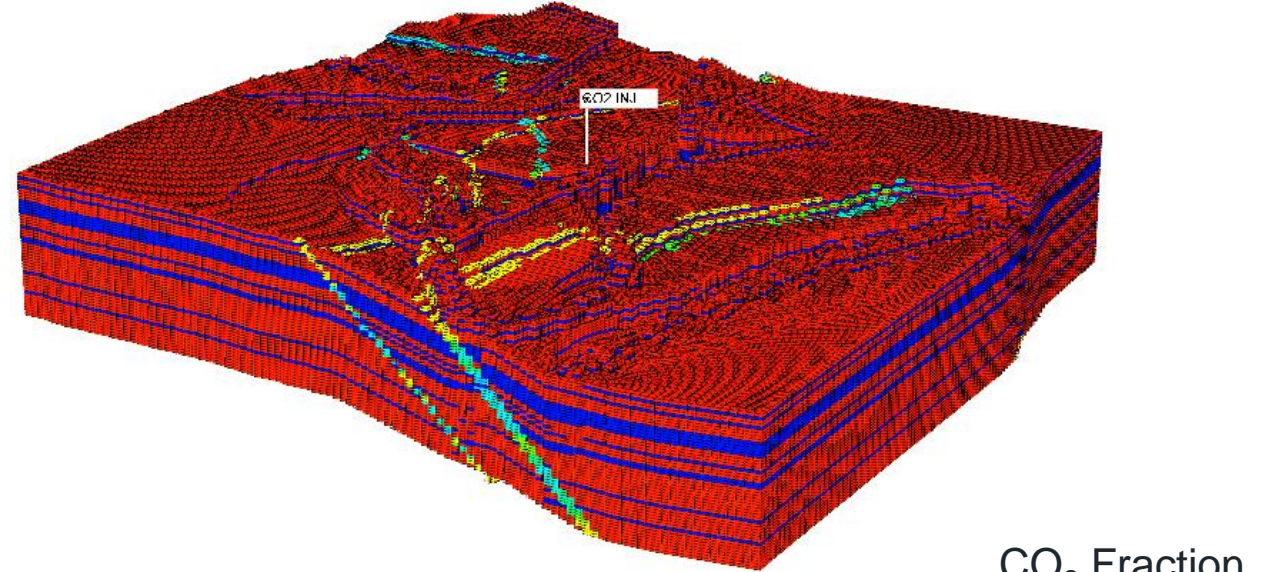
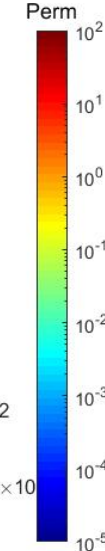
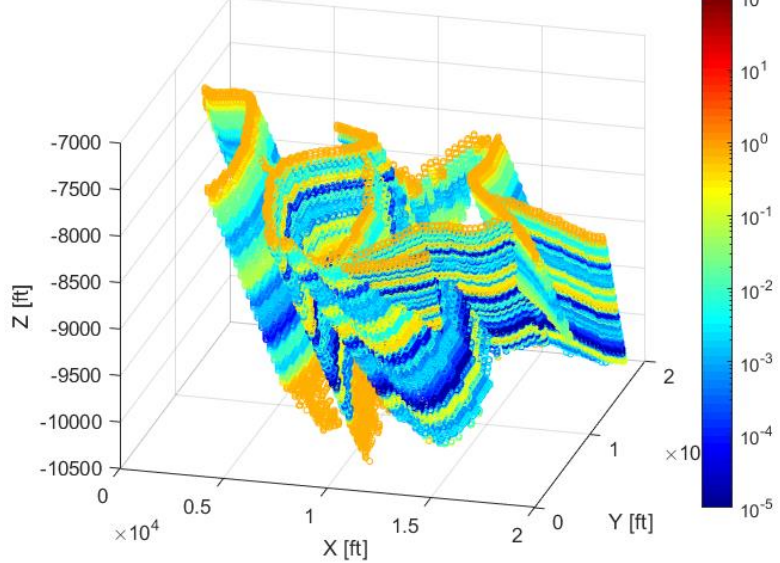


# $\text{CO}_2$ plume migration in a realistic block

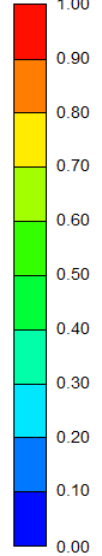
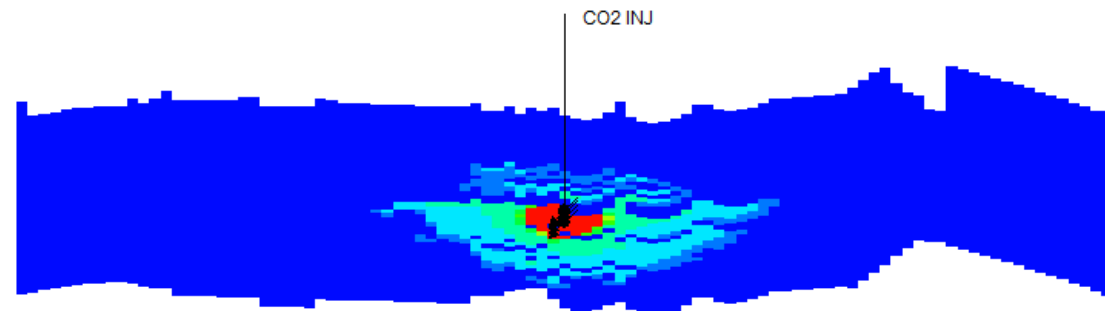


Permeability [mD]

SGR-based fault permeability

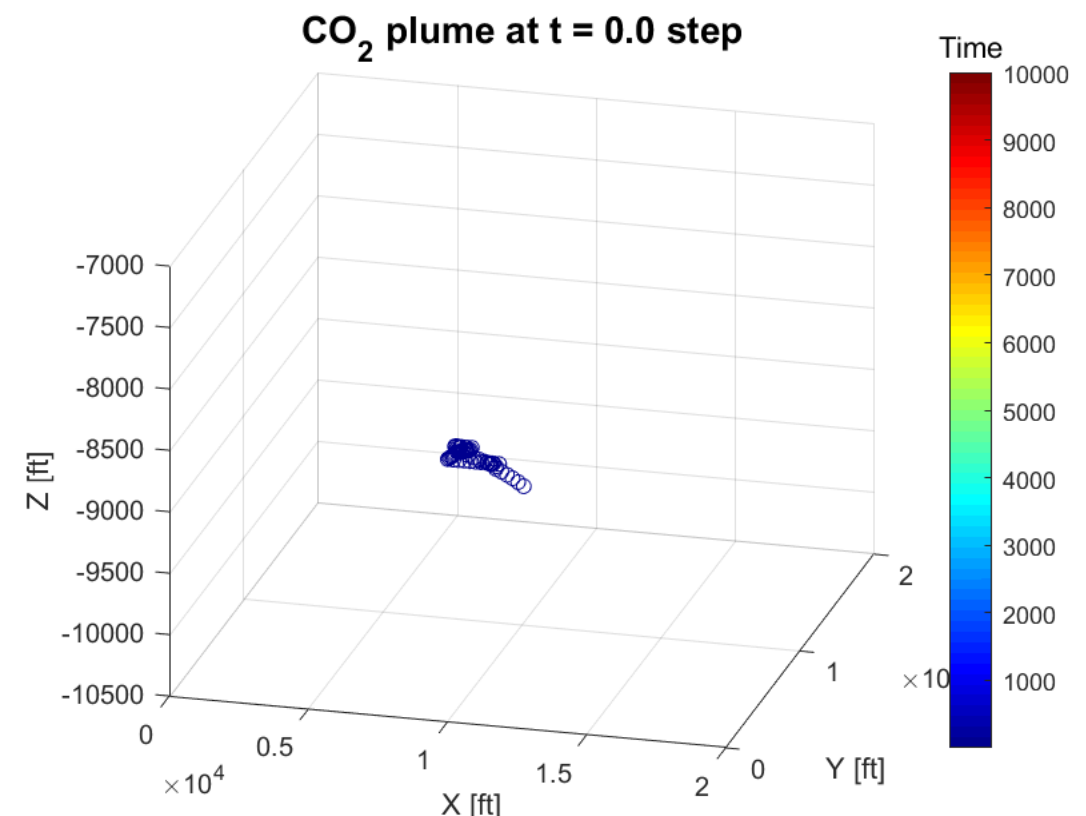
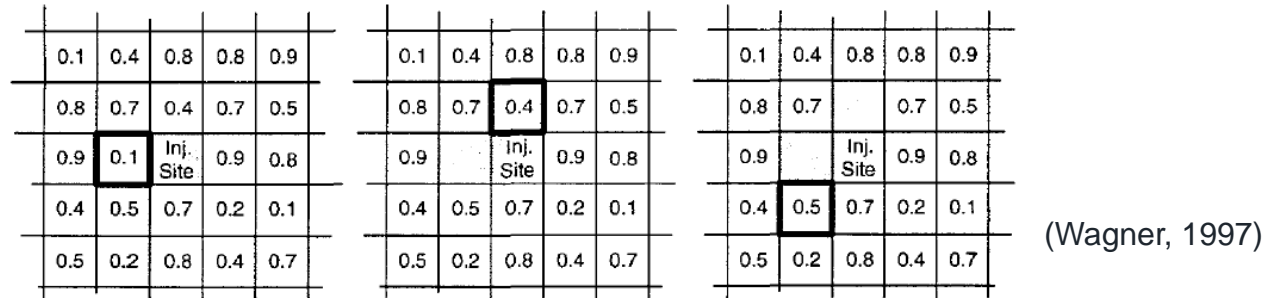
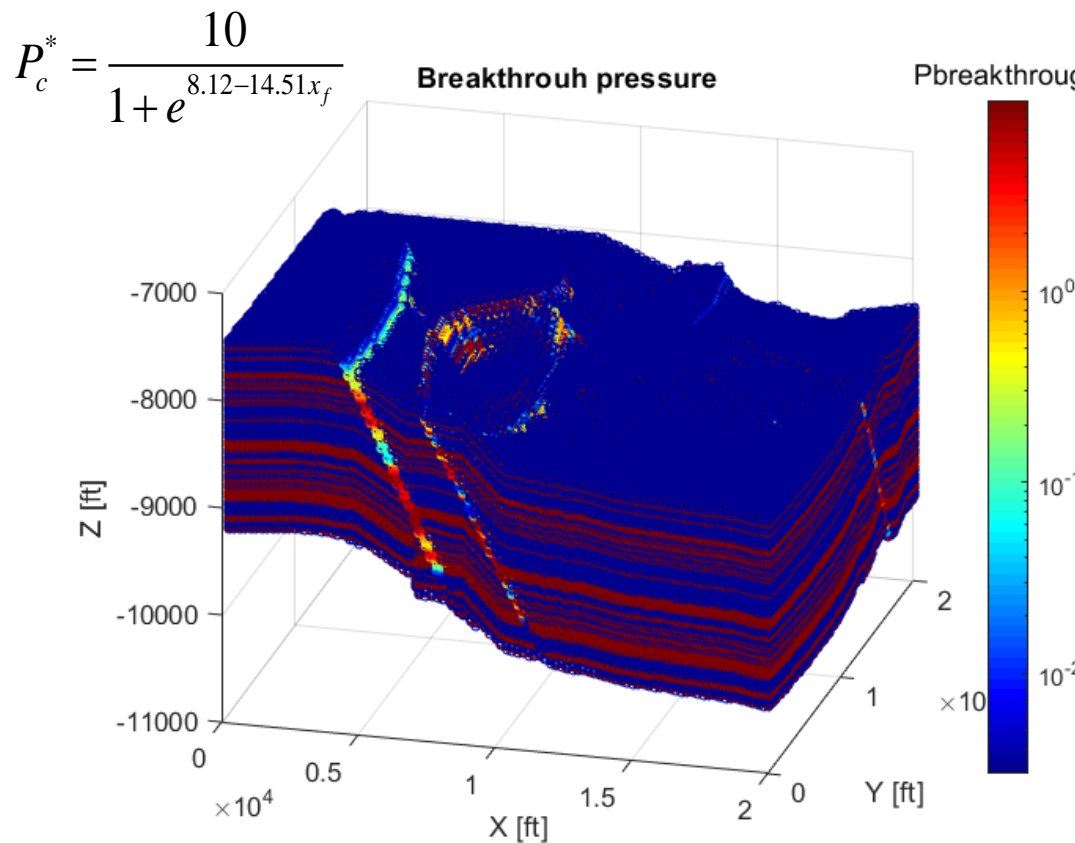


50 years

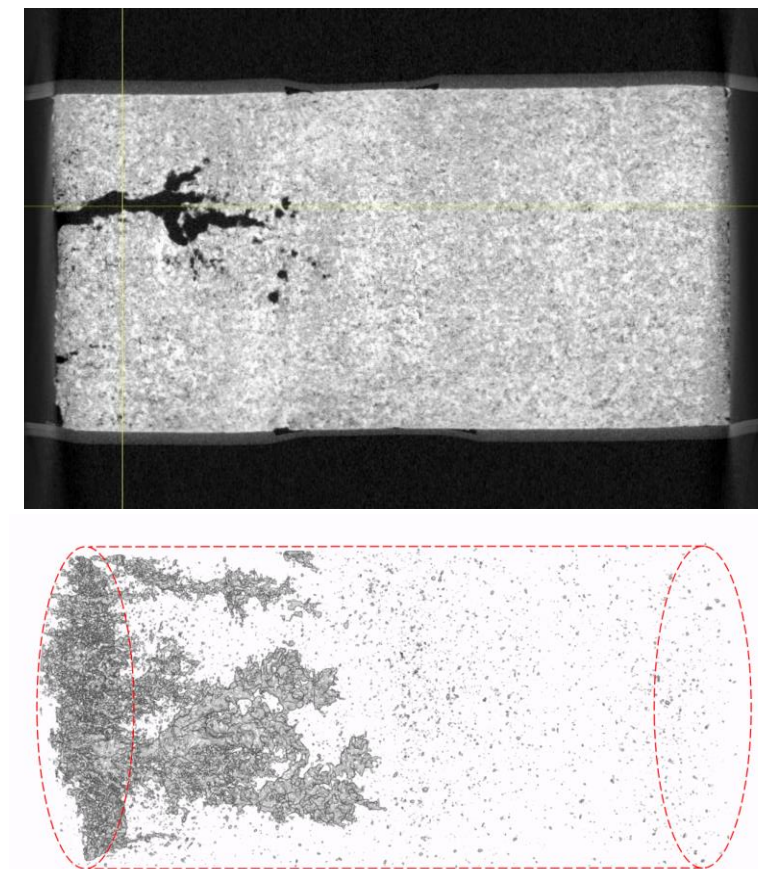
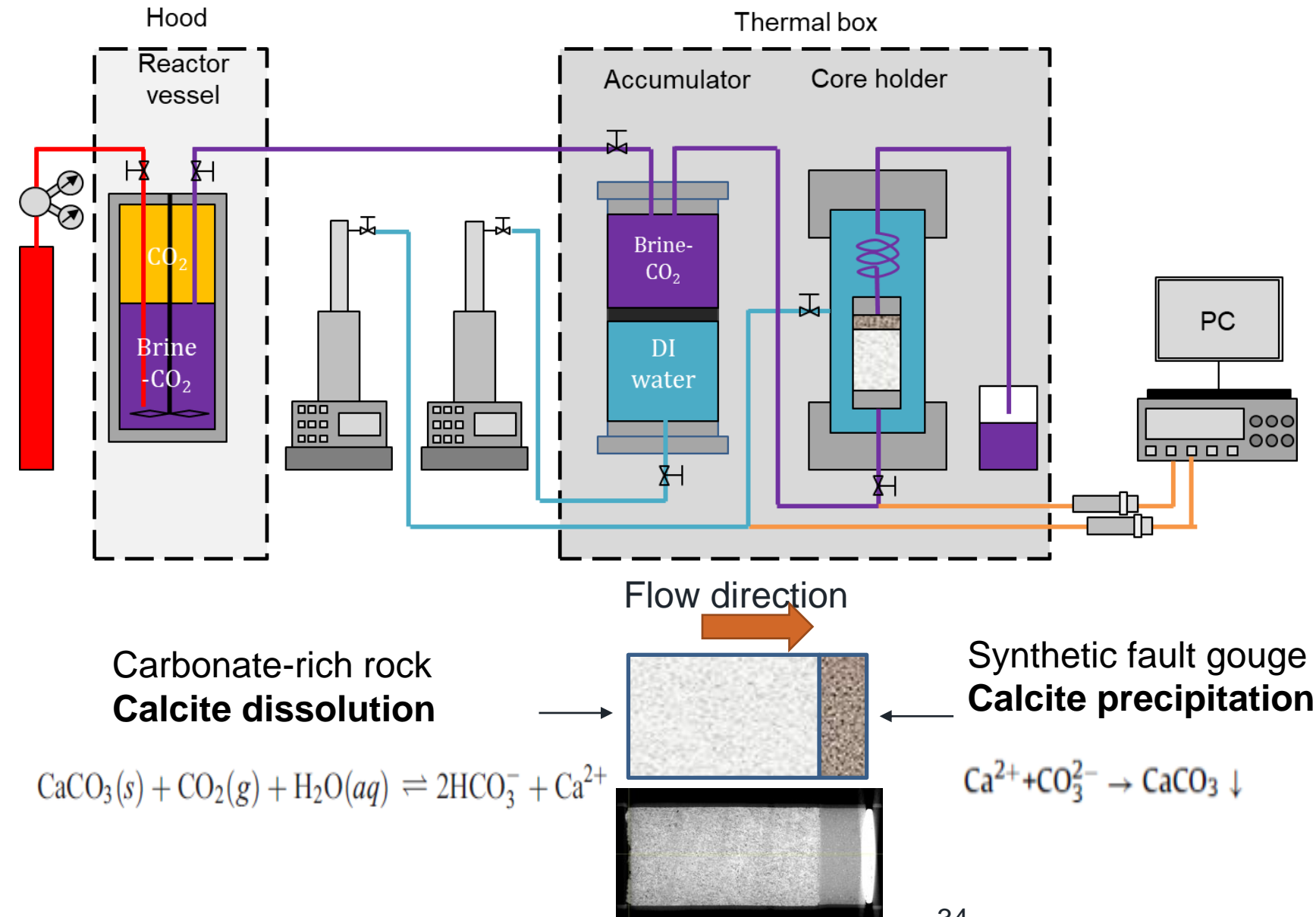


# Invasion percolation

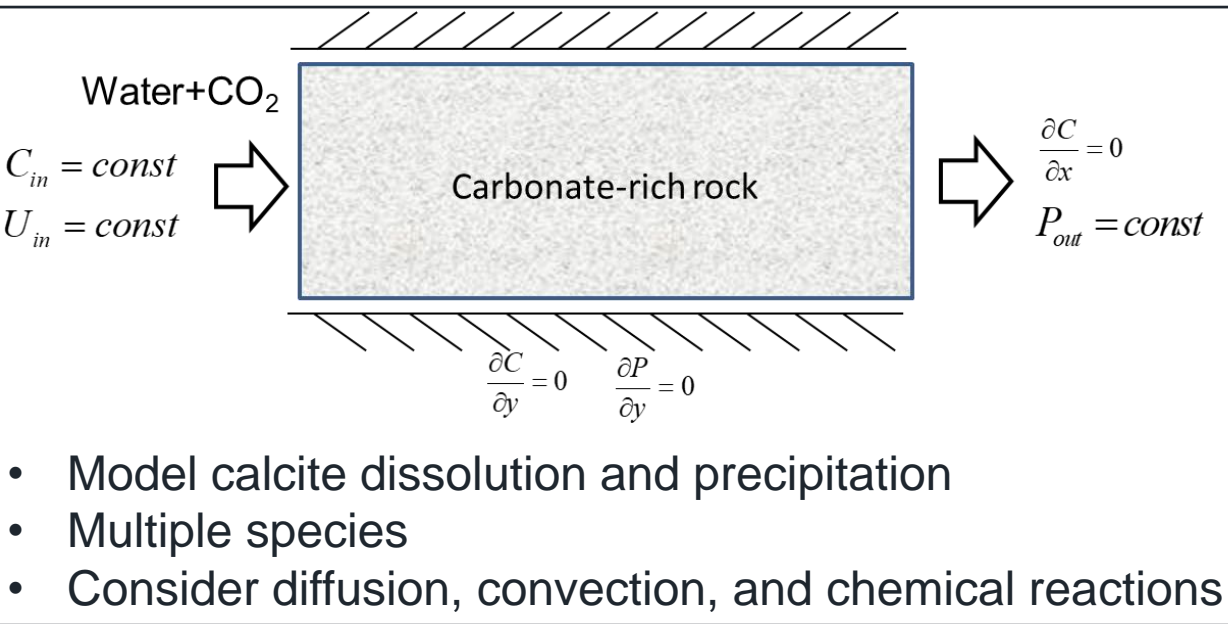
- Invasion occurs at  $P_{\min}$
- Assume constant flow rate
- Advance in one place at each step
- Total time step: 10,000



# Chemical alterations on fault gouge



# Multi-species reactive transport model



## Darcy scale model

$$\frac{\partial(\phi\alpha)}{\partial t} + \nabla \cdot (U\alpha) - \nabla \cdot (\phi D \cdot \nabla \alpha) = S_e r_e + S_k r_k$$

$$\frac{\partial \phi}{\partial t} = \frac{R_{net} M_{CaCO_3} a_v}{\rho_{CaCO_3}}$$

$$\frac{\partial \phi}{\partial t} + \nabla \cdot U = 0$$

$$U = -\frac{1}{\mu} K \cdot \nabla P$$

## Pore scale model

$$K = K_0 \frac{\phi}{\phi_0} \left( \frac{\phi(1-\phi_0)}{\phi_0(1-\phi)} \right)^{2\beta}$$

$$r = r_0 \sqrt{\frac{K\phi_0}{K_0\phi}} \quad a_v = a_0 \frac{\phi r_0}{\phi_0 r}$$

$$k_c = \frac{D_m}{2r} \left( Sh_\infty + 0.7 Re_p^{1/2} Sc^{1/3} \right)$$

$$D_x = D_m \left( \alpha_{os} + \lambda_x Pe_p \right)$$

$$D_y = D_m \left( \alpha_{os} + \lambda_T Pe_p \right)$$

## Equilibrium reactions

$$H^+ + OH^- \rightleftharpoons H_2O \quad K_4 = \alpha_{H^+} \alpha_{OH^-} = 10^{-14}$$

$$H^+ + CO_3^{2-} \rightleftharpoons HCO_3^- \quad K_5 = \frac{\alpha_{H^+} \alpha_{CO_3^{2-}}}{\alpha_{HCO_3^-}} = 10^{-10.329}$$

$$Ca^{2+} + HCO_3^- \rightleftharpoons CaHCO_3^+ \quad K_6 = \frac{\alpha_{HCO_3^-} \alpha_{Ca^{2+}}}{\alpha_{CaHCO_3^+}} = 10^{-1.106}$$

$$2H^+ + CO_3^{2-} \rightleftharpoons H_2CO_3 \quad K_7 = \frac{\alpha_{H^+}^2 \alpha_{CO_3^{2-}}}{\alpha_{H_2CO_3}} = 10^{-16.7}$$

(Akanni, 2015; Golfier et al., 2002; Panga et al., 2005; Ratnakar et al., 2013; Holzbecher, 2012; Eppner et al., 2015; Saaltink et al., 1998; Plummer et al., 1978)

## Kinetic equations

$$CaCO_3 + H^+ \rightleftharpoons Ca^{2+} + HCO_3^- \quad k_1 = 10^{\left(0.198 - \frac{444}{T}\right)} / 100$$

$$CaCO_3 + H_2CO_3 \rightleftharpoons Ca^{2+} + 2HCO_3^- \quad k_2 = 10^{\left(2.84 - \frac{2177}{T}\right)} / 100$$

$$CaCO_3 + H_2O \rightleftharpoons Ca^{2+} + HCO_3^- + OH^- \quad k_3 = 10^{\left(-5.86 - \frac{317}{T}\right)} / 100 \quad (T < 25^\circ C)$$

## Net rate of calcite precipitation and dissolution

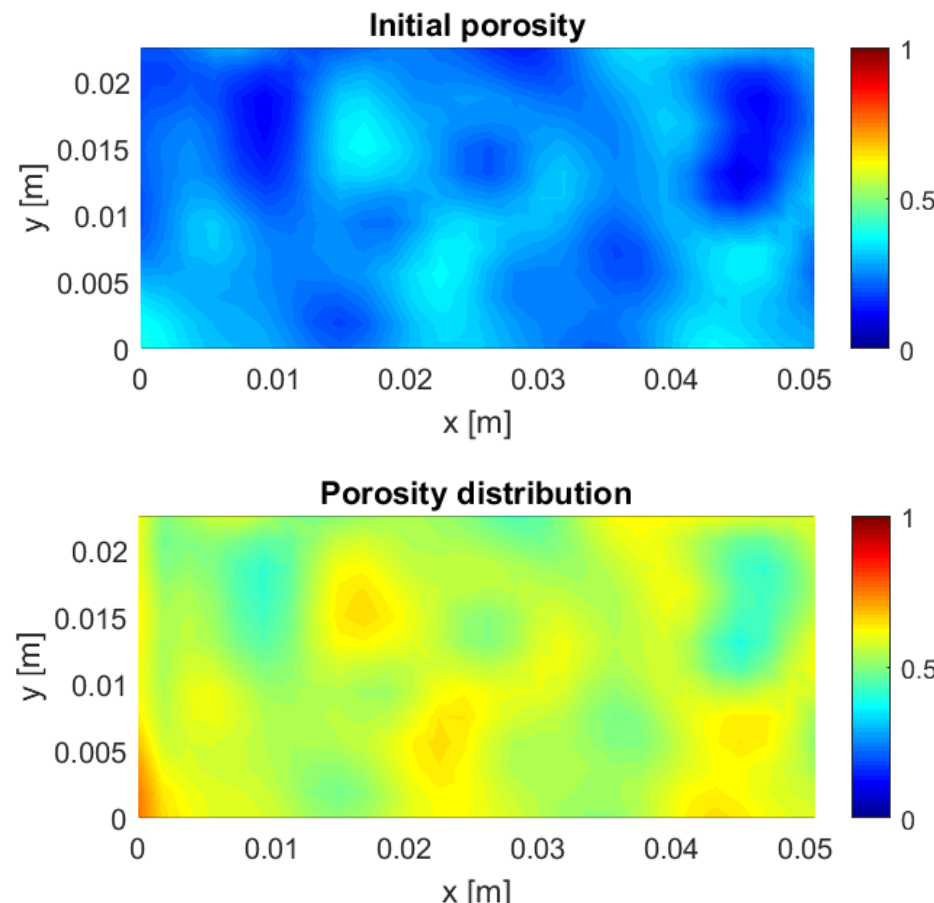
$$R_{net} = k_1 \alpha_{H^+} + k_2 \alpha_{H_2CO_3} + k_3 \alpha_{H_2O} - k_{-1} \alpha_{Ca^{2+}} \alpha_{HCO_3^-} - k_{-2} \alpha_{Ca^{2+}} \alpha_{HCO_3^-}^2 - k_{-3} \alpha_{Ca^{2+}} \alpha_{HCO_3^-} \alpha_{OH^-}$$

Rnet > 0: dissolution; Rnet < 0: precipitation.

# Preliminary results

## Randomly-correlated porosity field

- Initial porosity field is generated by Gaussian distribution
- Average value is 0.27



## CO<sub>2</sub> injection condition

- Injection duration: ~14 days
- Injection rate: 5 ml/min
- Upstream CO<sub>2</sub> pressure: ~100 psi

